Coupling of electromagnetic waves into wires - experiments and simulations

by

Alistair Paul Duffy, B.Eng, M.Eng

Thesis submitted to The University of Nottingham for the degree of Doctor of Philosophy, October 1993.

CONTENTS

ABSTRACT

Electromagnetic Compatibility (EMC) problems may occur in many environments. This Thesis considers a particular sub-set of coupling within shielded enclosures. The actual systems studied are the coupling between a dipole and either one or two rods in a screened room and the effect of a cavity and apertures on a signal travelling along a wire.

Experiments are described for the screened room which investigate the repeatability of the measurements and the effects of two closely spaced conductors on the coupling results. The cavity experiments also consider the repeatability of the measurements and the effects of the apertures.

Transmission-Line Modelling (TLM) is compared with some other popular modelling methods and generally described. It is applied to the modelling of the experimental systems already discussed. An inherent error associated with the modelling of wires in TLM, manifesting itself as an apparent decrease in the resonant frequency of a wire-like structure, is investigated. The source of the error is deduced and a method of minimising it is proposed.

The experimental results are applied to the validation of TLM, and its error correction. Very good comparisons between the experiments and simulations are reported. Correlelograms are investigated as a method of comparing the modelled and experimental results.

ACKNOWLEDGEMENTS

A debt of gratitude must be paid to my supervisors, Professor Christos Christopoulos and Dr. Trevor Benson, for their good humoured assistance during the course of the project and for knowing when to direct me and when to let me go my own way. I would also like to thank Dr. Phil Naylor for help with 'getting started' with TLM and Dr. Jon Herring for the numerous lengthy discussions on many aspects of TLM.

The work presented here was sponsored by the Defence Research Agency, Fort Halstead (formerly RARDE). I would like to thank the DRA for their funding and particularly Dr. John Lyons, Dr. Richard Clement, Mr. Chris Thomas and Mrs. Joyce Stone (DRA, Farnborough) for their comments, suggestions and probing cross-examination during the progress review meetings. Also many thanks to my colleagues in the labs and the Department's technicians for their help and advice - solicited and otherwise.

Finally, thanks to Sue for her patience and support.

CHAPTER ONE
INTRODUCTION

This chapter introduces the basic definition of electromagnetic compatibility (EMC); why wires are important in EMC; the rôle of modelling in EMC, and the importance of Transmission-Line Modelling (TLM); why experimental verification tests are required, and an outline of the rest of the Thesis

1.1. ELECTROMAGNETIC COMPATIBILITY

The theme of the Thesis is an experimental and modelling study of the coupling of electromagnetic energy into wires, which is fundamental to electromagnetic compatibility (EMC). This section briefly overviews EMC and discusses some of the areas where wires can be found in EMC situations.

1.1.1. The definition of EMC

EMC is defined by the International Electrotechnical Commission, IEC[1] as

> "The ability of a device, unit of equipment or system to function satisfactorily in its electromagnetic environment without introducing intolerable electromagnetic disturbances to anything in that environment".

There are many texts on EMC and its associated topics, however, a very good introduction and practical overview can be found in the book "EMC for Product Designers" by Williams[2] where he succinctly notes that the term EMC has two complementary aspects, namely the ability of a system (either electrical or electronic) to operate without causing any interference to other equipment, and that such systems should operate as designed in a specified electromagnetic environment. These aspects essentially imply that, although it is impossible to totally eliminate all unwanted electromagnetic interference (EMI), any piece of equipment should not cause any other piece of equipment to malfunction through extraneous electromagnetic radiation, nor should a piece of equipment fail if it is subject to EMI below a specified maximum.

Much of the impetus for EMC compliance in Europe has arisen because of the EC directive[3], to be adopted by all member states, requiring that all electrical equipment placed on the market complies with the necessary European standards (which are overviewed in reference 2). Implementation of the directive becomes mandatory in 1996. There are several methods of demonstrating compliance[4], these are:

self certification, where the manufacturer declares conformance.

a technical construction file which can be presented to a competent body who will review it and issue a certificate, should the equipment be suitable.

equipment tested and certified by an independent test house.

It was noted in the Atkins report[5] that demand for facilities, to test for compliance, would exceed available capacity, both at start-up and subsequently. This would have a deleterious effect on product launches, and hence investment would be required in both test facilities and personnel.

The reliance on prototype, and pre-prototype, testing can lead to revenue loss through lost sales. This may come about because of an excessive time in the design-test-redesign loop, or, if the non-compliance of some equipment can be demonstrated (by a competitor, for example), the manufacturer will be required to remove that equipment from the market.

There are three components to an EMC problem, namely a source of interference, a propagation channel (which may be either radiated or conducted) and a coupling mechanism by which the extraneous signal affects the victim equipment. Where radiated emissions and susceptibility are considered, the source and victim equipment will involve wires and wire-like structures.

It can be seen that it is important to understand the mechanisms by which the EMI is generated and the mechanisms by which it interferes in order to minimise both.

There are essentially four main methods of gaining such understanding:

analytical methods requiring the direct solution of Maxwell's, and associated, equations for a given system.

extrapolation, which requires that the knowledge gained for one piece of equipment is extended to a new piece of equipment.

measurement, which requires that the equipment is built and tested according to the required standards.

numerical modelling requiring computer based numerical tools which allow systems to be analyzed in a relatively straightforward manner.

Of these, the first provides highly reliable results for simple situations. As the complexity of the problem increases, so the difficulties in implementing analytical solutions increase - rapidly becoming insurmountable. The extrapolation method is a key method of design such that the EMC designer's experience is heavily drawn upon and his "feel" for the situation, and hence judgement, is the single most important factor. There are many situations when this approach is of great benefit, especially in circuit design. However, it should be noted that even small changes to a design can completely change the electromagnetic behaviour of a piece of equipment. Measurements, although the most tangible of the methods, can be costly and time consuming, particularly in a commercial environment, if several modifications need to be made to a design. Numerical modelling offers the benefits of the analytical methods without the drawbacks of either extrapolation or measurements. To date, the applications of numerical modelling have been limited, this is partially due to the computer memory and run time requirements for large problems and partially the lack of integrated CAD packages using modelling methods required for widespread use in Industry. The natural resistance of potential users to something which, to them, is new and unproved is also a factor limiting the industrial use of modelling. This will probably change over a period of time as more experimental verification is provided, to which the practical EMC engineer can relate, computer resources are improved and more efficient, easy to use, algorithms are developed.

1.1.2. Wires in EMC

The occurrence of wires, or other conductors, whose main purpose is signal or power transfer, is fundamental to EMC problems. Wires may occur singly or as wire looms and bundles, such as control wires for various vehicles. Other conductors may occur as tracks on circuit boards. An interesting review of printed circuit board EMC, which is a separate subject area and not considered specifically here, has been recently been undertaken[6]. Further, wires may exist just as signal carriers such as in telecommunications applications.

Unintentional 'wires', such as support spars or electrical ducting, may also be problematical when treated as EMC components. It is probable that the methodologies used to study wires can also be applied to treat a number of other structures, such as an aircraft fuselage whose diameter is smaller than its length.

It can be seen that the study of coupling to and from wires, or similar conducting structures, is fundamental to EMC and is one of the major areas of interest for general EMC applications.

1.2. NUMERICAL MODELLING

It was remarked that numerical modelling can be a valuable tool for the EMC engineer. Transmission-Line Modelling (TLM)[7,8] was chosen as the modelling tool for the studies described in this Thesis. Chapter 2 will describe the TLM method, as it pertains to the simulations undertaken later in this Thesis, and note some of the main features of several of the other major modelling methods.

However, it is helpful at this stage to briefly describe the basis of numerical modelling and the justification for using TLM in this work.

1.2.1. The basis of numerical modelling

Numerical modelling is used primarily as a means of determining the behaviour of a physical system without the need to actually build it. A physical study of a system may either be impractical or impossible due to cost or size limitations, or where measurements are required which can not be obtained experimentally without 'loading' the system in some way due to the presence of the measuring device.

In the case of electromagnetics, the behaviour of most systems can be described by the relevant differential or integral equations. However, it is unusual to have a system which can be described effectively by a set of equations which can be solved directly: the systems are usually too complex for this to occur. It is more usual to discretise the equations in time or frequency, and in space. Each element of the problem is described by the governing equations, the parameters of which may differ slightly from those of its neighbouring (in time, frequency and/or space) elements. These equations can then be solved, usually using a computer, and the result of the first solution of the equations is used to seed the second-pass solution, and so on. Some methods require such an iterative solution so that the answer converges to a steady state whereas others model the system dynamically. In general, frequency domain methods converge to a steady state and time domain methods give a dynamic model of the system behaviour.

Some of the more widely used methods in EMC studies are Finite Element, Finite Difference, Finite Difference - Time Domain, Method of Moments and Transmission-Line Modelling (TLM). These will be briefly described in §2.1.

1.2.2. TLM in EMC modelling

As will be seen in §2.2. and §2.3. TLM possesses a number of features which suit it to the modelling of EMC systems[9]. Some of these are listed here without discussion (they will be discussed further in Chapter 2):

all six field components can be determined at the same point in space.

it is inherently stable.

the controlling algorithm is straightforward and it is a conceptually simple method.

it is a time domain method.

wires can be included using one of a number of methods depending on the problem to be solved.

variable meshing techniques permit the use of small features in a large work-space.

material properties are easy to alter from the free-space values.

For this project, a method of modelling wires in which they are incorporated directly into the model using reflective boundaries to represent the metal surface of the wire (the integrated solution method) was favoured due to its flexibility and ease of visualisation. However, when restricting the cross-section to one node (for reasons described in §3.2.), an error manifesting itself as a reduction in the resonances was observed[10], this is referred to as 'resonance error'. The resonance error affects the wire resonances, the resonances of any cavities present are not subject to it. This error is investigated in Chapter 3, its cause is determined and a solution is proposed for it.

1.3. VERIFICATION EXPERIMENTS

In general, out of the several hundred journal and conference papers on TLM there are relatively few which relate to experimental verification. Thus, a main motivation for this work was to verify TLM experimentally and, more specifically, to verify TLM for the modelling of systems involving the coupling of electromagnetic waves into wires.

There were two mutually supportive parts to the work undertaken and described in this Thesis. The experimental part investigated the accuracy and repeatability of measurements undertaken in a screened room and an enclosed cavity. The modelling part simulated the same structures used in the measurements. The common thread was that the experimental results were used as verification tests for the TLM. The validation of TLM included not only its use as a means of studying coupling into wires but also the validation of the multigrid method[11], aperture models and the modelling of complex cavities. The rest of this section will describe the rationale for using experimental results for verification of numerical modelling tools and will overview the systems used in the study.

1.3.1. The rationale for experimental verification

For any tool to achieve widespread use its fitness for purpose needs to be demonstrated. In the case of tools required for the study of physically realisable systems, verification against results from physical systems is of significance because it imparts confidence in the numerical results. Analytical comparisons

are only of limited use because of the restrictions which would be imposed by the fact that analytical approaches become rapidly intractable as the complexity of the system being studied increases.

Whereas analytical solutions, in the absence of simplifying assumptions, can potentially provide results of a high certainty, the results of experiments, especially those inside screened enclosures, have a high initial uncertainty. Thus, a substantial amount of work has been directed to minimising those uncertainties.

1.3.2. Systems studied

Two structures form the basis of the experiments undertaken in this work; these were a screened room and a smaller screened enclosure with apertures of various sizes in one of the walls[12] leading to free space.

More generally, the (reverberating) screened room is one of a number of EMC test facilities[13], the others including anechoic chambers, open area test sites, TEM cells and GTEM cells[14]. The open area test site is often regarded as the better facility for EMC-type measurements[15] due to the relative unlimited size of the equipment under test and the absence of resonances, although there may be problems of high ambient radiation levels. Often, other test facilities, such as the TEM/GTEM cells try to emulate this performance.

The screened room has the benefit over the open area test site of cost (one to two orders of magnitude less). However, when being used at frequencies up to approximately 30 MHz the inherent uncertainty in the results is generally below 3 dB if care and appropriate correction is used, this figure rises to up to 40 dB at radio frequencies[16]. Hence, verification tests involving radiation in a screened enclosure at high frequencies must ensure that there is very little uncertainty about

the results. Potential problematic areas need to be investigated and unknowns eliminated.

The smaller enclosure, containing one or more apertures, can be used to represent several practical configurations such as equipment cabinets with apertures for input/output devices, and simplified scaled versions of aircraft and terrestrial vehicles with windows.

A high correlation between simulation results and experimental results has been obtained, indicating that uncertainties in the measurements have been largely eliminated. Also, it indicates that the method used for the simulations is correct.

1.4. OUTLINE OF THESIS

The remainder of this Thesis is organised as follows:

Chapter 2 describes numerical modelling in electromagnetics including an overview of the Transmission-Line Modelling method.

Chapter 3 investigates the resonance error: its cause and a method for its minimisation.

Chapter 4 describes the development of the experimental verification tests.

Chapter 5 describes the experimental configurations and the TLM models used in the verification tests.

Chapter 6 presents the results of the verification tests.

Chapter 7 discusses the results and other points regarding the Thesis and the conclusions drawn from this work.

Chapter 8 gives the publications referenced in this Thesis and those arising from the work reported.

CHAPTER TWO
NUMERICAL MODELLING AND TLM

This chapter discusses the reasons for TLM being chosen for modelling the coupling of electromagnetic waves into wires. It presents a brief discussion of some of the more common numerical methods before considering in detail the features of TLM which suit it to EMC problems. Finally, a discussion of wire modelling using TLM is presented.

2.1. NUMERICAL MODELLING IN ELECTROMAGNETICS

Chapter 1 stated that significant benefits could be enjoyed by using numerical modelling tools for the study of EMC phenomena because only relatively simple systems can be solved analytically[17] and experimental studies are not always feasible. This section describes some of the more common numerical modelling methods used in electromagnetic simulation. There are a number of methods which are regularly applied to various problems[18-22] and it would be unrealistic to try to describe them all fully here, hence, a only a brief overview is given.

It is possible to categorise numerical modelling methods in many ways, however, it is usual to choose two particular classification schemes. Firstly, the model may

be either a differential or integral method. Secondly, the method may be time domain or frequency domain, depending on whether the results of the model are at a single frequency or whether it produces output with incremental time.

2.1.1. Finite Element (FE)

This method was originated from the study of mechanical problems[23], such as the mechanical resonances of bridges. However, more recently it has found uses in electromagnetic applications[24]. The method works by assuming that a complex problem can be approximated by reducing it to a set of smaller structures, or finite elements. The complex function governing the behaviour of the overall structure is simplified over each one of these elements. This is normally a frequency domain, integral method, although time domain schemes exist[25]. Inhomogeneities are easily included. It is also possible to account for irregular and arbitrary shapes by choosing the most appropriate geometries for the elements: it is usual to use triangular or square geometries, although other geometries have been studied[26].

A major drawback, and an active area of research, is the difficulty of data preparation because of the flexibility of the element shapes[27]. Also, open-boundary problems, such as a dipole in free-space, require that the mesh is truncated to approximate to a boundary at infinity due to computer memory and run-time limits.

2.1.2. Finite Difference (FD)

This method often, but not always, employs rectangular elements in a regular mesh. The resulting system of equations is sparse in comparison with FE, and is thus often regarded as being easier to program[28]. FD is a differential, frequency domain, method. It discretises space and iteratively determines the values of the fields at the mesh points which satisfies the governing differential equations. However, it should be noted that once the matrix equations have been set up, standard matrix methods can be used to determine the required eigenvalues and eigenvectors. Although, it is a straight-forward method, curved boundaries can not be handled as easily as with FE. Open boundaries need to be truncated in a similar way to FE.

2.1.3. Method of Moments

This class of models was developed in the 1960s[29]. The principle of the method is the solution of linear partial differential equations of the form

$$\textit{Operator (unknown function)} = \textit{known function} \qquad (2.1)$$

where the operator and the function to the right of the equation are known. The unknown function is to be determined. An example of such a form is Poisson's equation:

$$\nabla^2\Phi = -\frac{\rho}{\epsilon} \qquad (2.2)$$

The solution is obtained by solving the matrix equation resulting from the introduction of a finite set of basis functions to represent the unknown.

The method of moments may be used to solve both differential and integral equation systems.

2.1.4. Finite Difference - Time Domain (FD-TD)

This scheme, first proposed in the mid 1960s[30], was not widely applied to electromagnetic problems for about a decade[31].

FD-TD discretises the time dependent Maxwell's curl equations in time and space. Most applications employ rectangular grids, although other meshes can be used[32].

The standard method works by interleaving two grids, one giving the electric fields and the other the magnetic fields. A central difference algorithm is applied to the cells in the meshes, the electric field grid being used to determine the magnetic field and *vice versa*.

The calculations are straightforward and computer implementation is relatively simple. Being a time domain method, frequency domain data is easily determined by Fourier transforming the output from an impulse excitation. The drawbacks of this method are that open boundaries can not be modelled directly and require that the mesh is truncated, and the electric and magnetic fields are distributed throughout the cells and are not localised at one point, thus leading to potential ambiguities in the precise location of boundaries and excitation.

2.1.5. Transmission-Line Modelling (TLM)

There are many parallels between TLM and FD-TD[33-35]. However, whilst FD-TD is a direct discretization of Maxwell's curl equations in time and space, TLM is analogous with Huygens's principle of wave propagation, which is used to determine the electric and magnetic fields. Both space and time are discretised, blocks of space form nodes and time is discretised to allow the dynamic propagation of pulses to be accomplished on a computer. TLM gives all six fields at the centre of the node and also between the nodes, thus requiring a larger storage than FD-TD during the simulations. The calculations are, however, very straightforward.

TLM suffers, like FD-TD, FD and FE, from requiring the truncation of the mesh to model infinite boundaries.

Since a TLM model is effectively a passive network, stability is unconditional on the initial conditions and the structure of the modelled work-space.

TLM was chosen for the studies described in this thesis because of it being a time domain method (thus giving the flexibility for obtaining results over a wide frequency range using a Fourier Transform) and the ease with which simulations can be visualised. A more detailed description is given in §2.2.

A further weighting given to the selection of TLM was the significant amount of background knowledge available on TLM within the Numerical Modelling Group of the Department of Electrical and Electronic Engineering at Nottingham University.

2.2. ELECTROMAGNETIC MODELLING USING TLM

In this section the Transmission-Line Modelling method is described in more detail than in §2.1.5. It is impractical to consider all aspects of electromagnetic modelling using TLM here, but many of the main aspects of the method will be described. The fundamentals of the method will be described in §2.2.1. with §2.2.2. describing the two main variable meshing techniques. The main strengths of TLM over other numerical modelling methods will be outlined in §2.2.3.

2.2.1. TLM Fundamentals

Huygens[36] proposed that a wavefront was constructed from the superposition of smaller secondary wavefronts, the envelope of which caused the construction of further wave fronts. Due to the digital nature of modern computers, the implementation of a model based on such a principle requires discretisation of both time and space. The level of discretisation is such that the elemental units Δl, the elemental unit of length, and Δt, the elemental unit of time, be related by the expression:

$$\frac{\Delta l}{\Delta t} = v \qquad (2.3)$$

where v is the velocity of propagation for the wave system under investigation. For example electromagnetic propagation would require that[37]

$$\frac{\Delta l}{\Delta t} = kc \qquad (2.4)$$

where c is the speed of light in free space and k is a constant dependent on the structure of the node and the material properties of the problem space (for the symmetrical condensed node, described later, k = 2).

The computer based simulation of electromagnetic field problems using models of electrical networks, which were first described in the 1940s[38,39], was first proposed in 1971[7]. A two dimensional network of intersecting (ideal) transmission lines was solved and the solution compared with a two dimensional solution of Maxwell's curl equations. An equivalence was observed. This equivalence was then used to enable the modelling of electromagnetic problems, such as the solution of waveguide problems[40-44].

The extension from two to three space dimensions was made by the mid 1970s[45]. This expanded node structure comprised six 2D nodes (three series and three shunt nodes). It was later simplified into the condensed node[46], which overcame some of the problems of spacial separation of different field types and polarizations, and the placement of boundaries. The symmetrical condensed node[47] overcame the disadvantages of the condensed node (more properly referred to as the condensed asymmetric node) which were that, depending on the polarization of a pulse incident on a node, the type of 2D node first encountered was different, either series or shunt nodes; also, the arithmetic involved was lengthy. It has also been shown that the SCN exhibits a lower dispersion than the asymmetric nodes[48-50].

The fundamental algorithm for the propagation of a pulse through the mesh is the 'scatter and connect' algorithm. This can be represented as:

$$ {}_{n}V^{r} = S_{n}V^{i} \qquad (2.5) $$

$$ {}_{n+1}V^{i} = C_{n}V^{r} $$

where V^i and V^r are the incident and reflected pulses in the entire mesh in the time period n and n+1 indicates the subsequent time period. **S** is a supermatrix of scattering matrices, each of which operates on a single node. In the case of a regular mesh of symmetrical condensed nodes (SCNs) all the elements of **S** are the same. Figure 2.1 shows a SCN, without stubs.

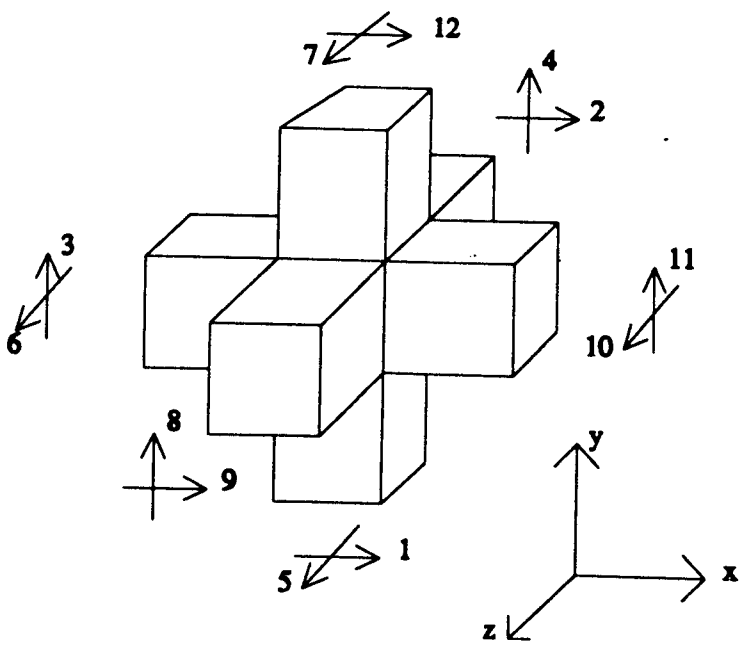

Figure 2.1 The symmetrical condensed node without stubs. The arrows correspond to the polarisation of the incident pulses and the numbers are the conventional port numbers.

The scattering matrix S representing its behaviour is given by[47]:

$$S = \frac{1}{2}\begin{pmatrix} 0 & 1 & 1 & 0 & 0 & 0 & 0 & 0 & 1 & 0 & -1 & 0 \\ 1 & 0 & 0 & 0 & 0 & 1 & 0 & 0 & 0 & -1 & 0 & 1 \\ 1 & 0 & 0 & 1 & 0 & 0 & 0 & 1 & 0 & 0 & 0 & -1 \\ 0 & 0 & 1 & 0 & 1 & 0 & -1 & 0 & 0 & 0 & 1 & 0 \\ 0 & 0 & 0 & 1 & 0 & 1 & 0 & -1 & 0 & 1 & 0 & 0 \\ 0 & 1 & 0 & 0 & 1 & 0 & 1 & 0 & -1 & 0 & 0 & 0 \\ 0 & 0 & 0 & -1 & 0 & 1 & 0 & 1 & 0 & 1 & 0 & 0 \\ 0 & 0 & 1 & 0 & -1 & 0 & 1 & 0 & 0 & 0 & 1 & 0 \\ 1 & 0 & 0 & 0 & 0 & -1 & 0 & 0 & 0 & 1 & 0 & 1 \\ 0 & -1 & 0 & 0 & 1 & 0 & 1 & 0 & 1 & 0 & 0 & 0 \\ -1 & 0 & 0 & 1 & 0 & 0 & 0 & 1 & 0 & 0 & 0 & 1 \\ 0 & 1 & -1 & 0 & 0 & 0 & 0 & 0 & 1 & 0 & 1 & 0 \end{pmatrix} \qquad (2.6)$$

2.2.2. Variable meshing techniques

Variable meshing techniques, such as hybrid variable mesh[51,52] and multigrid[53] which allow variable node sizes and regions of finer mesh size within a work-space, have alleviated the restriction that the node size in the bulk of the problem work-space is determined by the smallest feature in the whole of the model. The application of these techniques reduce the required memory, and hence increase the the size of the problem or the complexity of fine detail which can be modelled by a particular computer.

The problem of small features, such as wires, in a large volume, such as an aircraft fuselage, is frequently encountered within EMC problems. If the wire is 1 mm in diameter and the fuselage is 5 m in diameter the problems of having a node size dependent on the smallest feature can be seen to be impractical to solve on common computers. Methods to localise small nodes, for the modelling of fine features, can increase efficiency where memory or run-time is at a premium.

The two methods, graded mesh and multigrid, and regular meshing are illustrated schematically in Figure 2.2, which shows a slice through hypothetical work-

spaces.

Figure 2.2(a) shows a regular mesh, here Δl is constant for every node throughout the work-space: features need to be described relative to Δl. Figure 2.2(b) shows a graded mesh scheme, here the nodes are best visualised as slabs, each of a constant height, but the height may vary from slab to slab. Figure 2.2(c) shows the multigrid method. In this case, the smaller nodes are localised within a region of the work-space.

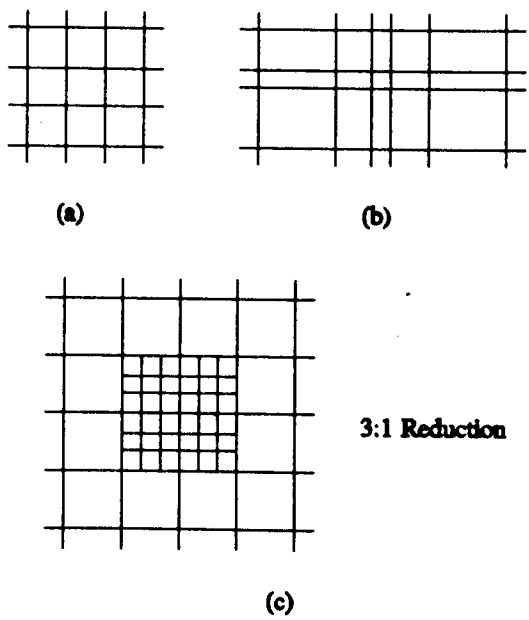

Figure 2.2 Different meshing schemes: (a) regular mesh, (b) graded mesh and (c) multigrid.

The basic method of operation for the graded mesh scheme is that extra inductance and capacitance is added to the node either by stubs or by altering the inductance of the link-lines and adding extra capacitive stubs to ensure synchronism of the pulses (the latter is referred to as the hybrid method). The important consideration for graded mesh schemes is that all pulses should reach a node and scatter from it together.

The multigrid method, being a regular mesh within a regular mesh, requires that signals are passed to and from the fine mesh region at the correct rate (for both meshes). Other considerations include the conservation of charge and flux at the interface between the two meshes.

The graded mesh is also particularly useful for implementing non-rectangular meshes, e.g. cylindrical, spherical or general curvilinear coordinates[54,55]. Cylindrical coordinates have been used in this Thesis for some of the investigations into wire resonance error problems.

2.2.3. Strengths of TLM

The main strengths of TLM over other modelling methods for studying the coupling of electromagnetic waves into wires are:

it models all six electromagnetic field components directly and located at the same point in space, unlike standard FD-TD which displaces the electric and magnetic fields. This means that there are no problems with the placement of the boundaries and the choice of the most appropriate field components to excite the system and obtain the output, i.e. either at nodes or between nodes.

it is inherently stable due to the analogy with the solution of passive RLC circuits. This analogy also makes TLM more easily visualised by users unfamiliar with the theoretical basis of the method.

it relies on a straightforward, simple, algorithm, with a high degree of latent parallelism, suiting it to implementation on digital computers or parallel processing engines. Although the governing procedure is the Scatter and Connect algorithm, the matrices can be simplified to discrete

operations[11,56,57].

it is a time domain method and hence frequency domain data can be obtained from a single time domain simulation. Also, being a time domain method, a dynamic, or transient, analysis of a structure is readily obtained.

it exhibits a lower dispersion than FD-TD[49] which means that larger, and hence fewer, nodes can be used for a given maximum frequency of operation.

Some interesting and potentially very useful recent advances in TLM are:

a method of modelling free-space boundaries has been presented[58] which used the angle of waves incident on a truncated free-space boundary to improve its behaviour. The modelling of open boundaries has also been enhanced by the 'Johns matrix' technique[59].

the removal of the restriction on the work-space that it must be an exact multiple (or half multiple) of the node dimensions has been proposed[60].

the operation of TLM with reverse time in order to determine the structure of a device or system based on its required frequency response[61,62].

2.3. THE MODELLING OF WIRES IN TLM

The importance of wires in EMC problems was discussed in §1.1.2. This section is concerned with the methods of describing wires in TLM.

The modelling of wires is often implemented by using short circuit nodes. These are symmetrical condensed nodes with the scattering matrix

$$\mathbf{S} = -\mathbf{I} \tag{2.7}$$

Alternatively, wires may be modelled by using shorted link-lines adjacent to the conducting boundary such that all the energy transmitted along a link line is returned with a 180° phase shift in the following time period. This method, where the wires are explicitly included in the model, is referred to as the integrated solution method. Integrated solution methods allow the modeller easy visualisation of the structure being simulated using only a one-pass solution. Computational resource limitations mean that it is usual to apply simplifications to the TLM model: these being that the wire should be modelled by a single node cross-section and a rectangular Cartesian mesh should be used for generality. When TLM is used to obtain the resonances of a wire the result of these simplifications to the model is a shift of the resonances, by approximately 5 - 10%, to lower frequencies[10], this will be referred to as 'resonance error'.

Another method used to model wires is the separated solution[63,64] method, where the field simulation and the wire simulation (using knowledge of the fields in the vicinity of the wire) are decoupled. The process of implementing a separated solution method is to simulate the structure under study and extract information about the fields local to the wire(s). This information is then used to generate distributed current and voltage sources along the wires in a 1-D model. Separated

solutions can produce accurate results, free of resonance error effects, but they allow no, or little, interaction with the environment and are thus limited to problems where certain simplifying criteria are permissible, such as the wire must not re-radiate significantly.

A further class of solutions exist which are referred to as wire nodes[65-68]. These involve embedding a wire-like structure within, or between, nodes. Wire nodes allow the modelling of wires with a smaller diameter than the node size in which they are modelled. However, they add extra complexity to the model due to the additional node types required.

In reference 65, Naylor and Christopoulos devised the scattering matrix of a three-dimensional symmetrical condensed node which had a wire running through it. This involved the addition of 'pseudo-stubs' in order to allow propagation along a wire with a diameter less than the node size. The model of Wlodarczyk and Johns[66] adopts a slightly different approach in that the wire is placed between adjacent symmetrical condensed nodes, rather than within a node. This approach allows the SCNs to be unaltered, but requires additional features to be included in the model. Finally the models of Porti *et al*[67,68] can almost be regarded as an hybridisation of the previous two, in that they adopt an approach similar to reference 66 but place the wire inside a SCN, in the manner of reference 65, with good results.

2.4. SUMMARY

This chapter has described the basis of numerical modelling in electromagnetics and some of the more commonly used methods. In particular electromagnetic modelling using Transmission-Line Modelling (TLM) has been described and emphasis placed on the modelling of wires using TLM.

TLM was chosen as the modelling method used for the work described in this Thesis because of the attractive features it possesses for EMC modelling. Within TLM, the integrated solution method of modelling wires has been chosen for further investigation because of its generality, self-consistency and ease of visualisation. It has the advantage over the separated solution and wire node methods of requiring only the symmetrical condensed node in a one-stage solution. One limitation on its usage arises from the resonance error which reduces the apparent resonances of a wire by 5-10%. In the next chapter, the cause of this error will be determined and a method to minimise it will be proposed.

CHAPTER THREE
INVESTIGATION INTO THE CAUSE OF THE WIRE RESONANCE ERROR

This chapter describes the resonance error encountered when modelling wires using the integrated solution method in TLM. It outlines the manifestation of the problem, identifies the cause of the error and proposes a solution to the problem.

3.1. MANIFESTATION OF RESONANCE ERROR

It was noted in Chapters 1 and 2 that a potential problem area, when using the integrated solution method to model wires in TLM, was the introduction of an error in the electromagnetic resonances of the wire when described by a single node-cross section[10] (wires, in this context, are regarded as conductors whose length is much greater than their diameter). The error was manifested as a shift of the resonance features, to lower frequencies, by 5-10%. In the time domain, this was seen as a progressive drift in the results[69]. The reasons for using a single node cross-section will be explained in §3.2. However, unless corrected, the presence of this error potentially limits the accuracy of TLM simulations for EMC applications.

In general, the EMC community accepts magnitude uncertainties of several dBs. However, they require the frequency position of features to be known accurately and so the resonance error is unacceptable.

A similar problem to resonance error has been seen in 2D TLM models, where other authors have referred to it as coarseness error[70] and attributed the error to the fact that nodes diagonally adjacent to an external corner have no direct contact with the wire. The solution proposed in this case was to introduce a stub to the 2D model such that direct interaction with the corner, by the adjacent corner node, was possible.

Three-dimensional models of strip-line structures have also been the subject of previous investigations[71]. It was noted that the resonant frequency of the strip was approximately 10% below the expected value, and it was suggested that the cause of this error was poor interaction of the corner nodes diagonally adjacent to the conductor. The solution proposed was to model the strip-line with two new node types - allowing accurate modelling of the conductor itself and of the edges - which embedded the conductor within the node, as opposed to the more usual method of modelling it by shorted link-lines.

In both the above cases, the cause of the error was stated without proof. The solution to the 2D and the strip-line problems was to introduce new node-types to compensate. The purpose of this work is to develop a procedure which eliminates the cause of the problem without recourse to a two stage solution nor a new node type. The acceptance criterion placed on the model was that it was presumed that the wire was modelled correctly if the resonance error was less than 1% using a single node to model the wire.

3.2. LIMITATIONS ON WIRE MODELLING IN TLM

Before discussing the nature and investigating the cause of the resonance error, it is appropriate to note the requirements which are placed on wires modelled in TLM.

The integrated solution method has been favoured for this work because it is a one-step solution (unlike separated solution methods, which require two separate simulations, one 3D and one 1D) and because, unlike the wire node solutions, it does not require a special node type, other than the symmetrical condensed node (unlike the wire node solutions). It is also straightforward to use, in that the technique of shorting link-lines to form the wire can also be used, without modification, to form other conducting structures, such as the bench in the screened room or an aircraft fuselage thus limiting the model to one type of conducting structure.

In constructing wire models, the following requirements were kept in mind.

the model should simulate a wire accurately by using no more than one node cross-section. This requirement is based on the fact that computing resources are limited. Hence, requiring from the outset that a single wire be modelled with several nodes cross-section risks requiring excessively long run-times and large storage.

the rest of the model should be affected as little as possible by the wire model, e.g. the resonant behaviour of any enclosure in which wires are positioned, if used, and the behaviour of other features in the model, should not be dependent on the particular wire model used.

resonant effects on the wires should be modelled accurately for both radiation from, and currents induced in, the wire.

terminations, such as those used for connection to coaxial-type equipment should be modelled correctly. The wire may also have its ends adjacent to metallic planes, such as when a wire passes through a bulkhead inside a vehicle.

These requirements were also borne in mind when developing the basic test systems described in §4.2.

3.3. IDENTIFICATION OF THE CAUSE OF THE WIRE RESONANCE ERROR

This section summarises the simulations undertaken in order to identify the cause of the resonance error. It describes the TLM 'test-structure' model used for preliminary investigations, the modelling of wires using a finer mesh description of the cross-section, it investigates the effect that changing the wire length has on the error and the modelling of the wire using a TLM mesh based on cylindrical coordinates.

3.3.1. Model for preliminary investigations

In order to investigate the manifestation, cause and possible solutions, of the resonance error, a simple test structure was used for simulations, as shown in Figure 3.1. This shows a two metre long wire placed between two large parallel plates such that the ends of the wire were coincident with the plates and normal to them.

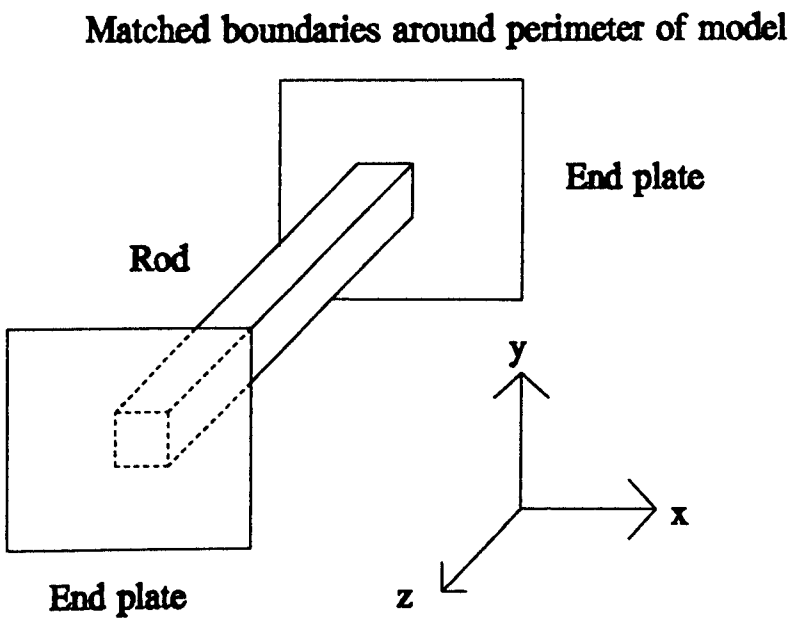

Figure 3.1 Single node cross-section wire between parallel end-plates.

In this system the resonances on the wire were enhanced by the end-plates, which also served to define the ends of the wire. The diameter of the wire was not important for determining its resonances since the plates eliminated edge fringing and any associated reduction in frequency with increasing wire diameter. This enabled meaningful comparisons to be made in cases where the number of nodes in the cross-section were changed.

The system was excited by a surface current at one end of the wire and the output was taken at a point approximately three quarters of the way along. This allowed the first four resonant frequencies to be determined: the theoretical values being 75 MHz, 150 MHz, 225 MHz and 300 MHz. In general, the fourth resonance (300 MHz) was used as the basis for error determination.

The 2m length of the wire was modelled by 20 nodes, each with a $\Delta l = 0.1$m. Based on the rule-of-thumb that the shortest wavelength of interest should not be less than $10\Delta l$, this is expected to give rise to low dispersion over the frequency range of interest.

When the structure of Figure 3.1 was modelled with no form of correction and with a single node describing the wire, a fourth resonance was obtained at 282 MHz, as opposed to the required 300 MHz, an error of 6%.

3.3.2. Finer descriptions of the wire cross-section

A first consideration given to the study of the resonance error problem was the actual description of the wire. One of the requirements placed on the integrated solution method in §3.2 was that no more than one node should be used to describe the wire cross-section. However, for the purpose of numerical investigation into the origin of the resonance error, the number of nodes describing the cross-section was increased. Figure 3.2 shows the effect, on the fourth resonance, of increasing the cross sectional area of the wire, from Δl^2 to $(8\Delta l)^2$. Clearly, there is a significant improvement as the cross-section was increased resulting in a negligible error at $(8\Delta l)^2$. The modelling of wires to such resolution is not acceptable, due to the memory and run-time implications, but it does show that the error is reduced as the number of nodes describing the wire cross-section is increased.

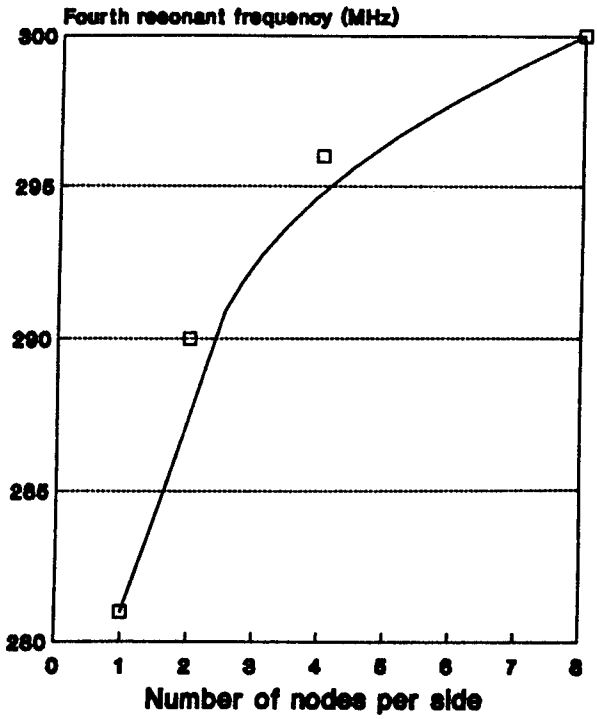

Figure 3.2 Fourth resonances of a square cross-section wire of varying nodes per side.

In order to approximate the geometry of the modelled wire cross-section to that of a cylindrical wire, a stepped approximation to the curved surface was used. Figure 3.3 shows the boundary descriptions used for two such approximations, with diameters of four and eight nodes, and Figure 3.4 compares the resulting fourth resonances with those obtained from a square wire. In this case, it can be seen that the improvement is not significant as the detail of the stepped boundary descriptions is increased. Further investigation indicated that the error depended on either, or both, of the number of nodes on a continuously flat surface per side (an increase giving a reduction in error) and the number of external corners in the cross section of the wire (an increase giving an increase in the error). The definitions used for internal and external corners are illustrated in Figure 3.5, where 'i' implies an internal corner and 'x' implies an external corner. Also,

node 'D' is the node diagonally adjacent to the external corner.

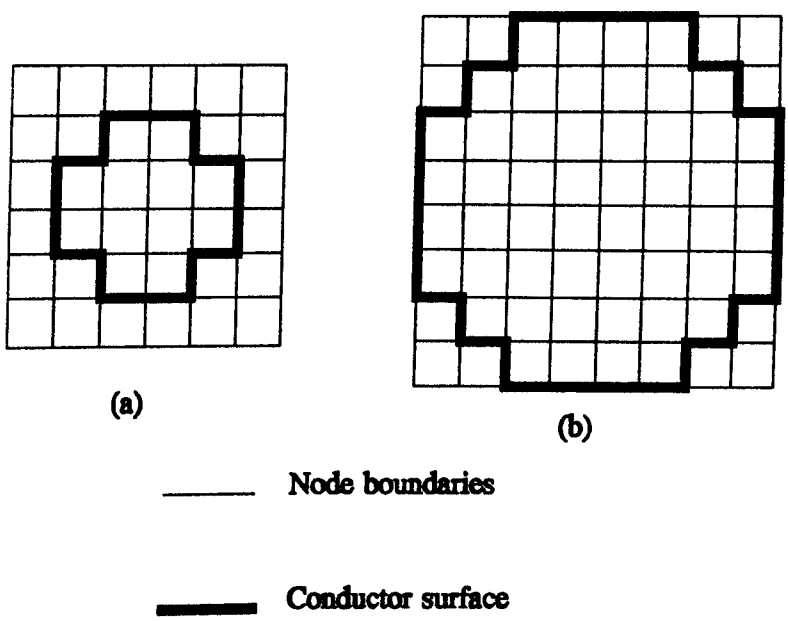

Figure 3.3 Stepped approximation to a cylindrical cross-section. (a) four nodes diameter, (b) eight nodes diameter.

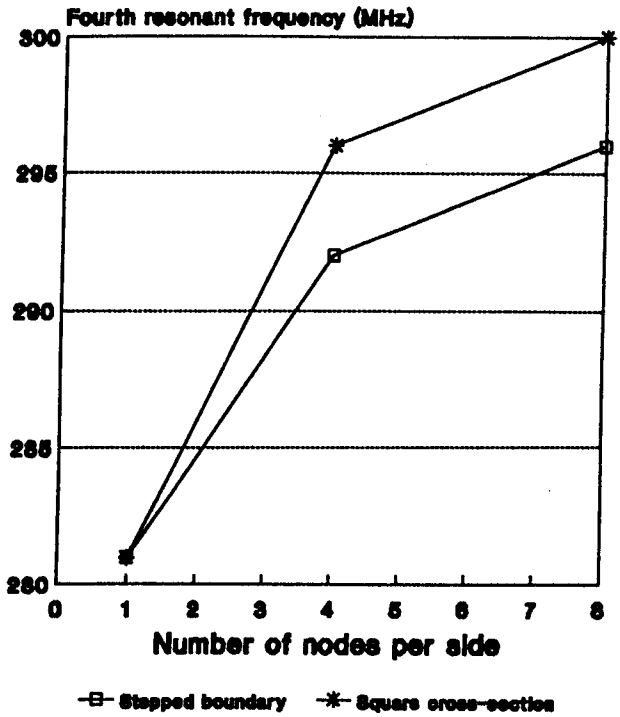

Figure 3.4 Fourth resonance frequencies for stepped and square boundary wires.

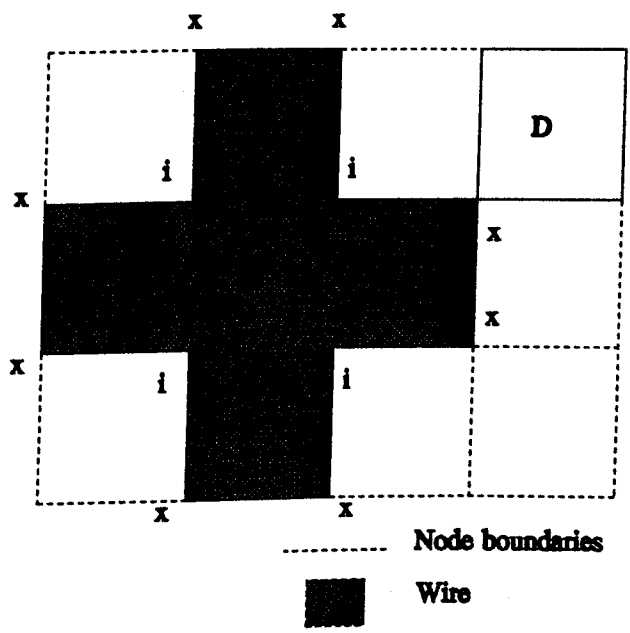

Figure 3.5 Wire corner convention.

3.3.3. Changing the description of the length of the wire

The above investigations concentrated on the cross-sectional description of the wires. A set of simulations were undertaken which kept the simulated length of the rod at 2m but changed the number of nodes, and hence the node size in this direction. The number of nodes varied between five and 50. Figure 3.6 shows the fourth resonance for various numbers of nodes.

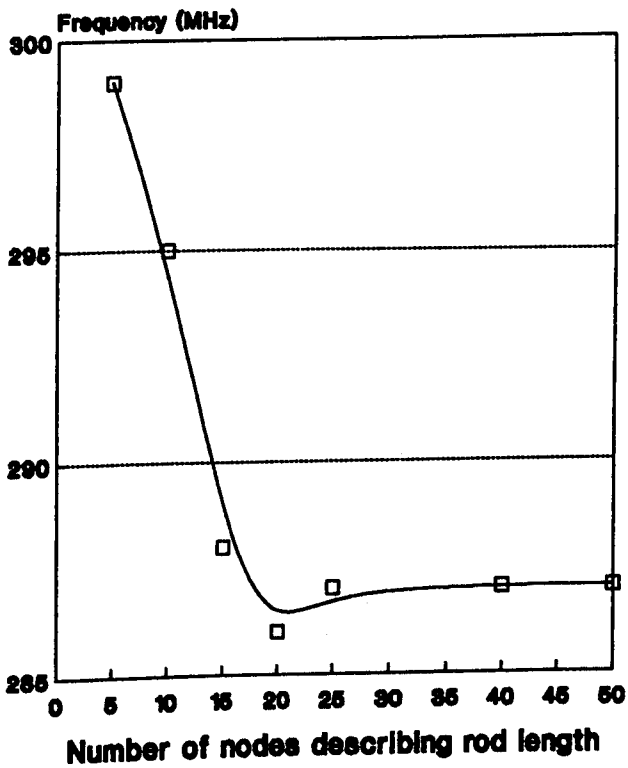

Figure 3.6 Effect of number of nodes describing the conductor length.

For lengths greater than 20 nodes, the location of the resonance remains fairly stable. Below this number, the resonant frequency increases, approaching the theoretical value of 300 MHz! However, it can not be stated that the reduction

in number of nodes improves the error, as the '10Δl' dispersion rule is being violated in this region. What is interesting is the fact that the error is stable above the 10Δl point (which occurs at 20 nodes for 300MHz) indicating that the length of the rod, in nodes, is of little or no consequence when determining the resonance error.

In a further test, the number of the nodes along the conductor length was maintained at 20, but the node sizes in the direction of the wire were changed and the resonances normalised to a 2m wire length for comparative purposes. The purpose of this study was to determine the dependence of the resonance error on the length of the nodes relative to their cross-section, i.e. on the aspect ratio of the nodes. Normalization was performed using:

$$f_{norm} = \frac{f_a f_{e2}}{f_e} \qquad 3.1$$

where f_{norm} = normalised frequency

f_a = actual resonant frequency

f_e = theoretical resonant frequency for the given length

f_{e2} = theoretical resonant frequency for 2m rod

It can be seen from Figure 3.7 that the magnitude of the resonance error is not significantly influenced by either the size or the number of nodes describing the length of the wire. The results of Figure 3.7 do show some variations but these are small and are not considered significant.

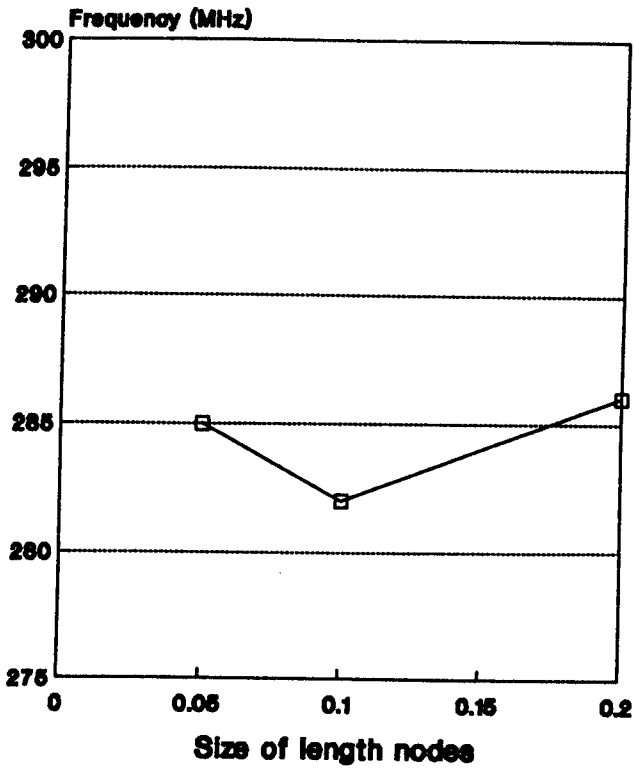

Figure 3.7 Normalised resonances for different sized nodes describing the conductor length.

3.3.4. Wire described in cylindrical coordinates

It was established in the previous sections that the cross-sectional description of the wire was of fundamental importance in determining the level of resonance error. It was found that a rectangular cross section exhibited a lower error than a corresponding stepped approximation to a curved boundary. It was also noted that the length of the wire had little effect on the error. It can be stated that the external corners, used in the description of the wires, are responsible for the error. In order to eliminate the effects of the external corners, a cylindrical version of the 2m long wire between two parallel plates model was used.

Cylindrical coordinate systems have been adequately described in[55] and will only be briefly described here. Graded mesh nodes were used whose sizes were allowed to vary in order to represent the changes in width of the cylindrical segment, as shown in Figure 3.8. The length of the corresponding link-lines were chosen to be the mean length or width of the node, as indicated. Essentially, this allowed the rectangular (x,y,z) coordinate system to be 'wrapped' round to form the (r,θ,z) cylindrical system.

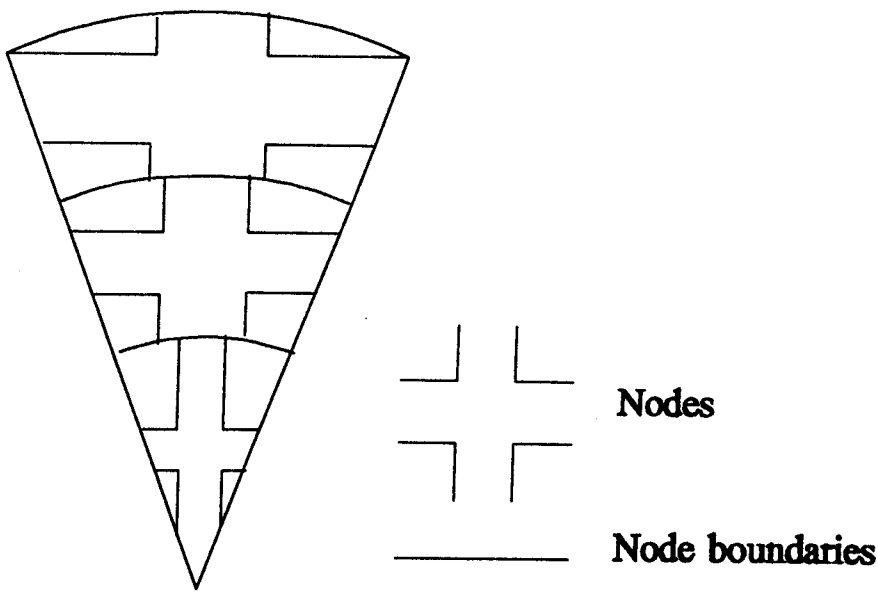

Figure 3.8 Cylindrical segment showing changes in node size.

The wire between plates system was modelled by a sector of the cylindrical system (thus exploiting the rotational symmetry of the system). Figure 3.9 shows the whole system.

Exciting the current on the rod and measuring the subsequent resonances gave frequencies which agreed with the theoretical predictions and were free from the resonance error.

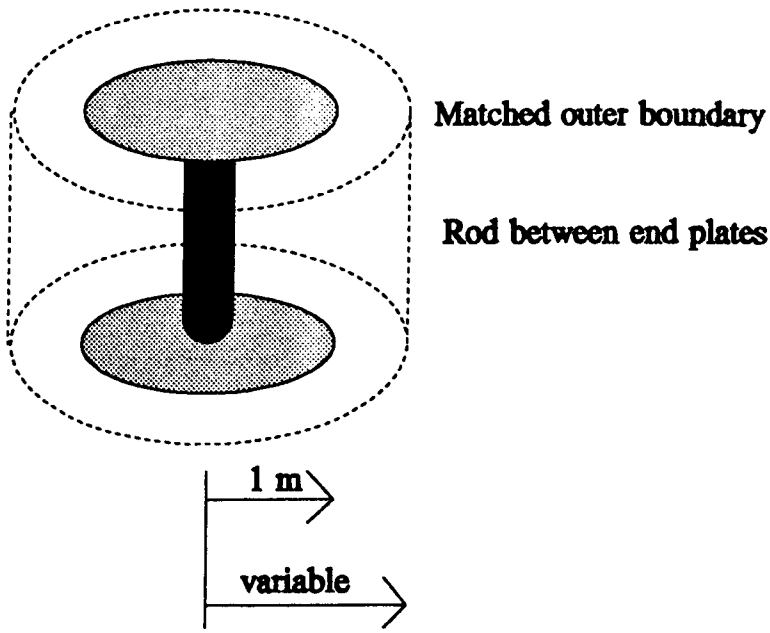

Figure 3.9 Cylindrical rod between parallel plates system.

3.3.5. Summary

The previous simulation studies have indicated that the cause of the resonance error is the external corner nodes delaying signals propagating around the circumference of the wire. The length of the conductor does not appear to have any effect on the degree of error (providing that the ten nodes per wavelength rule is observed). Changing the structure of the cross-section of the wire from a square to a stepped approximation to a curved boundary makes the relative error worse. The elimination of external corners by the transformation of the test structure to a cylindrical coordinate system eliminates the error.

The next sections will analyze the behaviour of the corner nodes and the pulse propagation around the corners and will propose a new method of modelling wires which reduces the error substantially.

3.4. THE ROOT OF THE RESONANCE ERROR AND A PROCEDURE FOR ITS MINIMIZATION

The nodes diagonally adjacent to the wire were identified as the source of the resonance error §3.3.

This section describes the cause of the error and a method by which it can be minimized.

3.4.1. The cause of the resonance error

In the TLM model of wires, pulses propagating around the circumference of the wire are used to support the current flowing in the wire. A more detailed analysis can be considered from Figure 3.10. Figure 3.10(a) shows the actual path taken by a TLM pulse as it travels around the corner. Distance AB is the path from the centre of the node to the adjacent node along the link line. Path BCD is the passage of the pulse through the diagonally adjacent corner node and path DE is the path to the centre of the next node. It will be noted that the distance from the section BCD to the corner of the wire is not constant, it increases from B→C and decreases from C→D.

The desired path is one where the distance of the propagating pulse to the wire remains constant (Figure 3.10(b)). This implies that the desired path at the corner node is a quarter-circle as shown by path GH. Thus, electromagnetically, the system being modelled is not equivalent to the physical system. In fact the path length ABCDE is greater than the path length FGHI and this will cause an apparent delay in the propagation of the TLM pulses around the wire in the

model. This delay is the origin of the resonance error.

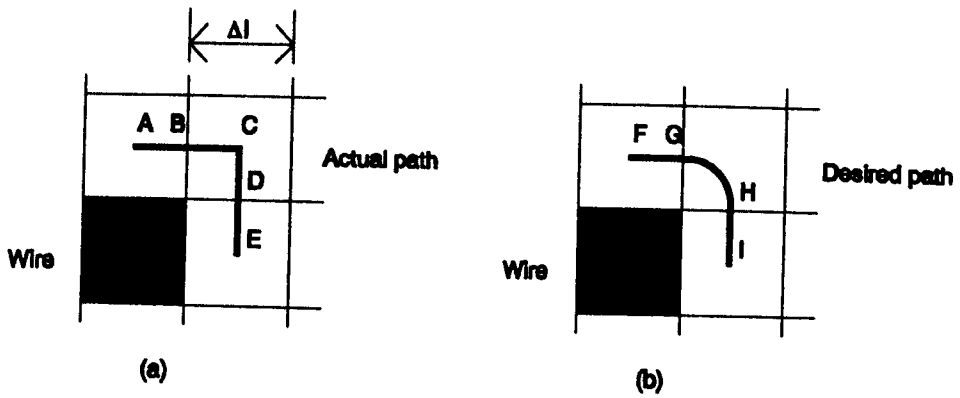

Figure 3.10 (a) actual path and (b) desired path around wire.

It is feasible to modify the structure of the corner node so as to correct for this error by reducing the distance the pulse travels, i.e. reduce the path length from that of path ABCDE to that of FGHI. The alternative method of producing the same result is to keep the propagation distance, i.e. the physical node size and shape, unaltered, but to increase the speed of propagation through the corner node so that it appears to have the desired path length. This method requires no new node type and will be described in §3.4.2.

3.4.2. Minimization of the resonance error

The method of increasing the velocity in the nodes around the conductor mentioned in the previous section can be implemented by reducing the relative background permittivity and permeability to less than one in the immediate vicinity of the wire, hence, increasing the velocity of pulse propagation around the wire. This can be realised in TLM by reducing the base time-step, Δt, and adding stubs to compensate for this reduction everywhere else. This approach eliminates the potential problems associated with introducing negative admittance stubs in the region adjacent to the wire.

The modified permittivity and permeability values were determined as follows. The actual path distance ABCDE in the TLM model is, from Figure 3.10:

$$(Actual\ length)_{ABCDE} = 4\frac{\Delta l}{2} \qquad (3.2)$$

The required path distance, FGHI, is

$$(Desired\ length)_{FGHI} = \frac{\Delta l}{2} + \frac{\pi}{2}\frac{\Delta l}{2} + \frac{\Delta l}{2} \qquad (3.3)$$

Thus, the velocity of propagation in the circumferential direction must be increased by a factor w, where

$$w = \frac{2\Delta l}{\Delta l + \frac{\pi \Delta l}{4}} = \frac{8}{4 + \pi} \approx 1.1 \qquad (3.4)$$

A further point which needs to be accounted for is that although the required velocity is wc, c being the speed of light, an incoming electromagnetic wave should experience no change of impedance as it approaches the wire. Thus, to implement the change in velocity, the relative permittivity and permeability are divided by w such that the following relationships hold:

$$v = \frac{1}{\sqrt{(\frac{\epsilon_r}{w})\epsilon_0 (\frac{\mu_r}{w})\mu_0}} = \frac{wc}{\sqrt{\epsilon_r \mu_r}} \qquad (3.5)$$

$$Z = \sqrt{\frac{(\frac{\mu_r}{w})\mu_0}{(\frac{\epsilon_r}{w})\epsilon_0}} = \eta\sqrt{\frac{\mu_r}{\epsilon_r}} \qquad (3.6)$$

where Z is the impedance of the medium and η is the impedance of free space. Thus, if $\varepsilon_r = \mu_r = 1$, as it will be in general for the problems discussed in this Thesis, the requirements described above will be met.

As the error is introduced by the corner nodes, it is also possible to apply a correction to these nodes only. Consider the actual path BCD in Figure 3.10. This is required to behave as desired path GH. Using a similar reasoning to above, the actual path is

$$(Actual\ length)_{BCD} = 2\frac{\Delta l}{2} \qquad (3.7)$$

whereas the desired path is

hence, in this case the required correction factor, w_c, is

$$(Desired\ length)_{GH} = \frac{\pi}{2}\frac{\Delta l}{2} \tag{3.8}$$

$$w_c = \frac{\Delta l}{\frac{\pi}{4}\Delta l} = \frac{4}{\pi} \approx 1.3 \tag{3.9}$$

which is to be applied only to the external corner nodes (the subscript 'c' indicating corner node correction).

The wire between plates simulations were re-run using the correction factors described above. The method of implementing the solution was to embed the wire in an isotropic region of reduced permittivity and permeability, which extended one node around the wire. An isotropic reduction of these parameters, such that the x, y and z directions were equally affected, was used because it eased data preparation.

The one node cross-section wire was embedded in a region where the local reduction of $\varepsilon_r = \mu_r = 1/w \approx 0.9$. This was found to give resonances as expected theoretically. Corner correction, i.e. correction only applied to the offending adjacent corner nodes, was applied with the local reduction $\varepsilon_r = \mu_r = 1/w_c \approx 0.8$, again resulting in resonances of the wire in agreement with those predicted from theory.

It was stated above that the corrections were implemented by isotropically changing the local material properties. In order to determine whether the improvement in resonance was due to the cross-sectional correction or whether the correction was due to a simple increase in velocity along the wire (an unacceptable 'fix'), the circumferential and longitudinal components were decoupled such that modification of the material properties was only undertaken longitudinally or in the plane of the cross-section without altering the properties in the other direction. It was found that no change in the location of the

resonances was observed for longitudinal correction only. However, the correct resonances were observed for the circumferential correction only, thus indicating the correctness of the identification of the source of the error, and its solution described previously.

Procedurally, the method of reducing the relative material properties around the wire is to determine the minimum time-step based on those values of permittivity and permeability and then decrease the velocity of propagation through the nodes everywhere else except around the wire by the addition of stubs. However, this requires extra memory and increased run time but does allow standard symmetrical condensed nodes to be used in the solution without additional node types and without recourse to a two-stage solution.

3.5. SUMMARY

This chapter has investigated the resonance error problem and a solution for it. It has shown that the error is attributable to the corner nodes diagonally adjacent to the wires. A method of minimising this error was developed and the preliminary results for a simple test structure were very encouraging and point to a workable solution. Results obtained using this method for more general EMC configurations incorporating wires are given in Chapter 6 where the general applicability of this approach is explored further.

CHAPTER FOUR
MEASURING ELECTROMAGNETIC COUPLING IN A SCREENED ROOM AND IN A CAVITY

This chapter describes investigations made into those factors affecting the accuracy and repeatability of coupling measurements in a screened room and an enclosed cavity, these measurements form the basis for subsequent experimental validation of TLM simulations. The first section in this chapter discusses the rationale behind the tests developed. The rest of the chapter is directed towards the basic study of the basic configurations adopted. The actual configurations used in the validation tests are reported in Chapter 5.

4.1. INTRODUCTION TO VERIFICATION TESTS

It is important that any new tool is tested to determine its fitness for purpose. This enables the tool's designer to change or hone the design as required and it also allows the end user to have a certain amount of confidence that the tool they are using will perform in the way they expect. In terms of numerical modelling tools, it is important that the verification tests reflect 'typical' usage. EMC modelling is an area in which there are a wide range of potential applications and it would be naïve to state that the results for a single set of tests give full

confidence in the application of the model under all circumstances. However, it is required that tests are developed which give a high confidence to the user for a specific sub-set of applications. This Thesis addresses the coupling of electromagnetic waves into wires in screened or partially screened enclosures, hence the main elements of such systems need to be included in the verification tests. An EMC problem can be considered as having three component parts, as illustrated in a simple graphical form in Figure 4.1. These parts are a source of interference signal, a propagation channel from source to victim and a means of coupling into the victim equipment. Here, the concern is only for radiated coupling paths. The validation tests should, where possible, be self contained, comprising:

a source of radiation, such as a half wavelength dipole or a travelling wave type antenna.

a propagation path between the source and the victim.

a victim equipment, or other conducting structure into which electromagnetic coupling can take place.

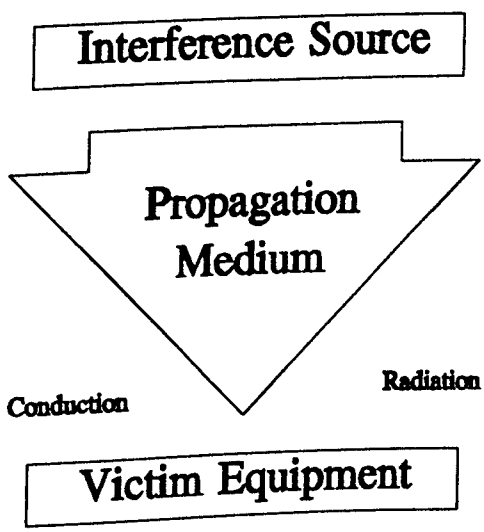

Figure 4.1 The EMC problem.

Further points which have been incorporated in the test structures used, as they increase the confidence in the subsequent comparisons, are:

near field interaction, which are notoriously difficult to predict because of the r^{-2} and r^{-3} terms (r being the distance from the source). This has been included for the purposes of validating models as it can occur in practical problems. (It should be noted that far-field predictions using TLM would depend on the ability to model free-space boundaries and the size of the computer memory to allow the model to be undertaken.)

system connections, such as 50Ω coaxial connections, which are used for exciting the system or for obtaining output values from the system have been included to allow the representation of practical systems.

wires with a much smaller diameter than their length. These are generally required to be modelled for EMC purposes.

wires placed close and parallel to a conducting surface.

Two environments were chosen for further study, these are shown in Figures 4.2 and 4.3. The first is the coupling between conductors in a screened room and the other is a small conducting enclosure with an internal wire. Both avoid uncertainties introduced by 'free-space' measurements, namely the effect of ambient radiation levels on the comparisons. Thus, both are ideal systems to be used for validation tests. Also, both systems represent self-contained EMC problems since both contain sources of interference, a coupling mechanism into the victim and a propagation path. In the case of the screened room, the source is the dipole, the victim is represented by the rod above the conducting bench and the propagation path is within the screened room itself. The conducting enclosure is slightly different, in that there is only a single conductor. The EMC problem here is the determination of the effects of the enclosure on the signal flowing along the wire.

The actual configurations used and the practical considerations for performing experiments on such systems are discussed in §4.2.

4.2. ENVIRONMENTS INVESTIGATED

This section describes the basic configurations of the two test structures and the basic measurement procedures.

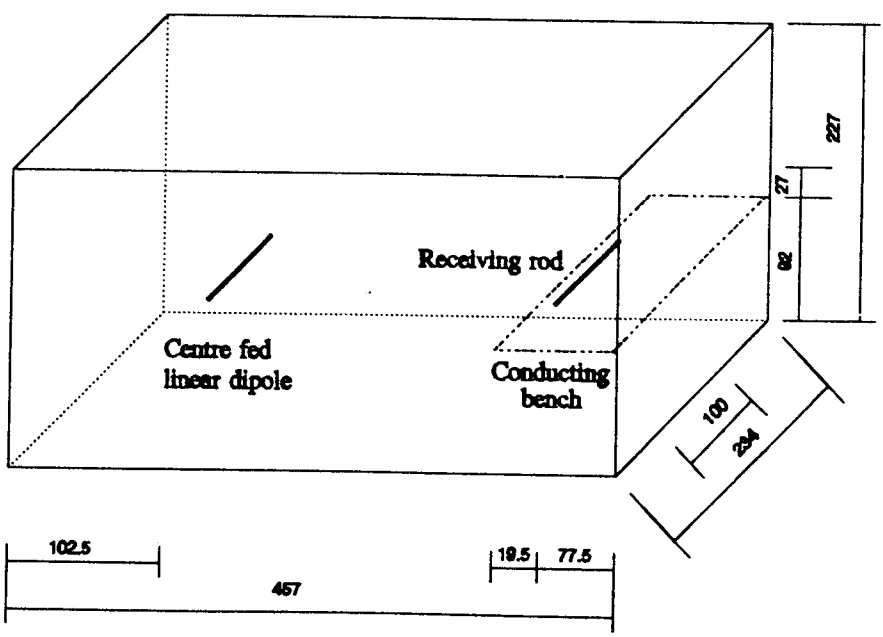

Figure 4.2 Screened room configuration. All dimensions are in cm.

In the screened room of Figure 4.2 the source dipole is centre fed and is connected to port 1 of a Hewlett-Packard vector network analyzer, model 8510B. Output was taken using a current probe (Eaton, model 94111-1) connected to port 2 of the network analyzer. The measurement taken was the S_{21} (system thru')

parameter[72,73]. The positions at which the output were taken were the midpoint of the receiving rod and 10 cm from the feed-point of the dipole along one or both of the arms.

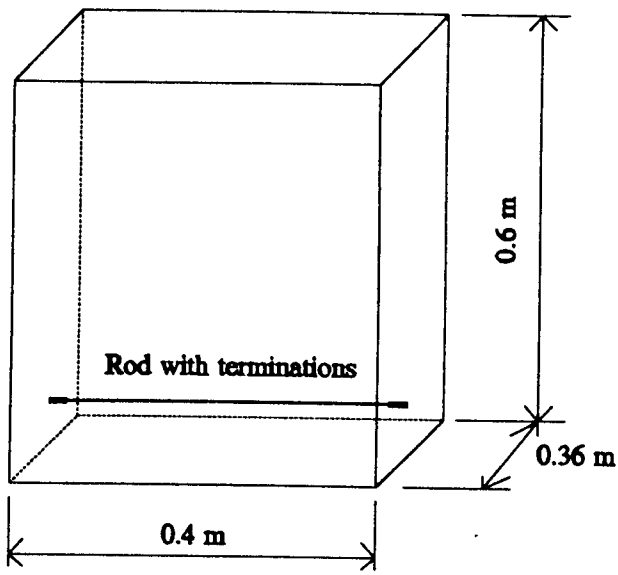

Figure 4.3 Enclosed cavity configuration.

The enclosed cavity of Figure 4.3 was excited at one end of the rod by connection to the network analyzer through a 50Ω BNC connector and output was taken at the other end of the conductor, via the corresponding connector, to the other port of the network analyzer. Again, S_{21} was used as the measured parameter.

These are the basic configurations for the systems, some variations were used to test particular features of the model, for example the single conductor in the screened room was replaced by two conductors and apertures were placed in one of the walls of the cavity for certain tests, these will be discussed further in Chapter 5.

The frequency ranges used in the measurements were 50 MHz to 250 MHz for the screened room studies and 400 MHz to 1.5 GHz for the cavity. The screened room range was chosen so that it included the main dipole resonance (located at approximately 140 MHz) and a number of room resonances. The lower frequency for the cavity studies was chosen because only a low Q rod resonance was present below this frequency. The upper frequency was chosen to allow adequate visual resolution of the resonances on the graphs.

In §4.1. several features which are common to EMC problems of coupling to and from wires were listed. These are addressed by the two test configurations thus:

near fields interactions take place in the screened room coupling studies and also in the enclosed cavity. The latter also includes travelling wave phenomena, since all signals propagate along the finite length of the wire, with a half wavelength less than the length of the internal wire.

connections to external systems are introduced by the feed of the screened room dipole and by the excitation points and output points of the enclosed cavity.

in both configurations, the dipole and rods can be constructed such that the diameter is much smaller than the length.

in both configurations, the resonant cavity formed by the enclosure or the screened room and the natural resonances of the radiators fall in the same frequency ranges, giving rise to a compound resonant structure.

both the screened room and the enclosed box have wires placed close to conducting surfaces. In the case of the screened room, the ends of these rods are not connected to any other structure. The enclosed box is similar to the test structure used in Chapter 3 in that it has the ends of the conductor close to the metal walls of the box.

The accuracy and repeatability of measurements undertaken in screened rooms have been questioned[16]. It was found that similar measurements undertaken in several screened rooms could show a variation of up to 40dB! The inherent similarities between the screened room and the box used in these studies, indicates that the problems inherent to the screened room may also affect the box. Hence, a principal aim in developing verification tests is to ensure that the tests themselves are repeatable and accurate. The difficulty with such an aim is that there is no 'standard' to compare with: the very act of introducing measurement equipment leads to further uncertainties. As a consequence, many of the factors which could give rise to uncertainties in the measurements were investigated as independently as possible. The following sections investigate many of the variables which may give rise to errors in the results.

4.3. SCREENED ROOM EXPERIMENTAL PROCEDURES AND UNCERTAINTIES

There are a number of factors which can give rise to potential uncertainties in results obtained from screened room measurements. Those considered to be of fundamental importance are general metrology, the cables and errors in positions of the source and receiver. These are discussed in this section.

4.3.1. Metrology

This section discusses a number of aspects of taking measurements in the screened room.

Network analyzer calibration. In order to eliminate the effects of the cable attenuation and phase shift on the measurements, calibration was undertaken according to standard practice[74], shifting the calibration planes to the ends of the cables connected to the dipole and the current probe. A simple thru' response calibration was generally undertaken as this was found to produce results almost indistinguishable from the more accurate, but also more lengthy, one path - two port measurements. A full description of error paths and correction can be found in reference 74.

The network analyzer itself was calibrated by the manufacturers, giving results potentially traceable to standards.

Network analyzer timebase selection. There are three frequency sweep options for the network analyzer. The first is cw (continuous wave - operating at a single frequency) and was not used for the work undertaken in this Thesis. The fundamental difference between the other two options, 'step' and 'ramp', is that 'step' phase locks at every measurement frequency and 'ramp' only phase locks at the start frequency and then the output follows the input without further phase lock until the start of the next cycle, giving the potential for drift. The 'step' mode is inherently more accurate, due to the phase lock, and was used for the majority of the experiments undertaken.

The 'step' mode takes longer to perform a single measurement than the 'ramp' mode - of the order of several seconds compared with several tenths of a second for the 'ramp' mode. This increase in time was of no inconvenience for the experiments undertaken.

In order to obtain a measure of the repeatability of the experiments, several sets of experiments were undertaken with the variable in question altered. Each measurement was recorded. The sets of results were scanned to find the maximum and minimum value of the received signal at a particular frequency. These will be referred to as the maximum and minimum variation curves, and will be used to highlight the repeatability of the measurements.

Current probe position. It was found that the current probe could be misplaced on the dipole and rod by several cm from its nominal position without resulting in any perceivable change in the measured response. Figure 4.4 shows the maximum and minimum values of the rod response as the current probe was displaced from the mid-point by ±5 cm, the maximum likely accidental displacement. The two curves are virtually superposed.

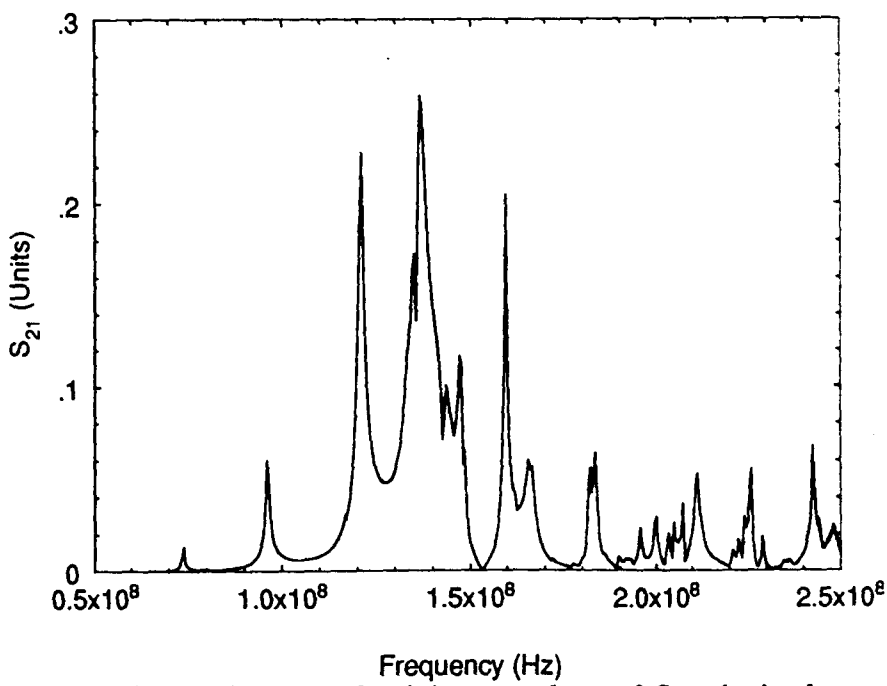

Figure 4.4 Maximum and minimum values of S_{21} obtained as a function of frequency with changes in the position of the current probe.

4.3.2. Cables

In the screened room measurements, cables were necessary to enable the network analyzer to excite the dipole and for the signal picked up by the current probe to be passed back into the network analyzer. Initial experiments were undertaken using braided cable. This proved unsatisfactory due to the high level of coupling through the braid. Clearly, standard braided coaxial cable is unsuitable for experiments undertaken in screened rooms. As a result, triple-braided cable was used (referred to as super-screened cable), this gave noise-floor-level coupling through the braid.

Super-screened cables were not without their problems, however. When the coupling experiments were undertaken as before but with super-screened cable used in place of braided cable, the measurements of the current induced in the rod were still not repeatable. Significant differences in the results were observed for experiments performed at different times. To further investigate this phenomenon, measurements were taken of the current in the two arms of the dipole using the current probe, both the dipole feed and the current probe output cables were super-screened. The dipole was placed symmetrically in the screened room, i.e. the feed of the dipole was equidistant from the two side walls and the axis of the dipole was perpendicular to those walls. The measurement taken was the current profile along the dipole over the frequency range 50 MHz to 250 MHz, this is shown in Figure 4.5. The ideal response is one which has a plane of symmetry located at the dipole feed, thus the current profile in the 'left' arm is the same as in the 'right' one. Clearly, this is not the case. It was found that this response would be significantly different if the experiment was re-assembled.

The dipole was a simple, linear, half wave resonator, with no balun arrangement. The lack of balun was investigated as the cause of the demonstrated current imbalance. A torroidal balun was added at the feed of the dipole but no improvement was observed, a significant current imbalance was still present.

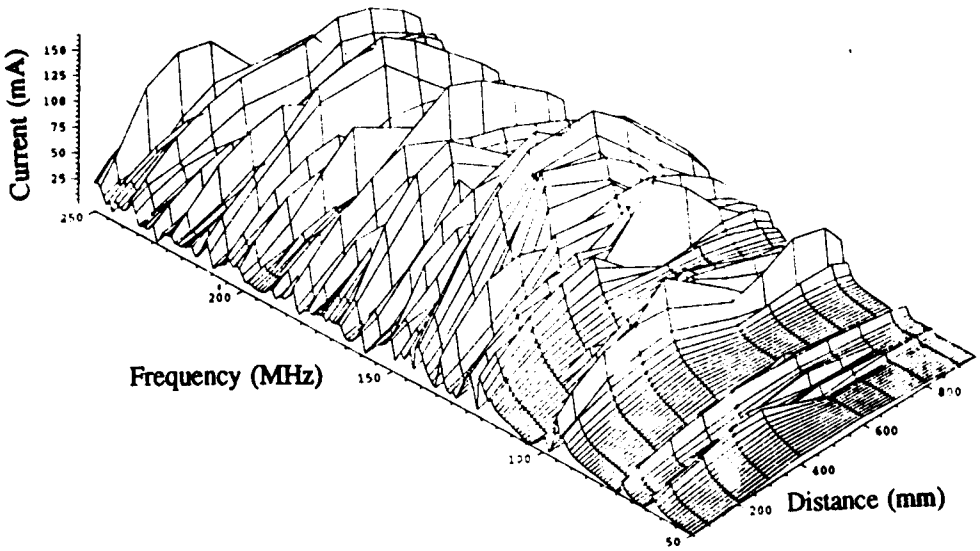

Figure 4.5 Dipole current profile with unloaded super-screened cables.

Further, it was noted that the positions of the cables had an effect on the actual imbalance. Changing the position of the dipole feed cable, such that as it dropped to the floor of the screened room it was either taken directly to the corner between the wall and the floor (so that the maximum single run length was close to this corner and the walls) or it was run along the centre of the room as far as possible and then taken to the bulkhead connectors, caused changes to the current imbalance. In no case could cable positions be found which balanced the currents in the dipole arms for all frequencies in the range studied.

Measurements were taken of the current flowing on the outside of the cables. This current was found to be comparable in amplitude with the signals induced in the rod. Thus, it was concluded that the cause of the imbalance was that currents were being induced on the outer conductor of the cable by the dipole illumination. In turn, these currents were causing re-radiation from the cables and hence a modification to the field patterns in the screened room and thus the currents flowing in the arms of the dipole.

The addition of small ferrite clamps (Chomerics, part number B2025-000) was found to be of great benefit. They were placed round the cables with a separation of about 0.3m, the actual separation of the clamps was variable. The current imbalance was found to be reduced to a small level, as can be seen in Figure 4.6. The ferrite clamps acted as a 'distributed balun', reducing the current flowing on the outer conductor of the cable.

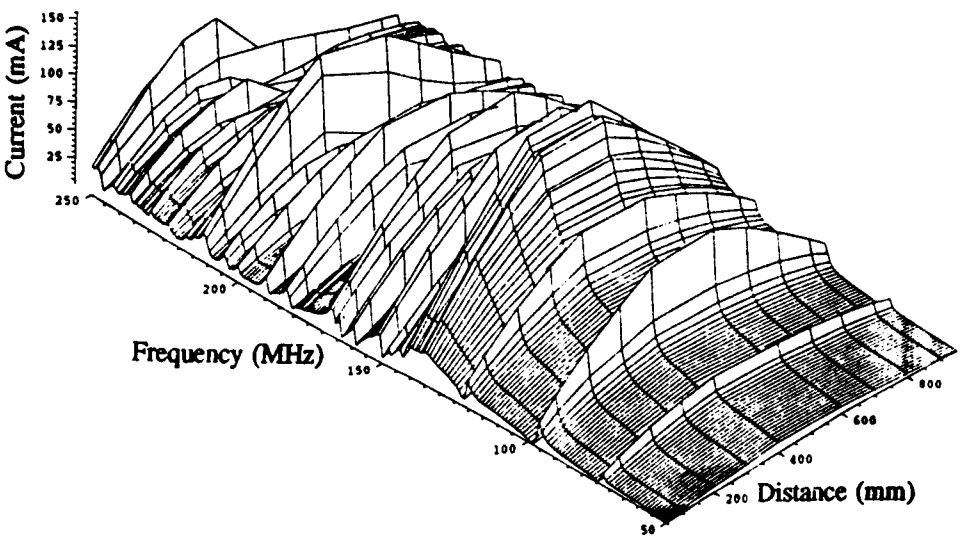

Figure 4.6 Current profile with ferrite loading of the cables.

Figure 4.7 shows the positions of the cables used in the screened room experiments to determine the dependence of the cables on the results. Although a great number of experiments would be needed to determine a true statistical confidence on the measurements, the following results will indicate the levels of repeatability expected. The cables were placed in all possible combinations shown in Figure 4.7 and the S_{21} parameter was measured on the mid-point of the receiving rod, with the positions of all other elements kept the same. The 'step' function of the network analyzer was used with a 401 point frequency span over teh frequency range of interest. Once the measurements had been taken, the results were scanned to find the highest value at a particular frequency and the

lowest value at a particular frequency. Figure 4.8 shows these two curves plotted on a linear amplitude scale. The two curves are almost indistinguishable.

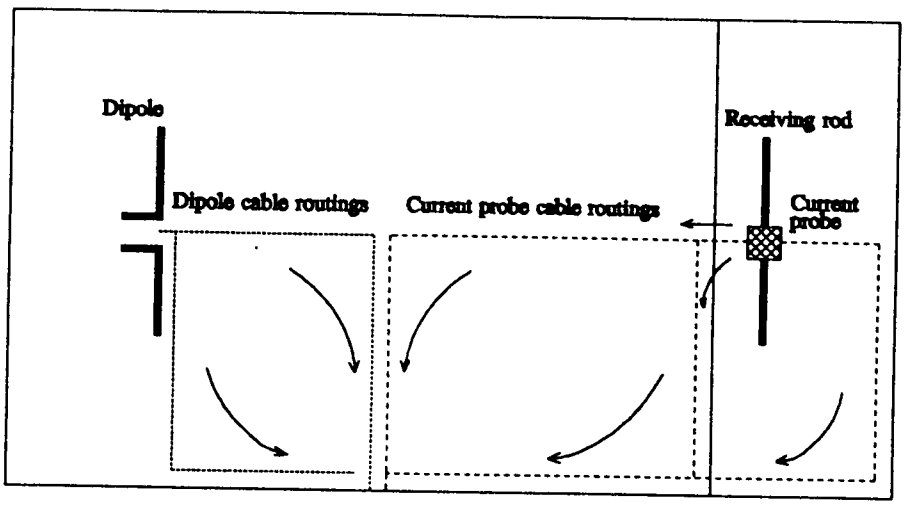

Figure 4.7 Locations of screened room cable runs.

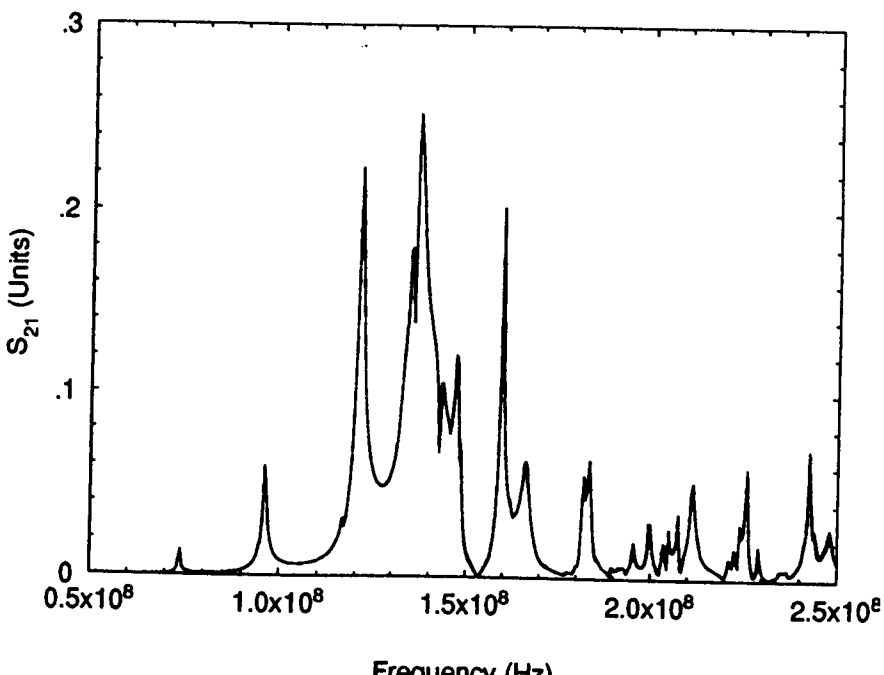

Figure 4.8 Maximum and minimum values of S_{21} obtained as a function of frequency with cable movement.

4.3.3. Dipole and rod positioning errors

It is likely that in the normal course of experimentation using the screened room configuration of Figure 4.2 there will exist small errors in the positioning of the dipole and the rod. These errors should be very small if the experiments are performed carefully, but they may still be present. Further, it was considered that a study of the positional effects may help in the interpretation of the behaviour of the screened room.

The errors will occur because of the dipole and/or the rod being slightly misplaced, or the dipole may be rotated about the vertical or the horizontal axes. These factors were quantitatively investigated.

It was envisaged that a normal error in the positions of the dipole and rod would be no greater than ±2 cm. This figure was based on practical experience. The amount of cross-polarisation was expected to be no more than approximately 3° in either plane - a greater angle could be visually detected.

The following list summarises the experiments undertaken.

Dipole movement. The variation experiments were undertaken for dipole movement of ±2 cm (towards and away from the receiving rod). S_{21} was measured and the maximum and minimum S_{21} values were obtained at each frequency as described for the current probe and are given in Figure 4.9. It will be seen that very little dependence on the dipole position is noted.

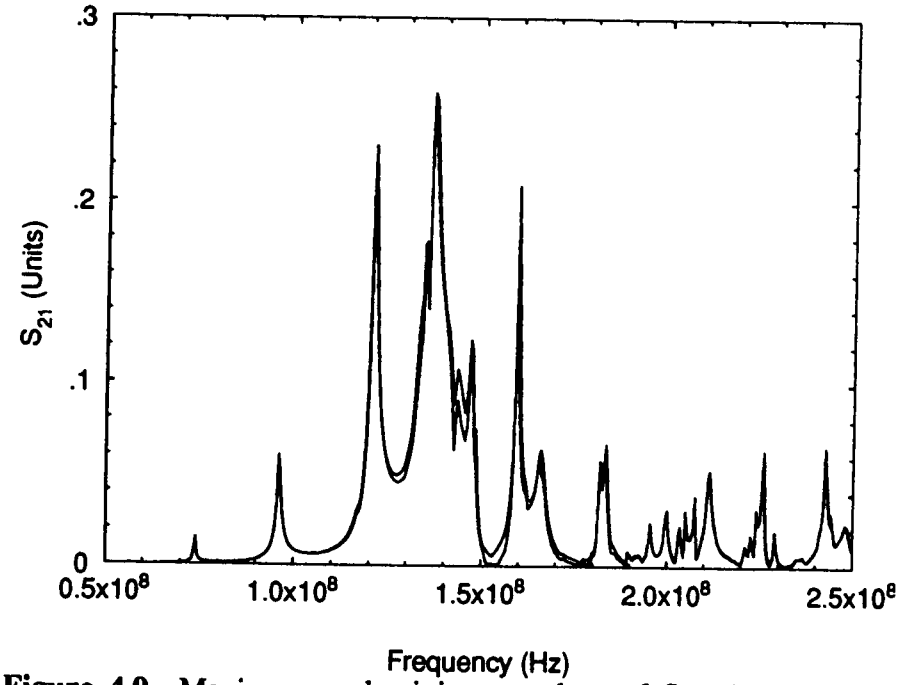

Figure 4.9 Maximum and minimum values of S_{21} obtained as a function of frequency with dipole movement.

Rod movement. When the rod was moved towards and away from the dipole, by ±2 cm similar results were obtained. The maximum and minimum values of S_{21} were recorded at each frequency and are shown in Figure 4.10. Little effect is noted.

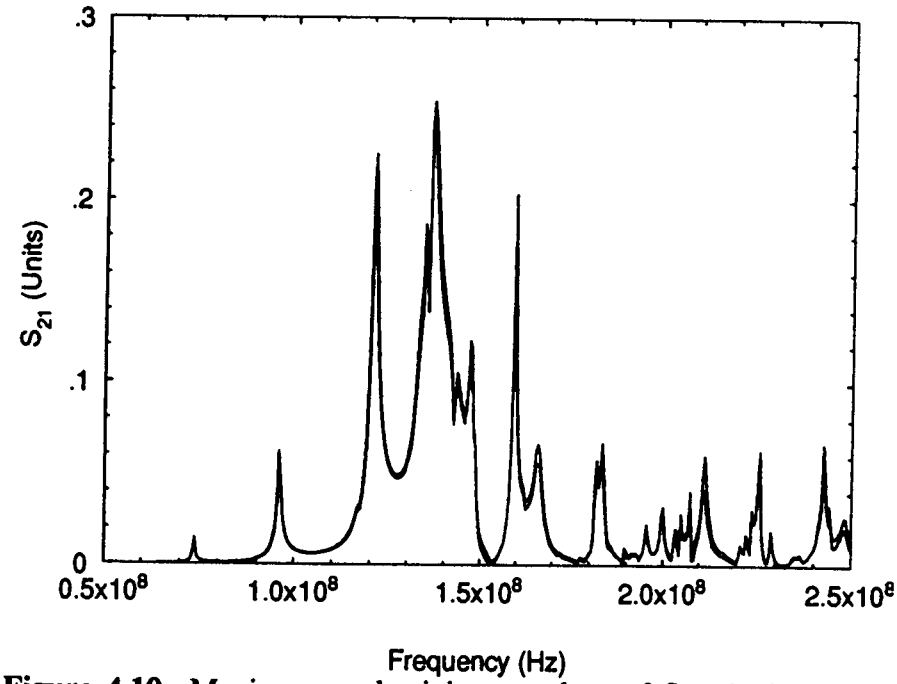

Figure 4.10 Maximum and minimum values of S_{21} obtaiend as a function of frequency with receiving rod movement.

Dipole and rod movement. When both the dipole and rod were moved by ±5 cm, the rod current showed very little perceivable change.

'Side-to-side' movement. The movement of either, or both, the dipole and the rod by ±5 cm from side to side (i.e. in the direction of their longest axes) resulted in only small and relatively imperceptible changes to the measured parameters.

Non-parallel elements (horizontal rotation). The dipole was rotated in the horizontal plane so that it and the rod were no longer parallel. Only small amplitude changes were noted in the measurements as noted in Figure 4.11 which shows the effects of approximately ± 3° horizontal rotation.

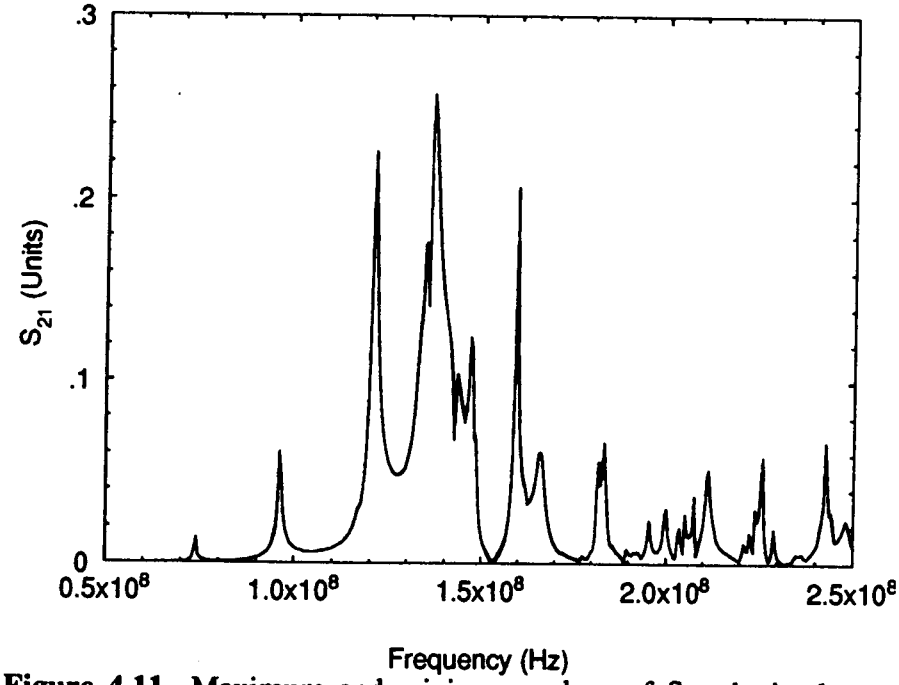

Figure 4.11 Maximum and minimum values of S_{21} obtained as a function of frequency with horizontal rotation of the dipole.

Cross-polarisation (vertical rotation). Although it was envisaged that the dipole and receiving rod could only be misaligned by up to 3° in practice, greater values being easily noticed 'by eye', a study of ±90° was undertaken to study cross-polarisation effects. The rod was maintained in its standard position and the dipole was rotated in the vertical plane. The current induced in the rod was recorded against the angle of rotation of the dipole from the horizontal. The measured rod current over the range of frequencies from 50 MHz to 250 MHz, with a 10° rotation, is compared with the parallel case shown in Figure 4.12. It will be noted that there exists very little variation. Further, the maximum and minimum value study, as described at the start of §4.3.3., was undertaken with ±3° rotation and the results are displayed in Figure 4.13. It will be noted here that no variation can be seen.

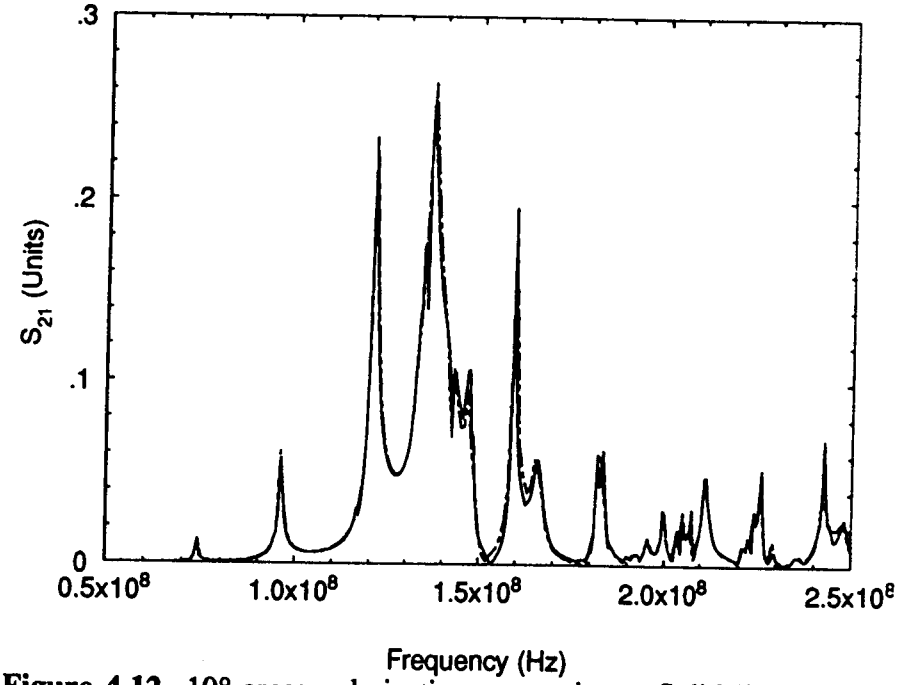

Figure 4.12 10° cross polarization comparison. Solid line parallel polarization of dipole and receiving rod, dashed line 10° rotation of dipole.

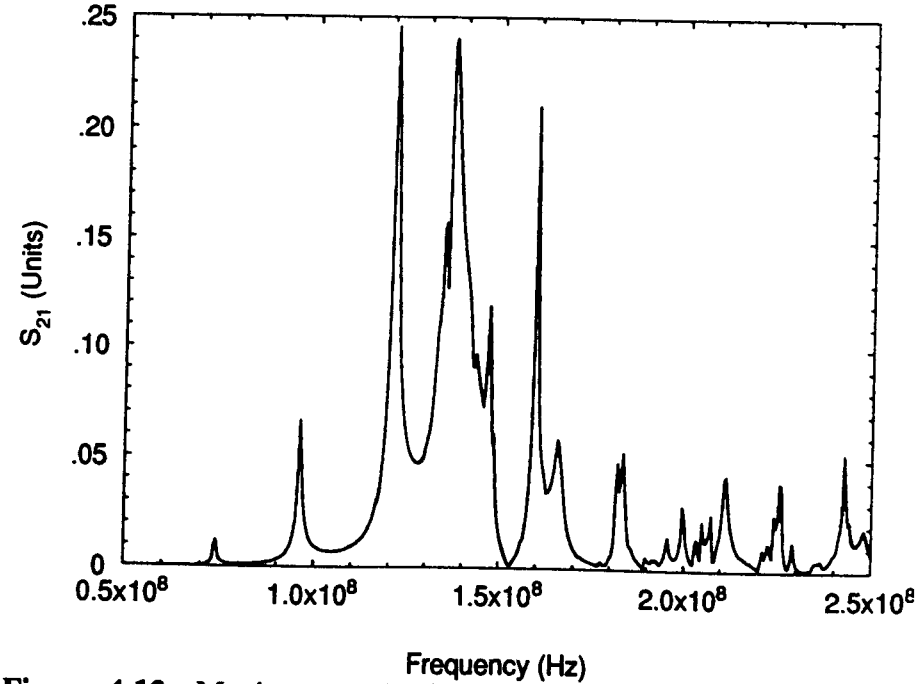

Figure 4.13 Maximum and minimum values of S_{21} obtained as a function of frequency with vertical rotation of the dipole.

It is interesting to note the effects of cross-polarisation (90° rotation) inside the screened room. Figure 4.14 compares measurements for the perpendicular and the parallel polarized cases, using a logarithmic amplitude scale to allow easy comparison of the curves. It will be seen that there is still a noticeable level of current induced in the case of perpendicular polarisation when compared with parallel polarisation.

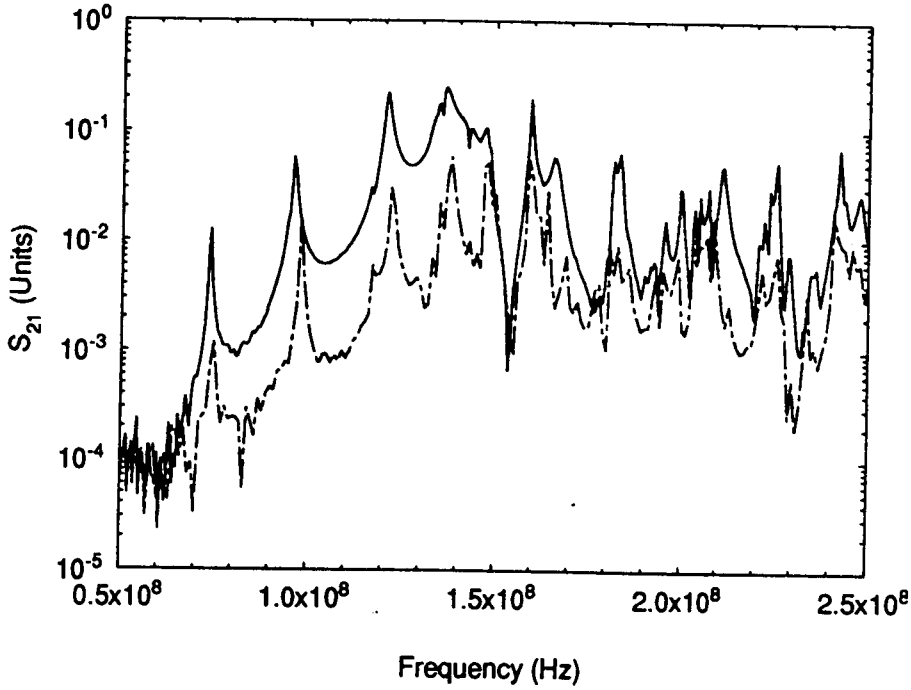

Figure 4.14 90° cross-polarization. Solid line parallel polarization of dipole and receiving rod, dashed line 90° rotation of the dipole.

4.3.4. Summary of experimental errors

In general small variations in the positioning of the dipole and rod, are unlikely to give rise to significant experimental errors.

After investigating the sources of probable error, it was decided that the measurements exhibited a high level of repeatability. It should be noted that the experiments have been performed on further occasions with fully repeatable results.

High frequency measurements. The frequency range chosen for the screened room coupling measurements represents the lower range of EMC radiation measurements. It is interesting to note some factors which would be important should the range be required to be extended beyond the 1 GHz limit currently specified in EMC standards:

cables and connectors would be required to operate up to the required frequency. The potential problem with the cables would be the re-radiation giving rise to imbalance on the dipole as in §4.3.2. and adversely affecting the receiving rod current. The solution may be to use a ferrite loaded wire[75] rather than add more ferrite clamps as this would render the cables bulky and difficult to work with.

screened room integrity, i.e. the shielding effectiveness of the seams, finger stock and windows, would need to be determined.

trunking and seams are internal structural features which, in the case of the Nottingham screened room, have a feature size of between 5 cm and 15 cm. Cross-sectional TLM simulations have indicated that they have little effect at lower frequencies, such as those being used in the experiments reported in this thesis. However, it was noted that they begin to cause variations in the positions of the room resonances from those of a smooth cavity at frequencies above approximately 500 MHz. Hence, it may be more appropriate to perform verification experiments in an anechoic, or semi-anechoic chamber.

positional variation errors would need to be reassessed for the an increased frequency range. This is due to the positional uncertainties being relatively larger, in terms of wavelength, as the frequency increases.

4.4. CAVITY EXPERIMENTAL PROCEDURES AND UNCERTAINTIES

Some of the factors associated with the cavity measurements have already been covered in the screened room discussion above, i.e. calibration of the cables and selection of timebase mode on the network analyzer. The main cause of uncertainty in these measurements is the manner in which the connections between the cavity and the network analyzer are made, and the manner in which terminating impedances can be connected. There is a great deal of commonality between the methods of cable and termination connection, and consideration will only be given to the cable, or 50Ω system, connections. Apertures in the cavity were used, and consideration was given to the amount of 'clear-space' required above the aperture so that any environmental effects, such as reflections from other equipment would be avoided. The rest of this section will consider the connection and clear-space problems.

4.4.1. 50Ω system connection

It was required to connect the conductor, which runs through the box, to the outside world and especially to the network analyzer via the 50Ω cabling, see Figure 4.3. Experimental uncertainties are generated in: the transition region between the coaxial cables (connected to the network analyzer) and the internal conductor. In making the connections, the following must be ensured:

the transition region between the system coaxial cable and the internal conductor must have a low insertion and return loss.

the results must be independent of the type and length of the system cables used providing that standard calibration procedures are undertaken.

the results must be independent of the system cables' orientation and flexion.

In general, the most convenient way of connecting the internal conductor to the 50Ω system is to 'pig-tail' a coaxial cable and connect it so that the centre conductor is connected to the internal conductor of the cavity and the braid is connected directly to the outside of the cavity. Figure 4.15 shows such a means of connection. Several researchers have investigated pig-tail methods of connections[76-78] and have concluded on their unsuitability. Potential problems in the particular case of the cavity are:

there may be a relatively high insertion loss as the impedance changes from the 50Ω of the coaxial connectors to that of the internal conductor via the undefined impedance of the transitional region.

the results may not be independent of the system cables, the results would depend on the length and orientation of the pig-tails, which would change the impedance profile of the transitional region. This will result in unrepeatable results.

there is no clear calibration plane with such a method, thus the calibration cannot be performed with any confidence.

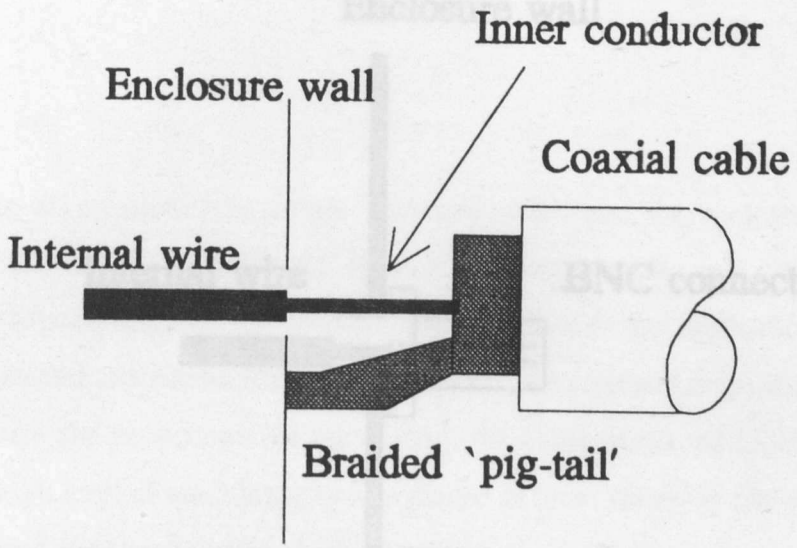

Figure 4.15 'Pig-tail' connection to the enclosed cavity.

It is difficult to determine the effect of the above factors analytically. However, some indicative tests were undertaken, which looked at the reflection of a signal from a short or open circuit at one end of the internal wire, with the other end connected to the network analyzer using a pig-tail. The short circuit was made by connecting the rod to the box by a small (but finite) length of wire. It was found that by altering: the length of the pig-tail, the area between the braid and the inner conductor, and the angle of the braid and inner to the enclosure wall, the results obtained were highly unrepeatable.

The connection method developed which fulfilled the system connection requirements is shown in Figure 4.16. The internal conductor spans all but a few mm of the length of the box. Its ends are connected to the inner connector of a BNC connector, the outer of which is connected to the box. This has the effect of avoiding pig-tails and of providing defined calibration planes close to the box and thus ensuring that the measurements are independent of the cables used.

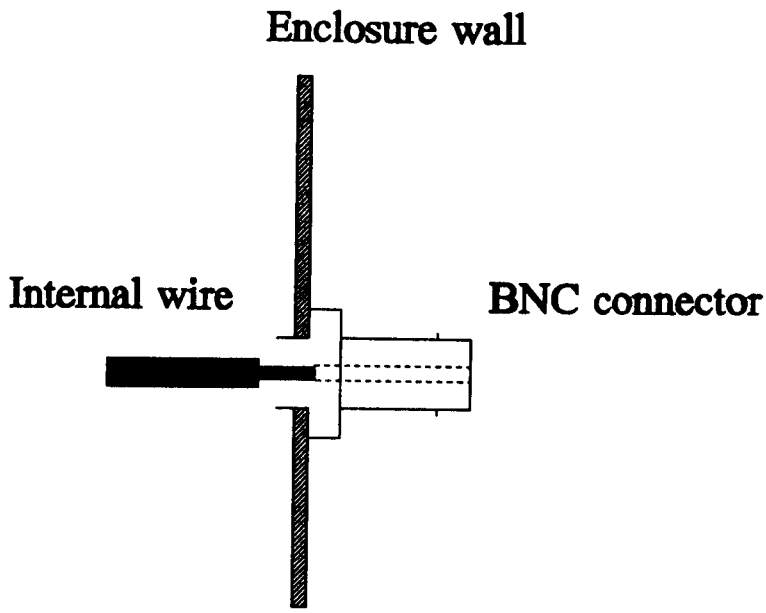

Figure 4.16 Enclosed cavity connection method used. The internal wire is connected to the inner conductor of the coaxial connector, the outer of which forms an electrical contact with the cavity wall.

4.4.2. Free-space for aperture measurements

A number of experiments were undertaken with an aperture incorporated into the lid of the cavity, which recorded the signal flowing along the internal conductor of the cavity. In order to determine the effects of the external environment, a large metal plate was placed directly above the aperture and close to it. As the plate was removed to a greater distance, the changes in the response of the cavity were noted. It was found that once the plate was removed to a height greater than approximately 30cm above the aperture, little further changes could be observed in the measurements. This indicated that measurements involving the aperture could be undertaken in the laboratory and would be little influenced by the laboratory environment.

4.5. SUMMARY

Results of measurements in the screened room and the enclosed box could potentially be highly uncertain, leading to unrepeatability and inaccuracy, and hence a poor level of confidence. However, with the application of certain experimental procedures (the ferrite clamps in the screened room and the defined conductor and connectors for the cavity), the experiments are highly repeatable and a high level of confidence can be placed in these results to allow comparison with simulations for verification purposes.

CHAPTER FIVE
VERIFICATION TESTS: EXPERIMENTS AND MODELS

This chapter describes the experimental and modelling configurations used for validating TLM in more detail. Further studies of the screened room behaviour will also be discussed.

5.1. EXPERIMENTAL SCREENED ROOM CONFIGURATIONS

There are two specific configurations used for the screened room comparisons: the basic system described in Chapter 4, consisting of a dipole illuminating a rod placed over a conducting bench, and a modification of this system in which a second similar rod conductor was brought into proximity with the first. Figure 5.1 shows the two conductor configuration. The single conductor configuration is as in the figure, but with the rod farthest from the dipole (rod 2) removed.

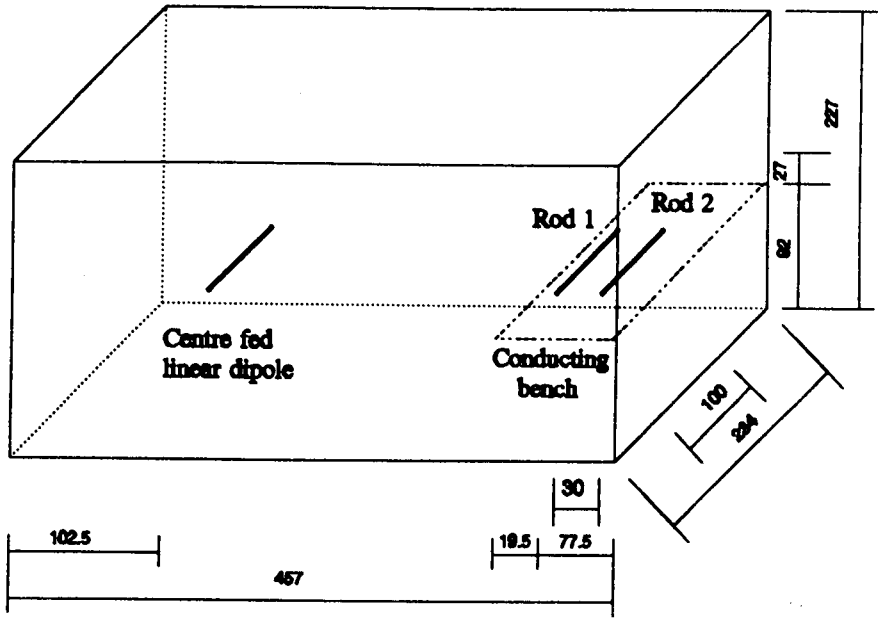

Figure 5.1 Two conductor, screened room configuration. All dimensions are in cm.

In general, the behaviour of the single conductor system was discussed in Chapter 4. The points noted are generally applicable for the two conductor system, however, it is interesting to study the influence of the second conductor qualitatively. If the two rods are considered as two similar half-wave dipoles it can be shown[79] that the total impedance of the first element of the two dipole array (and, by reciprocity, the second, although this will not be discussed separately) is equal to

$$Z_1 = Z_{11} + Z_{12}\frac{I_2}{I_1} \qquad (5.1)$$

where Z_{11} is the self impedance of the first dipole, Z_{21} is the mutual impedance of the two dipoles and I_1 and I_2 are the currents flowing in dipole 1 and dipole 2 respectively. The self impedance is determined by the length, diameter and wavelength of operation of the dipole, the mutual impedance is determined by the separation and the wavelength (given that the dipoles are approximately half wave dipoles within the frequency range of interest). Thus, for the two similar rods

described, the behaviour at a particular frequency will depend on the separation of the elements.

The resonance of a dipole occurs when its reactance is zero, hence, Figure 5.2 illustrates the approximate behaviour of the reactance of the system at approximately the natural resonance of a single element with a spacing of less than $d/\lambda = 0.3$, above which, the slope of the mutual reactance curve, X_{12}, becomes positive with respect to frequency. Figure 5.2(a) shows the trend of the self reactance as it varies with frequency. Figure 5.2(b) shows a family of curves of mutual reactance which decreases with both frequency and an increase in the separation. Figure 5.2(c) combines Figures 5.2(a) and 5.2(b) to give the resultant $\{X_{11} + X_{12}\}$. The family of these curves cut the axes at increasing frequencies as the separation decreases. Hence, it would be expected that the resonances obtained would increase as the separation decreases.

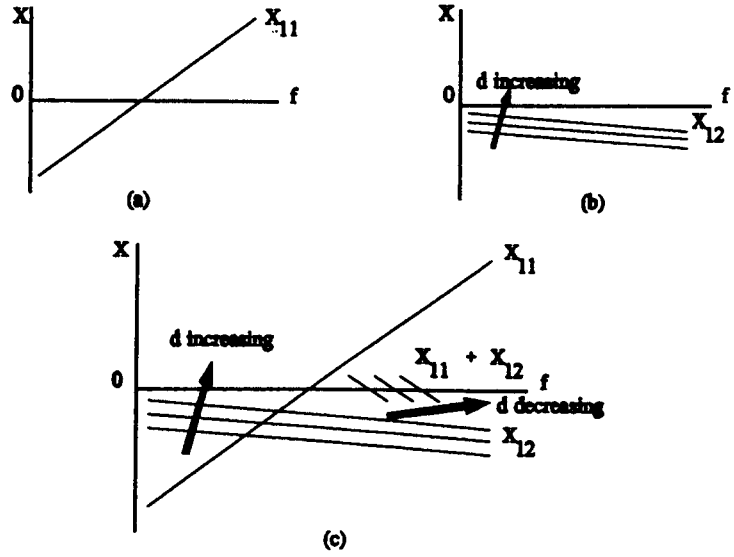

Figure 5.2 Effect on reactance of two dipoles of varying separation. (a) self reactance, (b) mutual reactance and (c) result of combining (a) and (b).

An experimental investigation of this is shown in Figure 5.3 which shows the resonances on rod 1 of Figure 5.1. The natural resonance of a 1 cm diameter,

1 m long linear dipole is approximately 140 MHz. The decreasing frequency of the peak as the separation increases agrees with the qualitative analysis. Although, it should be noted that the qualitative analysis does not account for any further interaction caused by the images of the rods in the bench and walls etc.

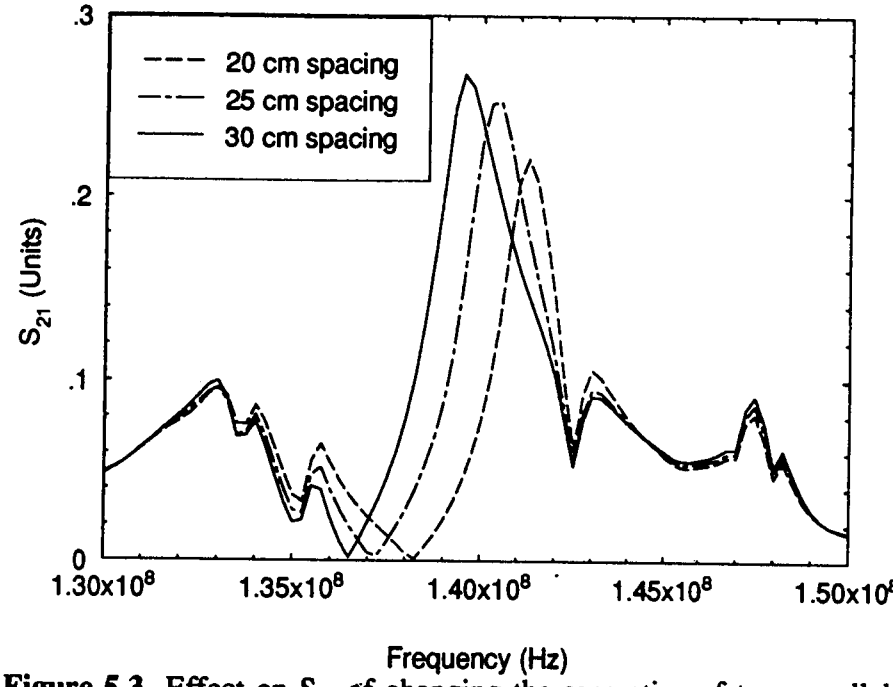

Figure 5.3 Effect on S_{21} of changing the separation of two parallel rods.

5.2. TLM SCREENED ROOM CONFIGURATIONS

In the TLM simulations of the screened room, the walls, floor and ceiling were modelled by introducing an external boundary reflection coefficient of $\rho = -1$. This is performed by shorting the link-lines forming the extremities of the workspace. The bench was modelled by internal boundaries with a reflection coefficient $\rho = -1$.

The work-space itself was modelled using a bulk node size of Δl = 5cm (the term 'bulk' is being used here to denote that these nodes extend throughout the whole of the problem space, smaller nodes are used to describe the wires and are included as fine mesh multi-grid regions, as will be described later). The choice of Δl = 5 cm allowed a reasonably accurate description of the screened room to be used, for a reasonably small usage in computer storage and run-time.

As stated previously, it is usual to operate TLM with a maximum node size determined by the 'ten nodes per wavelength' rule-of-thumb. The maximum frequency to which the comparisons are being made is 250 MHz, thus:

$$\Delta l_{max} = \frac{\lambda_{min}}{10} = \frac{c}{10 f_{max}} = \frac{1}{10}\frac{300\ 10^6}{250\ 10^6} = 0.12m \qquad (5.2)$$

Thus, it would be possible to operate the simulation with a bulk node size of Δl = 12 cm, however, this would result in a high reduction ratio for the multigrid sections resulting in a large number of fine mesh nodes, which would tend to negate the beneficial effects of having few bulk workspace nodes[11].

The errors in the modelled dimensions of the room were fairly small, a maximum of approximately 2cm in each of the three ordinate directions. At 300 MHz, 2 cm is approximately $\lambda/50$, and was considered to be an acceptably small error. Although some slight variations may be observed in the location of some of the room resonances these would be less than approximately 1%.

The multigrid fine-mesh regions were included within the bulk workspace nodes as indicated in Figure 5.4. A reduction ratio of 5:1 was used giving a fine mesh region allowing a modelled 1 cm diameter for the wires with a single node cross-section. Figure 5.4 indicates how the fine mesh regions are related to the rest of

the work-space.

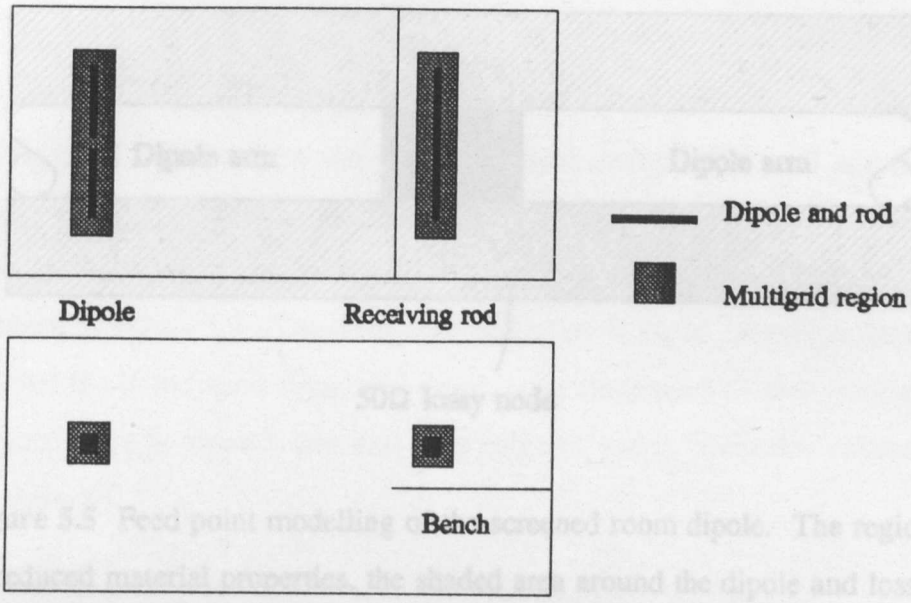

Figure 5.4 Screened room showing location of fine mesh regions.

The dipole and the receiving rods were modelled within the fine-mesh regions using the correction scheme introduced in Chapter 3. The region of reduced material properties was a one node thick layer around the one node cross-section conductors and extended one node beyond the ends of the rods. The dipole was actually modelled as two halves of equal length with a single lossy node between them for the feed. The correction region extended around the excitation as well as the rest of the dipole. In all cases the ends of the rods were closed off by internal boundaries, one node in extent, forming conductors with continuous surfaces.

Excitation was performed by placing a single lossy node of impedance 50Ω between the two halves of the dipole, as shown in Figure 5.5. Excitation was applied as a single impulse of unit amplitude at time T = 0. The ports excited on the node were those orientated in the direction of the dipole axis.

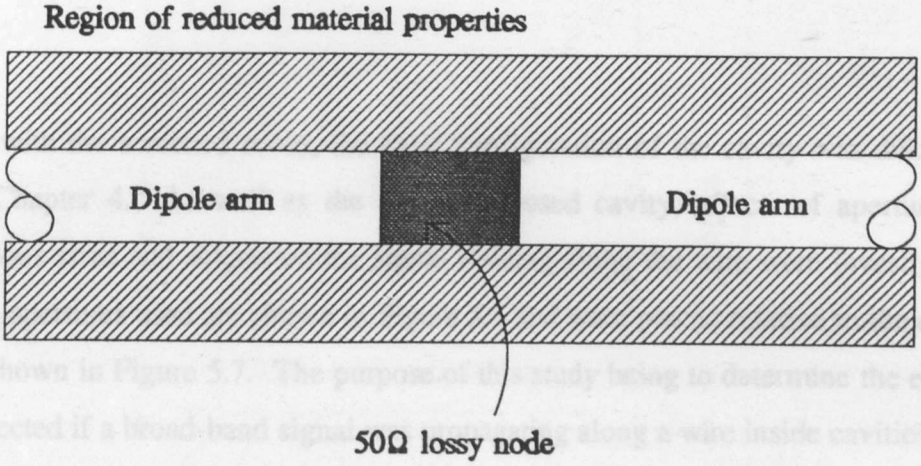

Figure 5.5 Feed point modelling of the screened room dipole. The region of reduced material properties, the shaded area around the dipole and lossy node, is a one node thick layer.

The output current was taken by recording the link-line pulse values on the surface of the dipole and receiving rods, again directed along the axis of the conductors, this being proportional to surface current.

The cables were not modelled as their influence on the response of the system had been effectively eliminated in the associated experimental work.

5.3. EXPERIMENTAL CAVITY CONFIGURATION

As with the screened room, the basic configuration of the cavity was discussed in Chapter 4. As well as the totally enclosed cavity, effects of apertures of various sizes and shapes on the signal flowing along the wire were investigated. The apertures used are shown in Figure 5.6 and were placed relative to the cavity as shown in Figure 5.7. The purpose of this study being to determine the effects expected if a broad-band signal was propagating along a wire inside cavities with apertures, such as aircraft, cars and other vehicles, and in equipment cabinets and rack systems.

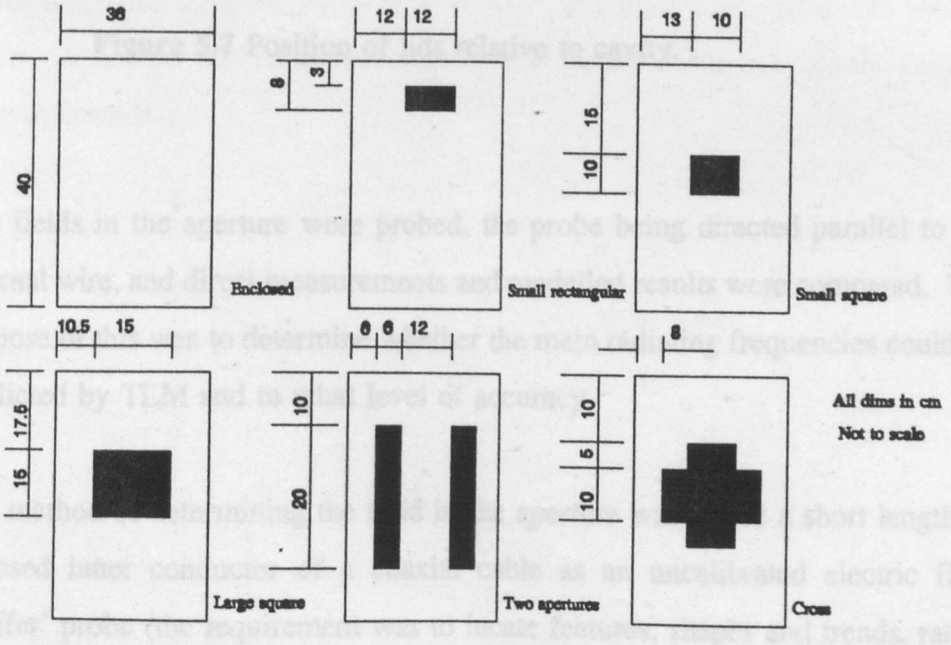

Figure 5.6 Cavity lids.

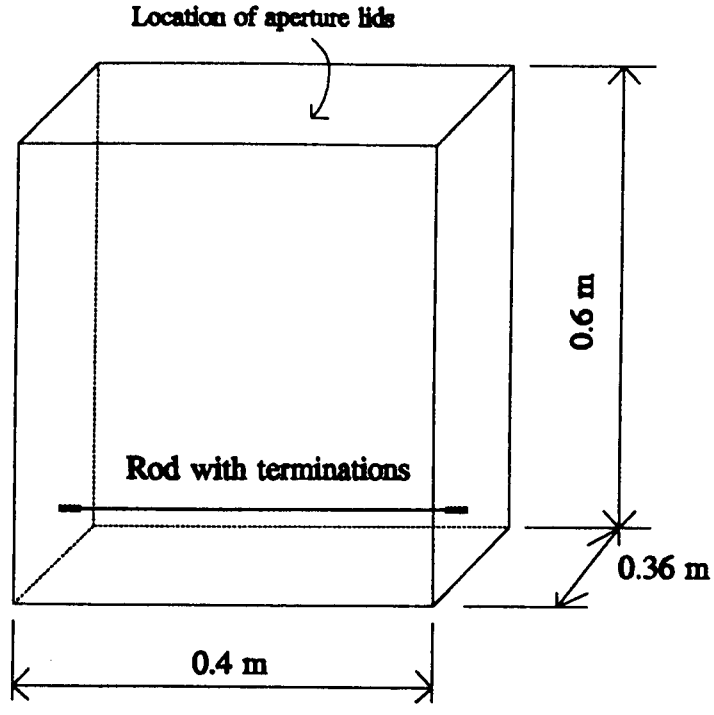

Figure 5.7 Position of lids relative to cavity.

The fields in the aperture were probed, the probe being directed parallel to the internal wire, and direct measurements and modelled results were compared. The purpose of this was to determine whether the main radiating frequencies could be predicted by TLM and to what level of accuracy.

The method of determining the field in the aperture was to use a short length of exposed inner conductor of a coaxial cable as an uncalibrated electric field 'sniffer' probe (the requirement was to locate features, shapes and trends, rather than to determine absolute field strengths).

5.4. TLM CAVITY CONFIGURATIONS

The external boundaries of the work-space were modelled as matched boundaries, thus absorbing the majority of the radiation incident upon them and approximating to matched free-space boundaries. The only exception was the boundary which formed the 'floor' of the box, that is the surface closest to the rod; this was modelled by a $\rho = -1$ boundary. Figure 5.8 describes the placement of the boundaries relative to the cavity.

The walls and 'lid' of the box were modelled by internal boundaries, placed half way between nodes, with reflection coefficients of $\rho = -1$. The workspace was constructed from a regular mesh of Δl = 1cm. The total work-space size was 60 x 64 x 100 nodes. 40 nodes were left between the top of the box and the parallel external boundary.

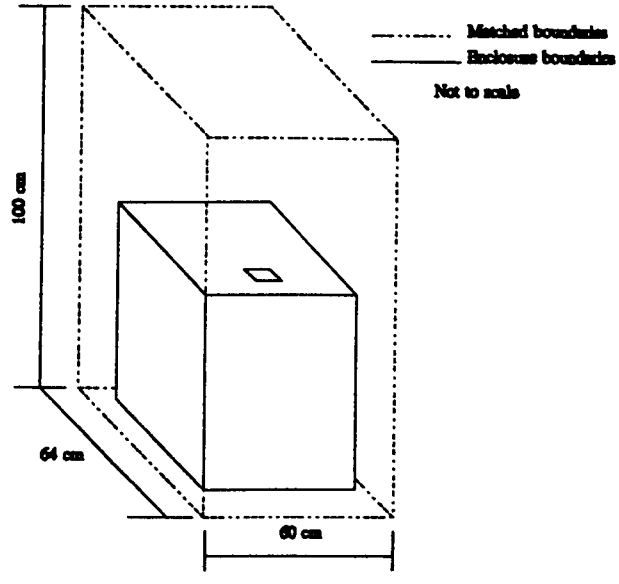

Figure 5.8 The cavity and the simulation external boundaries.

The 1 cm node size allows modelling, without noticeable dispersion, up to approximately 3 GHz, twice the frequency range used in the experimental work. The cavity dimensions could be modelled accurately due to the nature of the cavity construction, with only a slight, but relatively insignificant, misplacement of the internal conductor. The apertures were modelled as gaps in the internal boundaries used to form the lid.

The rod was modelled by a single node cross-section formed from internal boundaries. The 50Ω external system connections were modelled by single 50Ω lossy nodes, as shown in Figure 5.9. The wire and its terminations were embedded in the correction region of Chapter 3, similar to the rods and dipole in the screened room, which extended along the length of the rod from one side of the box to the other.

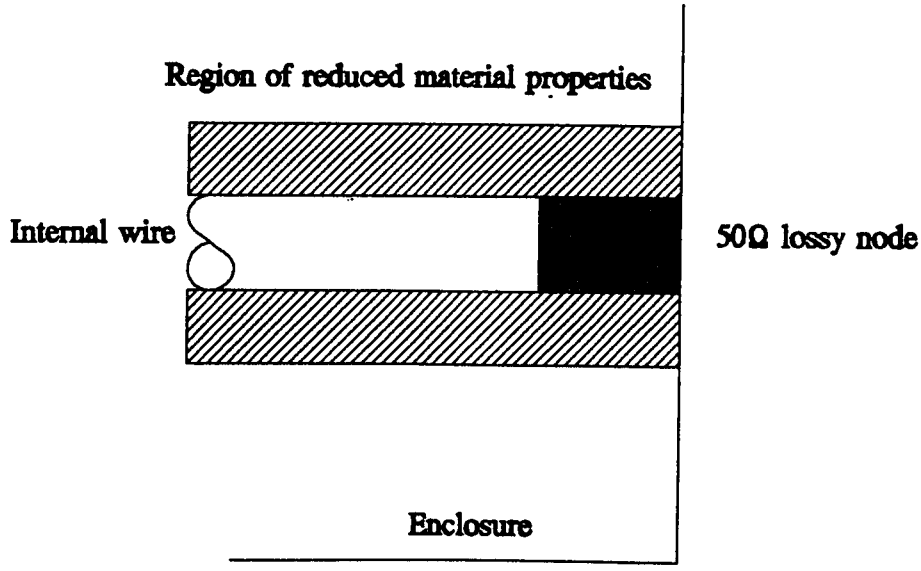

Figure 5.9 50Ω termination model in cavity. The region of reduced material properties, the shaded region around the wire and lossy node, is one node thick.

Excitation was performed by impressing a voltage across one of the lossy nodes, in a similar way to that of the screened room. Output was taken as the voltage in the terminating impedance, i.e. in the other lossy node.

5.5. METHODS OF COMPARING RESULTS

In order to determine the accuracy of the models and the measurements a method of comparison needs to be defined. The requirements, for the purpose of this study, are to determine the general agreement of the location, and relative variation, of features of the coupled signals. It was not necessary in this case to compare absolute values. In consequence, it was decided to compare the results of the models and measurements on the same graphs with the maximum amplitude of each response normalized to a peak value of one. Although further refinements could be made, such as to normalise to a mean energy level, the comparison made was considered as being adequate for the purpose of this study.

Because of the complicated structure of the results, simple comparisons between the experimental results and the simulations are difficult. In general, 'by-eye' comparisons have been undertaken. However, the use of correlelograms[80] appears to have some benefits - especially when wanting to place a numerical figure of accuracy to the comparisons - and these will be discussed further in Chapter 6.

5.6. SUMMARY

This chapter has briefly discussed some of the practical considerations of experiments and the models used for the validation tests and has introduced the range of comparisons used for the verification of the wire modelling method described in this Thesis.

CHAPTER SIX
RESULTS OF VERIFICATION TEST COMPARISONS

Chapter 5 described the configurations used for both the experimental and TLM tests. This chapter presents the results from those tests. Firstly, the results for the screened room dipole-to-rod coupling for both the single receiver and the two receivers cases will be given. Then, results from the cavity will be presented which will concentrate on the enclosed cavity amplitude and phase response with the various aperture lids and the results of the field probed in the small rectangular aperture. Finally, a discussion will be presented on the use of correlelograms for quantifying the comparison between experimental and modelled results.

6.1 SCREENED ROOM RESULTS

This section will consider the cases of the coupling of the linear dipole into the single receiving rod and the two receiving rods within the screened room. Results are presented which show how well TLM models the effect of coupling within the complex electromagnetic environment formed by the screened room itself, the bench and the dipole and rods. It will also be seen how well the effect of the modifications to TLM described in Chapter 3 are to overcome the resonance error problem in more general EMC configurations.

6.1.1. Single receiving rod

Experiments were undertaken involving a centre fed, linear dipole placed in the screened room illuminating a wire-like rod placed over a conducting bench as described in §5.1. The currents at the centre of the receiving rod and at 10 cm from the feed of the dipole were obtained in the frequency range 50 MHz to 250 MHz. Both the dipole and the rod were 1 m long and 1 cm in diameter.

The dipole and rod were both modelled inside multigrid regions with a bulk work-space node size of Δl = 5 cm and a grading ratio of 5:1, giving Δl = 1 cm in the fine mesh regions. Figures 6.1 - 6.4 compare experimental results with the results of TLM simulations.

Figure 6.1 is the normalized current in the receiving rod, the TLM model uses no resonance error correction and, although the results are similar, there is a noticeable difference between the two curves i.e. the TLM prediction of the main coupling peaks is at slightly lower frequencies than the experimental results. Figure 6.1 shows room resonances as sharp features superimposed on an envelope corresponding to the low Q response of a linear dipole. The peak of this envelope of the uncorrected TLM results occurs at approximately 135 MHz where the general shift of this envelope to lower frequencies can be clearly seen by comparison with the experimental results and with the corrected TLM results of Figure 6.2. However, both sets of dipole simulations (Figures 6.3 and 6.4) do show a number of features which occur in the experimental results, namely the peaks in the graphs show a smooth exponential-shaped rise and a sharp fall at frequencies below the maximum of the envelope and the shape of the peaks are effectively swapped round above the maximum of the peak of the envelope. This indicates that, neglecting the wire resonance error problem, TLM can model the fundamental behaviour of the radiator.

Figure 6.2 shows the same comparison as Figure 6.1, except here the dipole and rod are modelled using the resonance error correction scheme. The comparison of Figure 6.2 is seen to be better than in Figure 6.1, i.e. the envelope of the response has been corrected.

Figure 6.3 compares the measured dipole current with the TLM results obtained without using the correction scheme and Figure 6.4 compares the measured dipole current with the TLM results incorporating the correction scheme.

Figure 6.3 again displays the room resonances with the dipole envelope, but in this case the envelope is more marked than for the rod current as this element is being driven. The points discussed about Figures 6.1 and 6.2 can also be applied here, i.e. the uncorrected TLM simulation shows both an envelope shift and a slight shift in the precise location of features which were largely corrected by the correction scheme. The results indicate that the correction scheme is correcting the room resonances as well as the wire resonances.

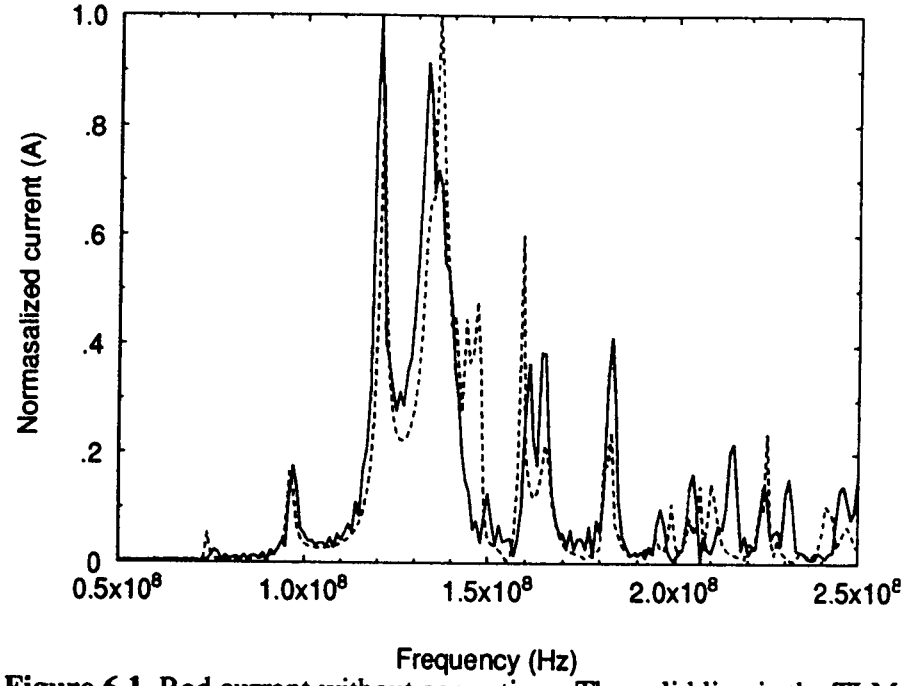

Figure 6.1 Rod current without correction. The solid line is the TLM simulation and the dashed line is the experimental result.

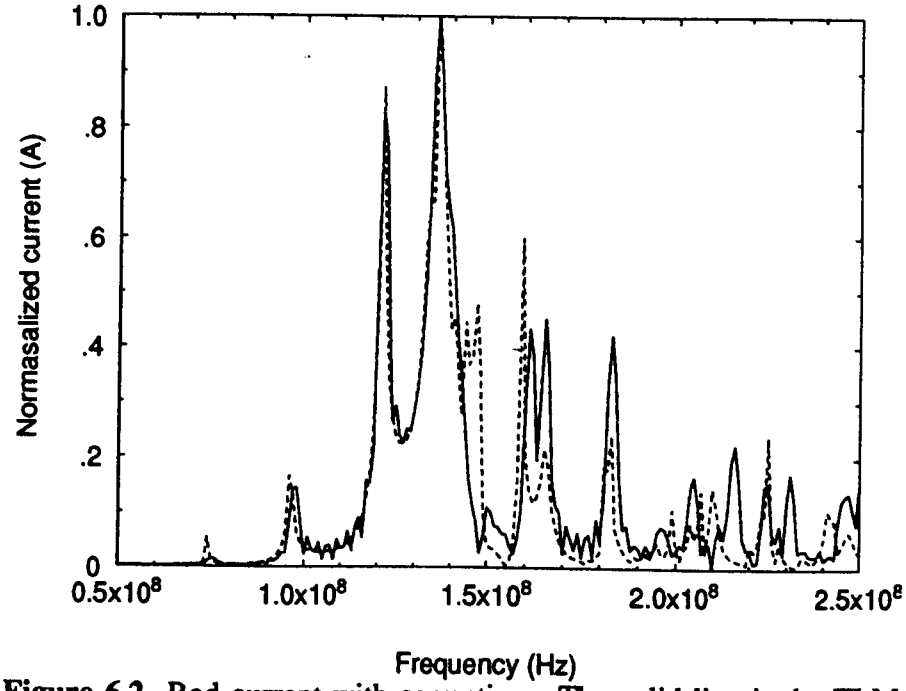

Figure 6.2 Rod current with correction. The solid line is the TLM simulation, the dashed line is the experimental result.

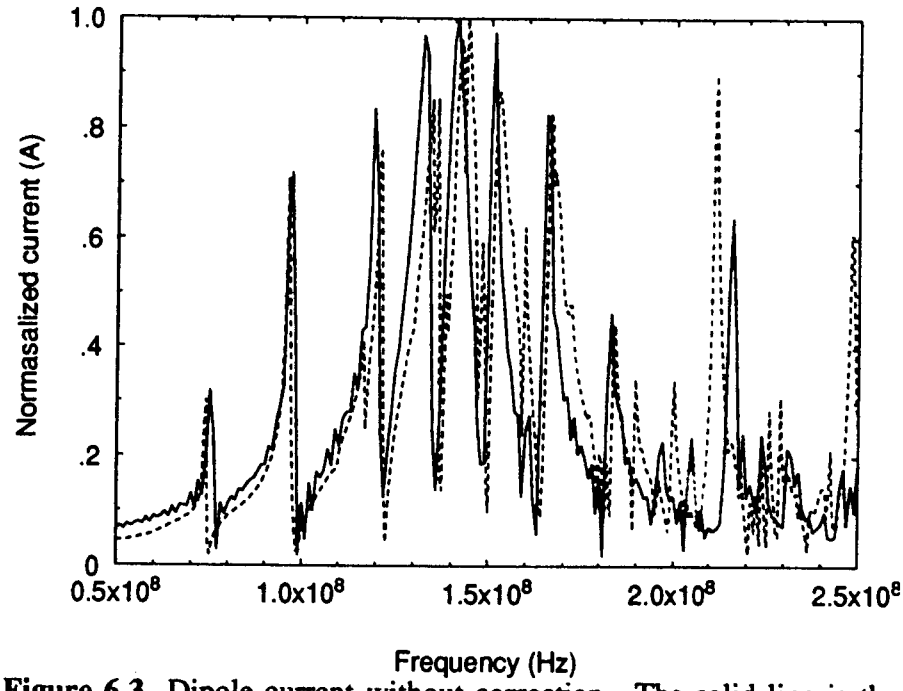

Figure 6.3 Dipole current without correction. The solid line is the TLM simulation, the dashed line is the experimental result.

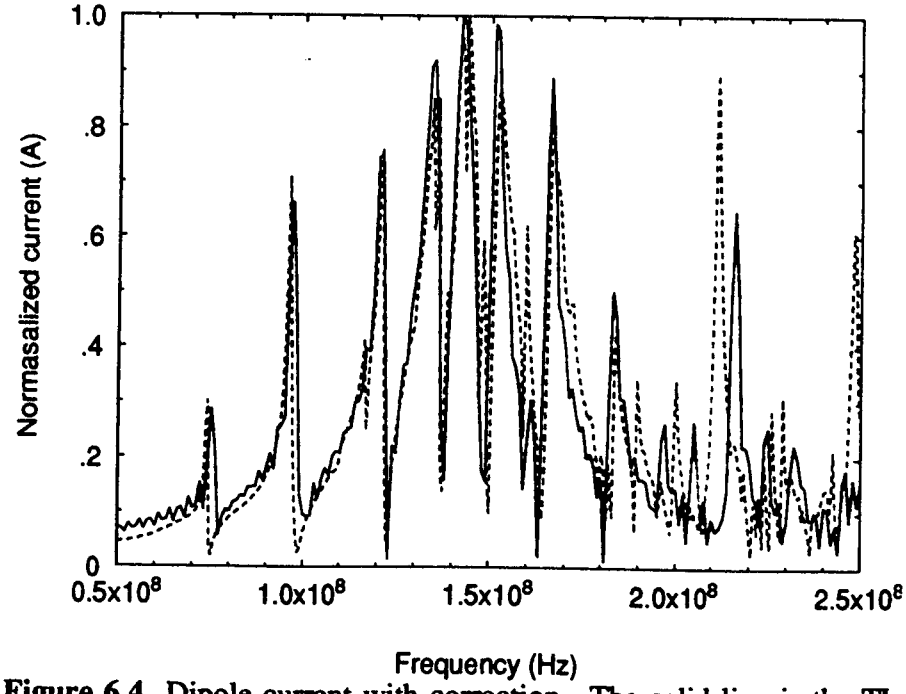

Figure 6.4 Dipole current with correction. The solid line is the TL M simulation, the dashed line is the experimental result.

The influence of the resonance error correction on the TLM results can be seen more clearly from Figures 6.5 and 6.6, which show the corrected and uncorrected modelled results for the rod and dipole currents respectively. It will be seen that the majority of the change caused by the resonance error correction, for the rod coupling results, is localised around the main coupling peaks whereas, for the rod coupling results, lower amplitude features are relatively unaffected.

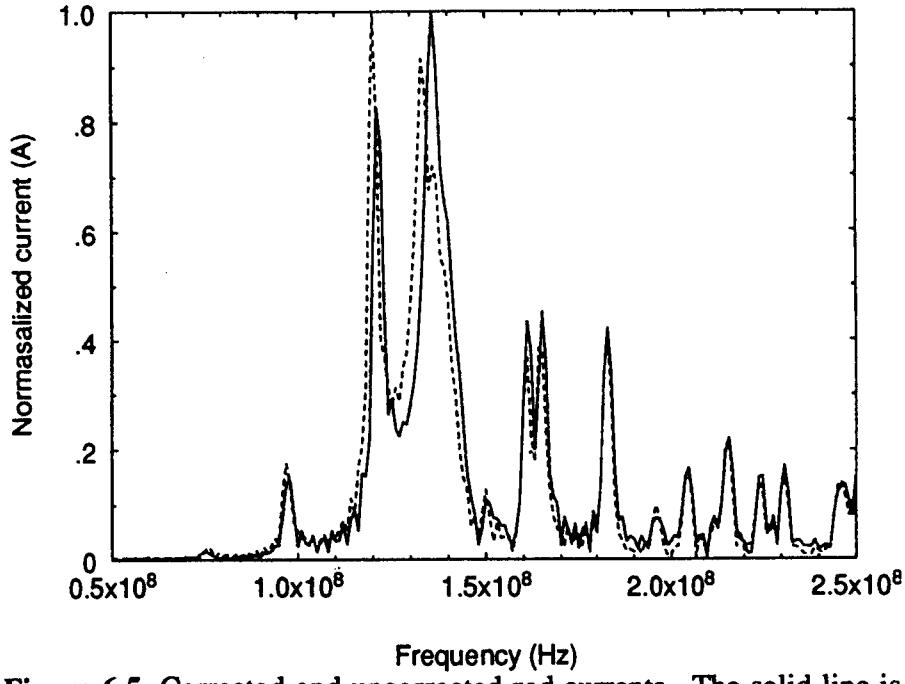

Figure 6.5 Corrected and uncorrected rod currents. The solid line is the TLM simulation obtained using resonance error correction, the dashed line is the TLM simulation obtained without correction.

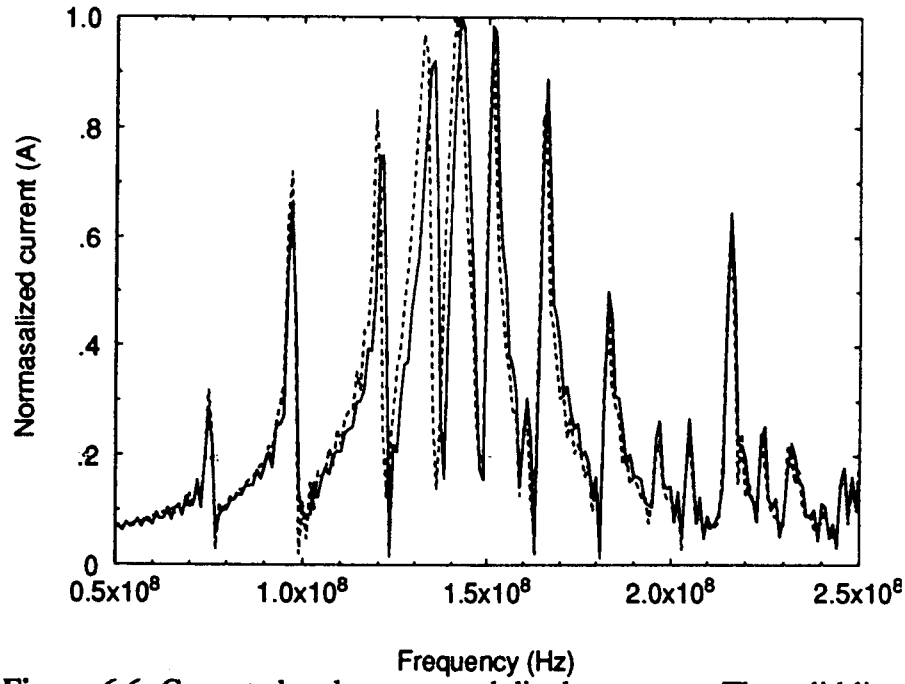

Figure 6.6 Corrected and uncorrected dipole currents. The solid line is the TLM simulation obtained using resonance error correction, the dashed line is the TLM simulation obtained without correction.

There are a number of observations which can be made regarding the results of this configuration. The coupling between a linear dipole and a rod of similar dimensions in a screened room with a conducting bench is a relatively simple problem. However, it does illustrate the dominance of the screened room on the electromagnetic environment, and coupling within it. This can be seen clearly from the current on the arm of the dipole; a smooth, low Q, response peaking between 140 MHz and 150 MHz (the prediction for a 1 m long 1 cm diameter dipole being 142 MHz) would be expected, however, the room is dominating the observed response with the peaks and troughs being caused by the room resonances.

The coupling within a screened room is a genuinely complex test for the validation of TLM, this difficulty is supported by the experimental discussions of Chapter 4. The high level of agreement indicates that TLM models the electromagnetic environment well. Further, the results indicate that although

unlined screened rooms are not recommended for radiated EMC tests, TLM could be used to determine optimum RAM placement in a partially lined room and, hence, some 'calibration' of the test facility. This has been the subject of research in recent years[81-83], which has concluded that although it is possible to determine the behaviour of a specific system, such as that described here, a generic calibration can not be performed in an unlined room and each new configuration would need to be calibrated separately[84].

It was noted above that this is a relatively simple coupling configuration, never-the-less, it is not one whose response can be readily determined analytically. Although it is important that simple configurations are considered, providing the foundations of a fuller understanding, the addition of further complexity should also be undertaken. The next section discusses a small change to the system which produces a substantial increase in the complexity of the overall system.

6.1.2. Two receiving rods

Although the two rod system is only marginally different to the one rod system, it adds further complication to the configuration by introducing mutual coupling of the receivers. The receiving system has practical application as two closely spaced wires or mechanical support spars. The addition of the second conductor extends the scope of the electromagnetic modelling problem, to include mutual coupling effects, without changing the experimental system excessively, and hence little additional experimental work on determining repeatability and accuracy was required.

Further, the two receivers configuration extends the generality of the resonance error correction by examining the effect of two closely spaced regions of material property change.

The first sequence of results in this section (Figures 6.7 to 6.12) compares the experimental and TLM results for the currents in each of the two rods and the dipole in the experimental configuration of Figure 5.1. Figure 6.7 shows the results for the rod closest to the dipole, without resonance error correction, Figure 6.8 shows the same comparison but with the resonance error correction used in the TLM results. Figures 6.9 and 6.10 compare experimental and modelled results for the conductor farthest from the dipole, again without and with resonance error correction respectively. Figures 6.11 and 6.12 respectively compare the experimental results for the dipole with the TLM results obtained without and with correction.

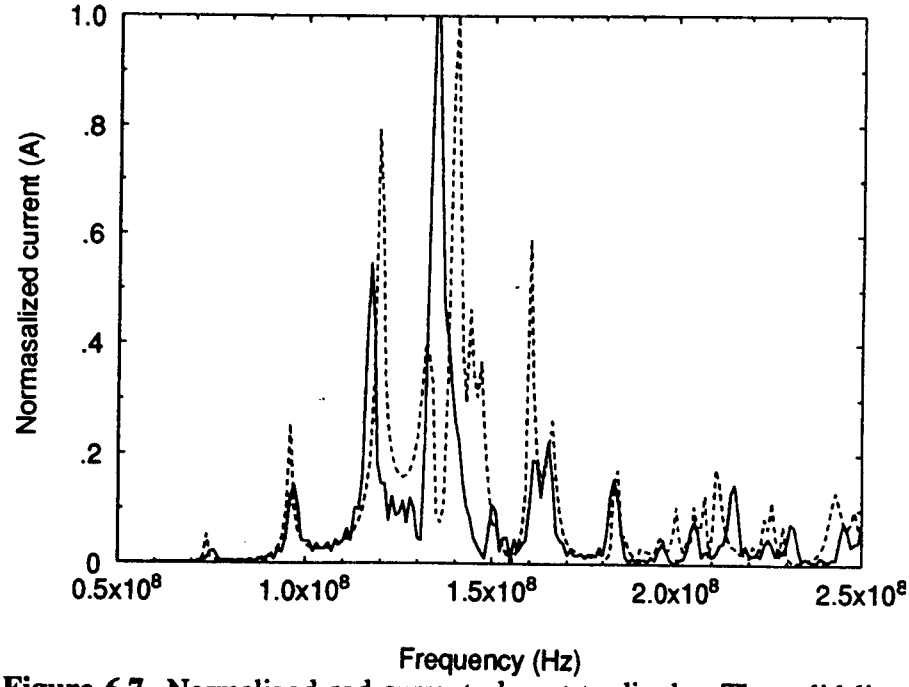

Figure 6.7 Normalized rod current closest to dipole. The solid line is the TLM simulation without resonance error correction, the dashed line is the experimental result.

There is a significant disagreement between the uncorrected TLM results and the experimental results of Figure 6.7, particularly between approximately 130 MHz and 150 MHz. This is more significant than the corresponding error for the case of the single receiving rod. The reason for the increase in the relative error is probably due to the resonance error having two effects. Firstly, it affects the self

resonant behaviour of the rods as illustrated in the single receiving rod case, and secondly, it will affect the relative coupling between the two receiving rods, further compounding the effect. This disagreement is minimised in Figure 6.8.

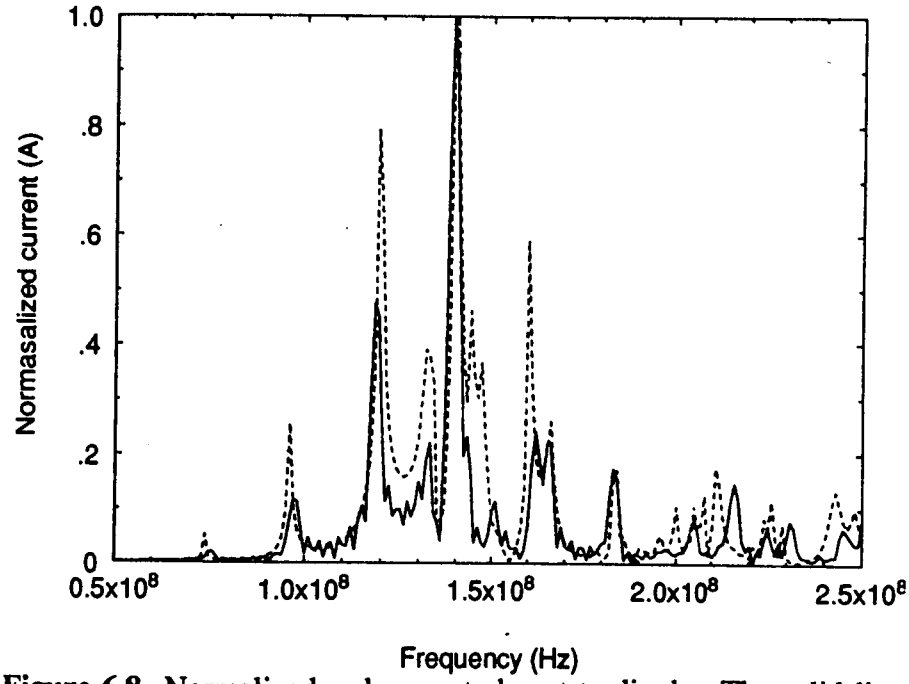

Figure 6.8 Normalized rod current closest to dipole. The solid line is the TLM simulation with resonance error correction, the dashed line is the experimental result.

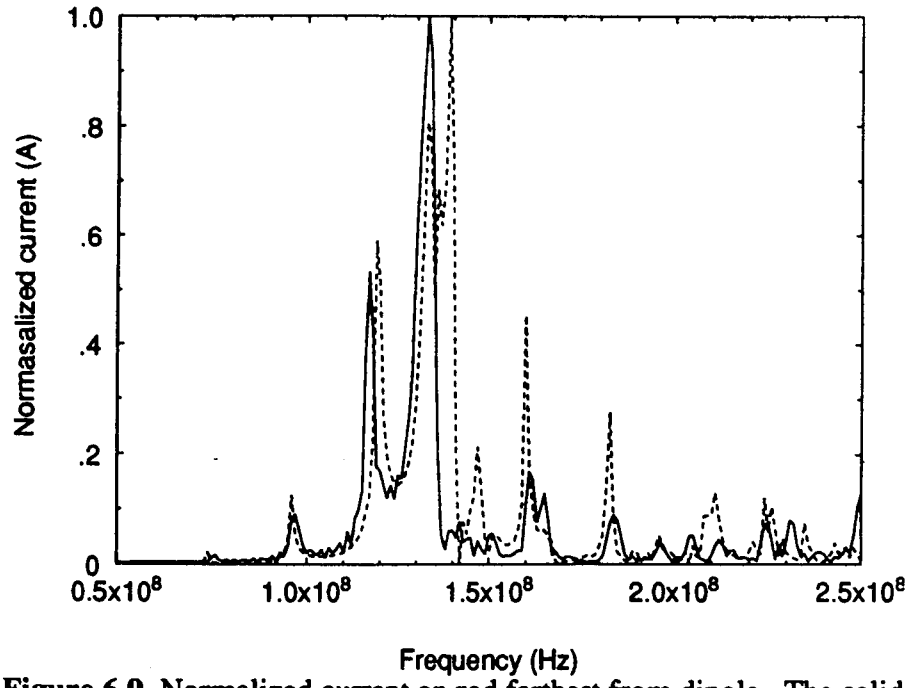

Figure 6.9 Normalized current on rod farthest from dipole. The solid line is the TLM simulation without resonance error correction. The dashed line is the experimental result.

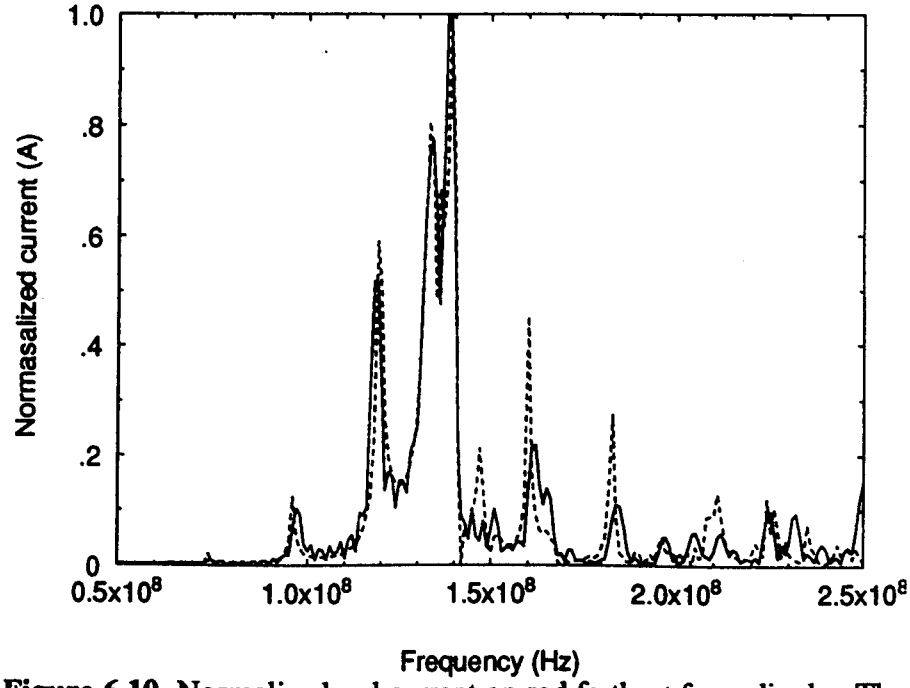

Figure 6.10 Normalized rod current on rod farthest from dipole. The solid line is the TLM result obtained with resonance error correction, the dashed line is the experimental result,

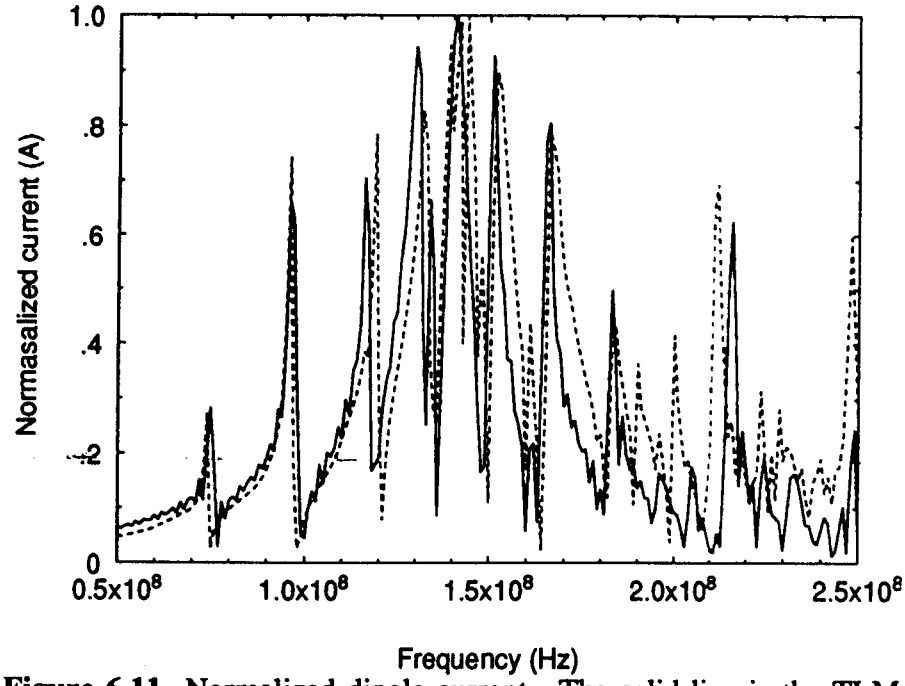

Figure 6.11 Normalized dipole current. The solid line is the TLM simulation obtained without resonance error correction, the dashed line is the experimental result.

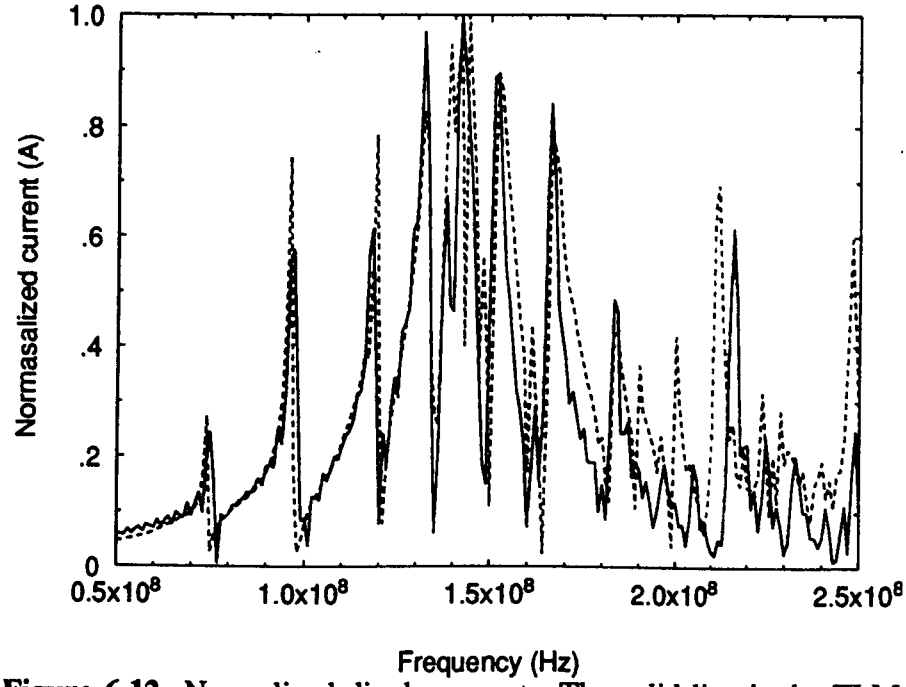

Figure 6.12 Normalized dipole current. The solid line is the TLM simulation obtained with resonance error correction, the dashed line is the experimental result.

The differences between the TLM and experimental results for the rods farthest from the dipole, shown in Figure 6.9, are also quite marked when modelled without using the resonance error correction, although the general shapes and trends do agree quite well. Specifically, the relative amplitudes of the peaks agree quite well, but the main response at about 140 MHz, which is actually a twin peak in the experimental results, has been shifted to lower frequencies in the simulation. The use of the correction scheme improves the results quite considerably and models the double peak.

The dipole current comparison shows a similar behaviour to that recorded in the case of the single receiving rod, i.e. the broad dipole envelope and the sharper room resonances. Again, the shape of the individual peaks can be seen to agree quite well for both comparisons. However, it should be noted that the wire resonance error correction scheme has little effect on the higher frequency features. This is attributed to the small differences in the modelled size of the screened room and the placement of the conducting bench compared with the experimental configuration giving rise to different resonant frequencies, which becomes more significant as the wavelength becomes smaller. Thus, it the differences are not caused by the wire resonance error, but are due to the resonances of the screened room.

The effect of the wire correction can be seen more clearly in Figures 6.13 - 6.15, which compare the corrected and uncorrected TLM currents for the rod closest to the dipole, the rod farthest from the dipole and the dipole respectively. One of the more interesting features of these graphs is that they appear to show greater shifts than Figures 6.5 and 6.6 which is attributed to the compound effect of the self resonance and the mutual coupling of the closely spaced receivers as described previously. Again, the TLM results agree much more closely with the experimental ones when the resonance error correction scheme is applied.

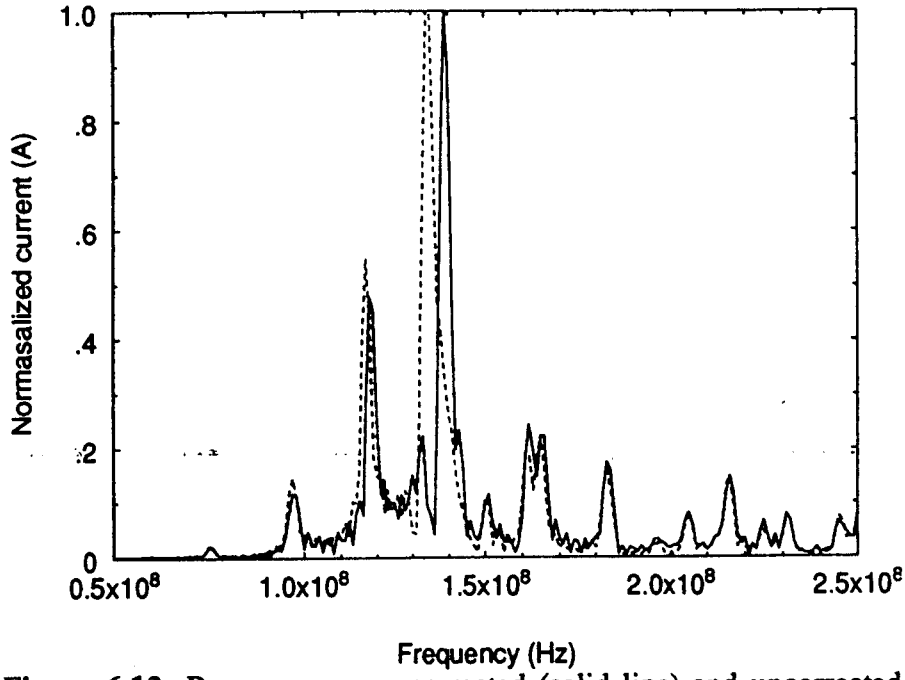

Figure 6.13 Resonance error corrected (solid line) and uncorrected (dashed line) TLM simulation currents for the rod closest to the dipole.

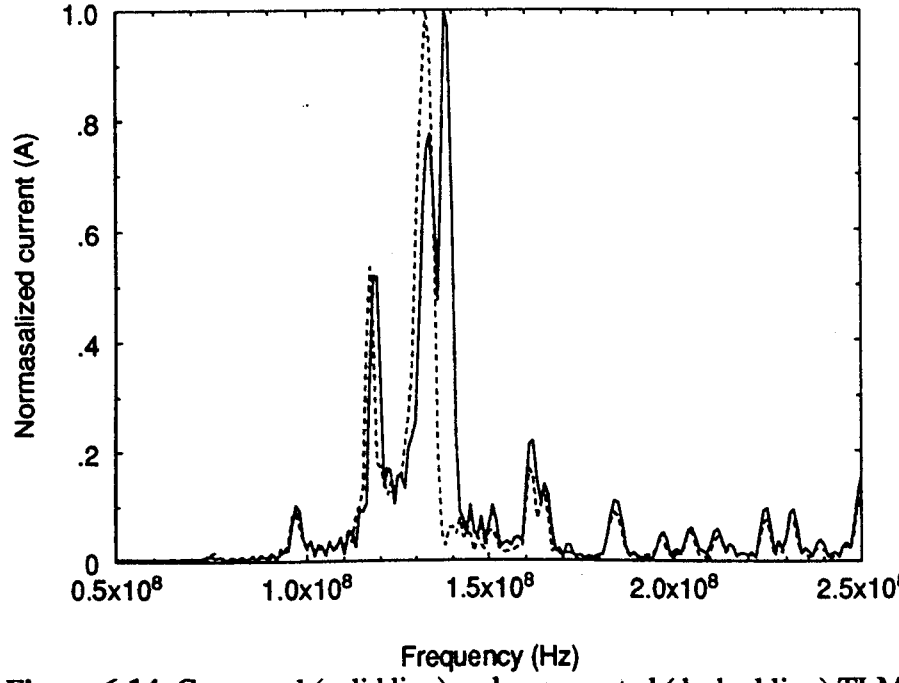

Figure 6.14 Corrected (solid line) and uncorrected (dashed line) TLM simulation rod current for rod farthest from dipole.

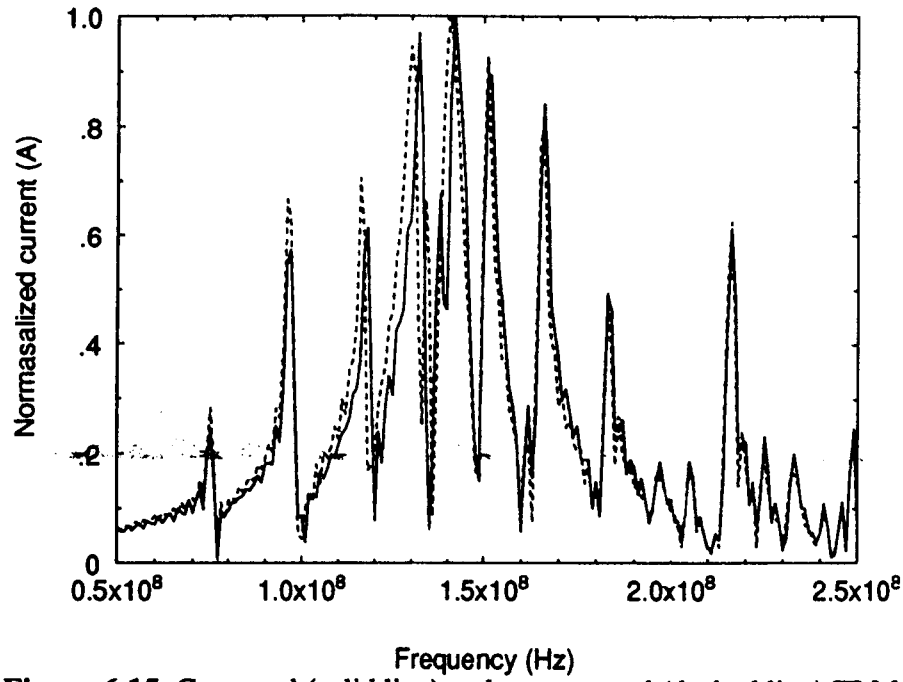

Figure 6.15 Corrected (solid line) and uncorrected (dashed line) TLM simulation dipole current.

The influence of the second conductor on the response of the receiving rod closest to the dipole can be seen in Figure 6.16 which compares the TLM simulations for the currents in the receiver of the single rod system and in the rod closest to the dipole of the two conductor system. Both results were obtained using the resonance error correction scheme. The second rod is shifting the resonant response of the first (in the two receivers case) to slightly higher frequencies, as expected from Figure 5.2.

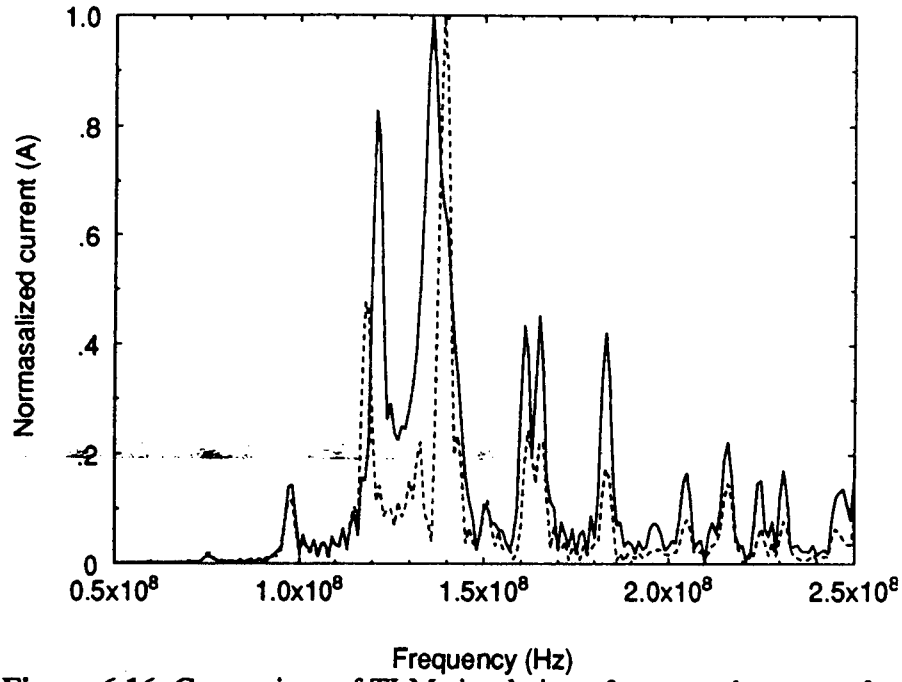

Figure 6.16 Comparison of TLM simulation of corrected currents for the single rod case (solid line) and the rod closest to the dipole in the two rods case (dashed line).

In Figure 5.3. it was shown that the likely effect of changing the separation, based on self and mutual reactance changes for two parallel, linear, dipoles of the same size, was that as the separation between the elements increased, the resonant frequency would decrease.

Figure 6.17 compares the change in location of the peak in the current of the rod closest to the dipole, at approximately 140 MHz, as the separation of the two receivers was changed. This Figure shows the TLM prediction and the equivalent experimental results. The prediction and the measurements agree well with each other and with the qualitative analysis presented in Chapter 5. The difference between the TLM results and the experimental results is approximately 1%, which is within the acceptable accuracy criteria set out in Chapter 3.

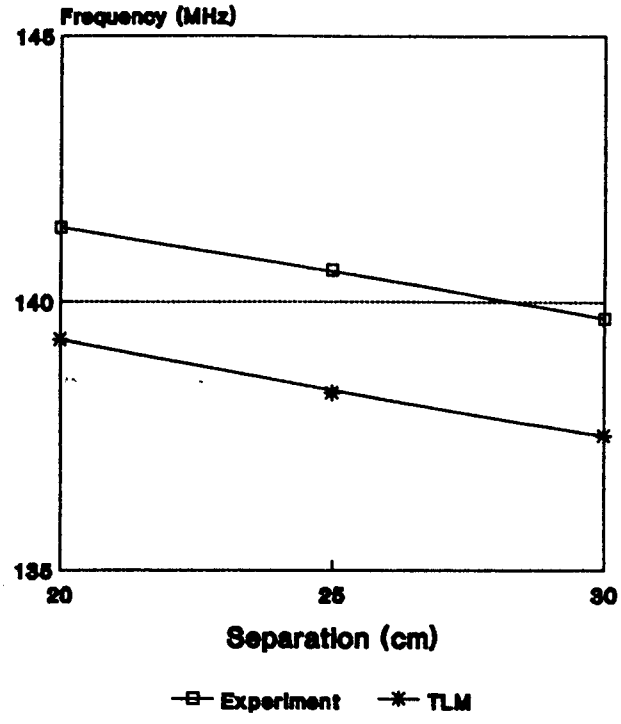

Figure 6.17 Magnitude of TLM and experimental frequency change with varying separation.

One of the points which should be noted in all the comparisons (both using and not using the resonance error correction) is that TLM simulates the general profile of the responses and the relative amplitudes of the experimental responses well. Further, the resonance error correction scheme works as well for two receivers as it does for a single one. This result is important when considering the organisation of wire looms or bundles and how individual conductors (or support spars) should be placed to obtain a specified frequency response. Depending on the particular circumstances, the prediction of the shifts in the frequency response may be of particular importance. It also provides further validation that TLM can provide a correct analysis of the effects of positional changes in such systems.

6.2. CAVITY RESULTS

Experiments and TLM modelling were undertaken for the cavity as described in §5.3 and §5.4. This section looks at the effects of the apertures on the amplitude and phase response of a signal passing along the internal wire. It considers the effect of the resonance error correction scheme of Chapter 3 on the magnitude and phase response for the enclosed cavity, and the field probed in the rectangular aperture.

6.2.1. Effect of wire model correction on TLM cavity model

Figures 6.18 and 6.19 compares the TLM simulation of amplitude and phase (obtained from one end of the wire, with the other end excited) respectively, without resonance error correction, with experimental results for the case of the enclosed cavity. Although the high Q features (the box resonance dependent features) are modelled quite accurately in both position and relative amplitude, the broader low Q features (the rod resonance dependent features) are not modelled with the same accuracy. Careful inspection of the graph will show that the undulating envelope of the rod resonance has been shifted to lower frequencies; the combination of which gives rise to the noticeably poor comparison, especially at approximately 750 MHz where the shifted rod resonance has combined with two box resonances to 'flatten' a portion of the graph which should have a pronounced slope.

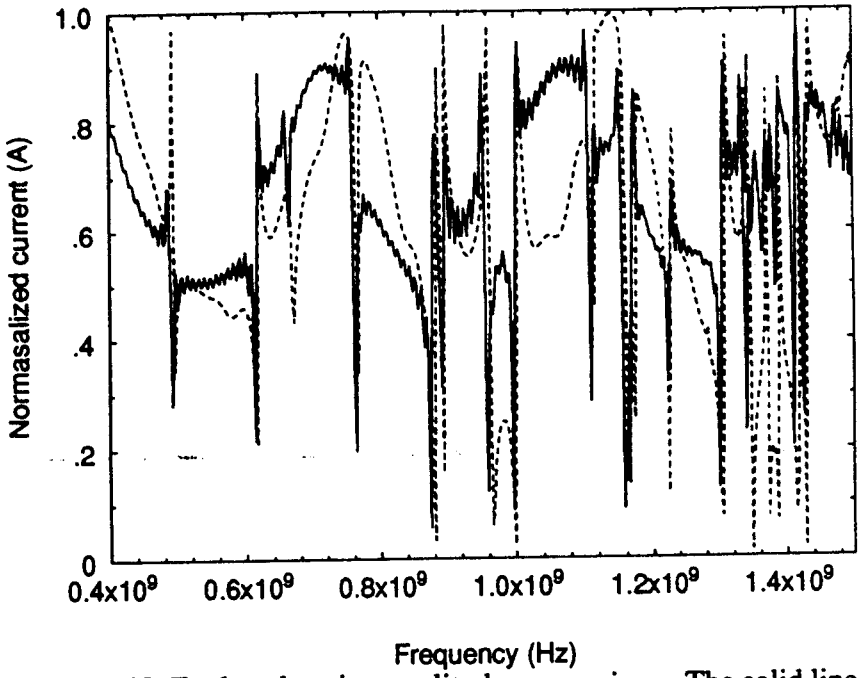

Figure 6.18 Enclosed cavity amplitude comparison. The solid line is the TLM simulation obtained without resonance error correction, the dashed line is the experimental result.

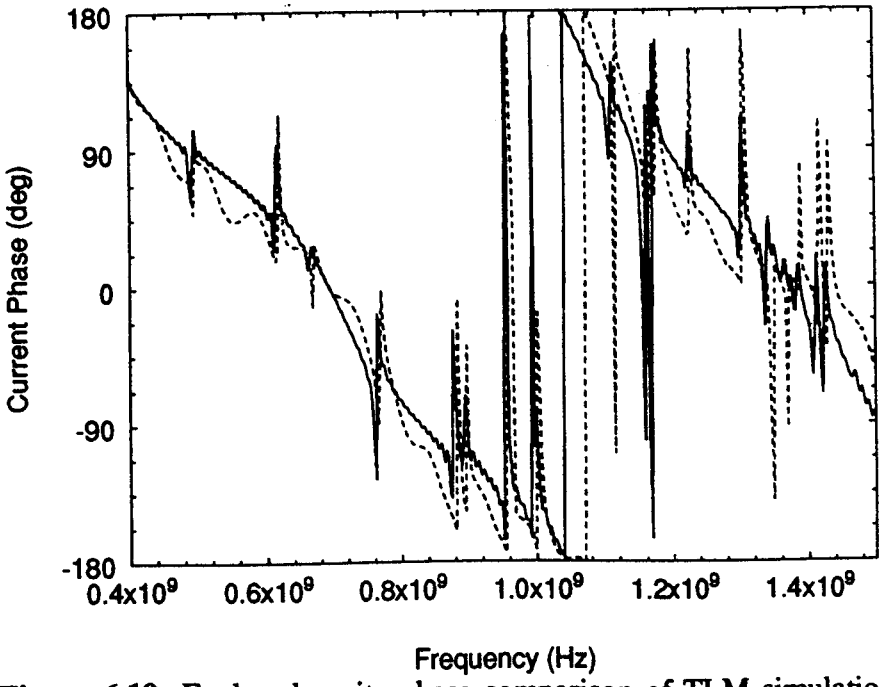

Figure 6.19 Enclosed cavity phase comparison of TLM simulatio n without resonance error correction (solid line) and experiment.

With the resonance error correction method applied to the internal rod, the amplitude and phase comparisons of Figures 6.20 and 6.21 were obtained. The overall response is clearly better. It should be noted that the correction scheme has no noticeable effect on the resonances of the box, but only of those of the wire.

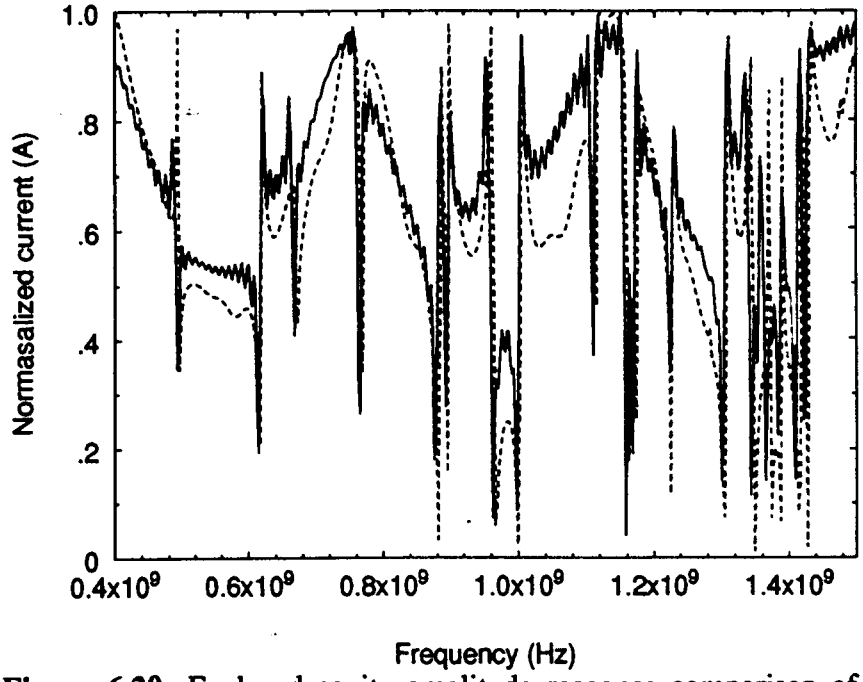

Figure 6.20 Enclosed cavity amplitude response comparison of TLM simulation obtained with resonance error correction (solid line) and experiment (dashed line).

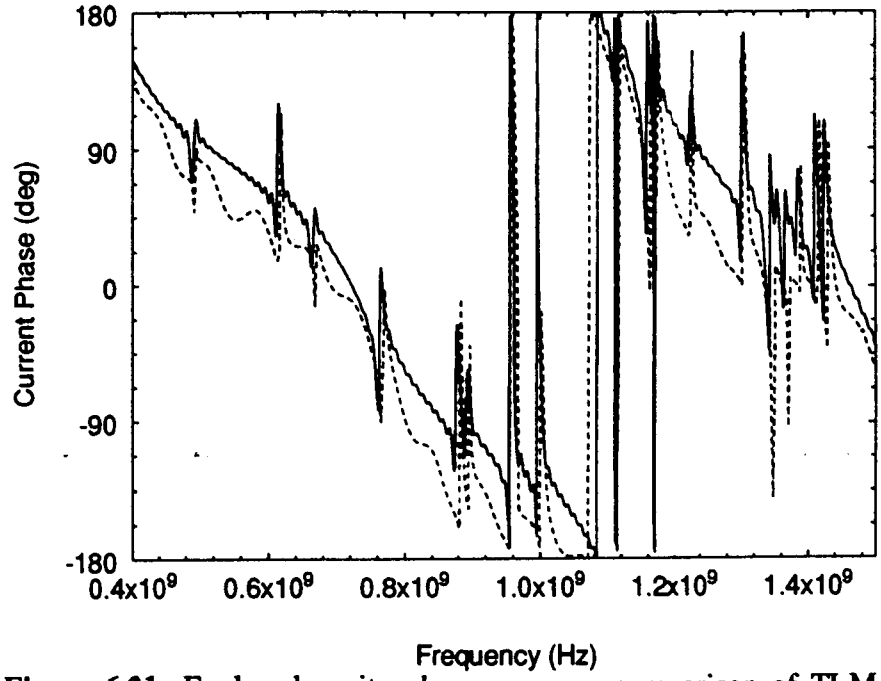

Figure 6.21 Enclosed cavity phase response comparison of TLM simulation obtained with resonance error correcetion (solid line) and experiment (dashed line).

6.2.2. The effect of apertures

The aperture lids were placed on the cavity in turn and the effect each had on the signal passing along the internal wire was recorded. The resonance error correction method was used to model the wire. The lids and box sides were modelled using internal boundaries, i.e. shorted link-lines. Figures 6.22 and 6.23 give the amplitude and phase responses for the small rectangular aperture. Figures 6.24 and 6.25 give the amplitude and phase responses for the small square aperture. Figures 6.26 and 6.27 give the amplitude and phase responses for the two aperture system. Figures 6.30 and 6.31 give the amplitude and phase response for the cross aperture.

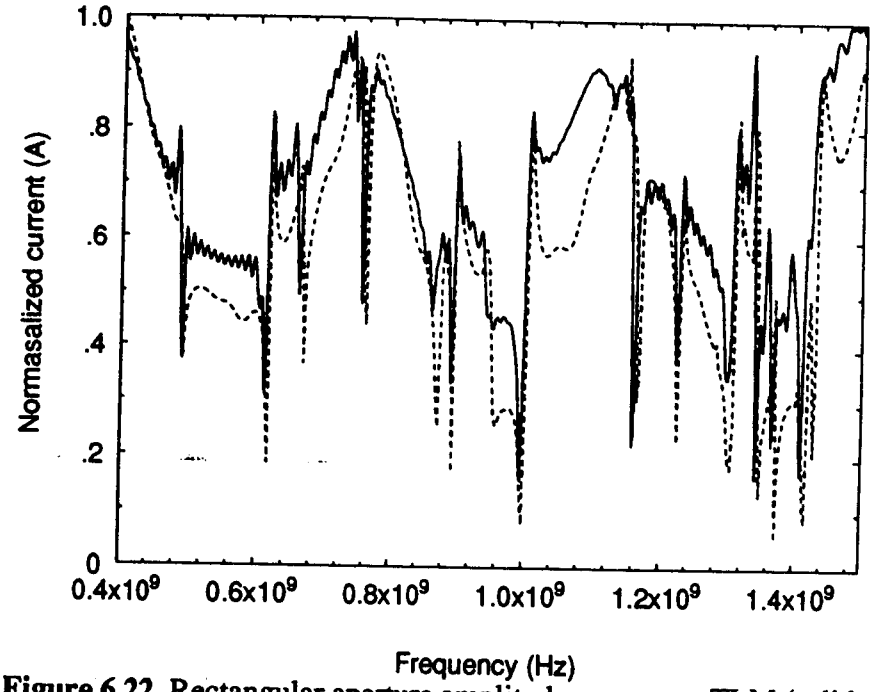

Figure 6.22 Rectangular aperture amplitude response. TLM (solid line) and experiment (dashed line).

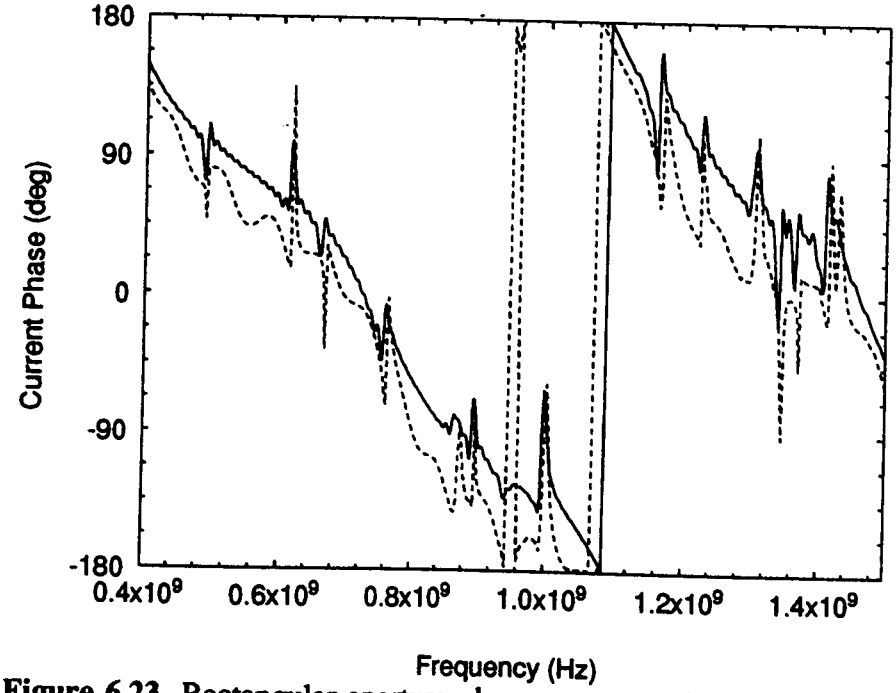

Figure 6.23 Rectangular aperture phase response. TLM (solid lin e) and experiment (dashed line).

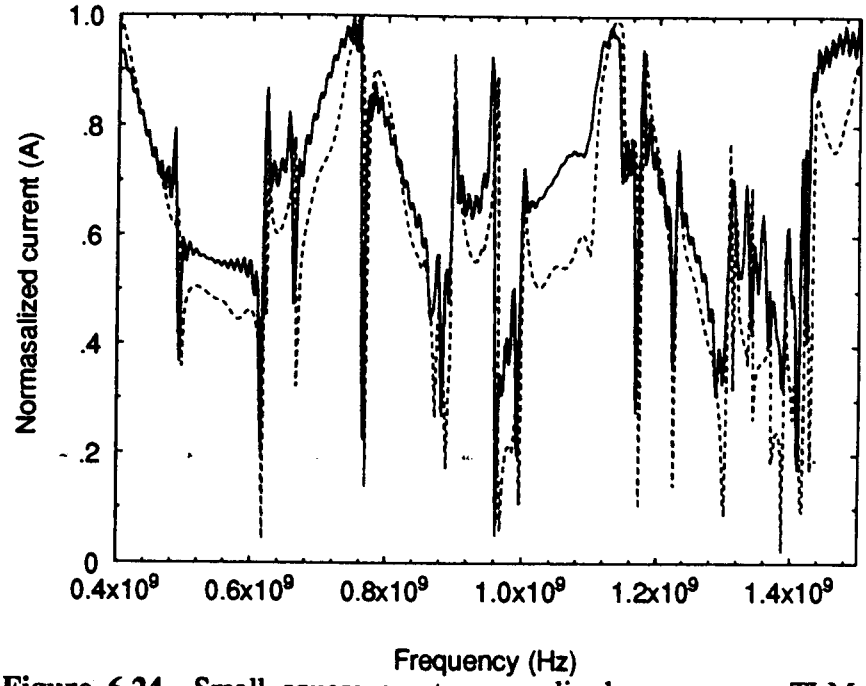

Figure 6.24 Small square aperture amplitude response. TLM (solid line) and experiment (dashed line).

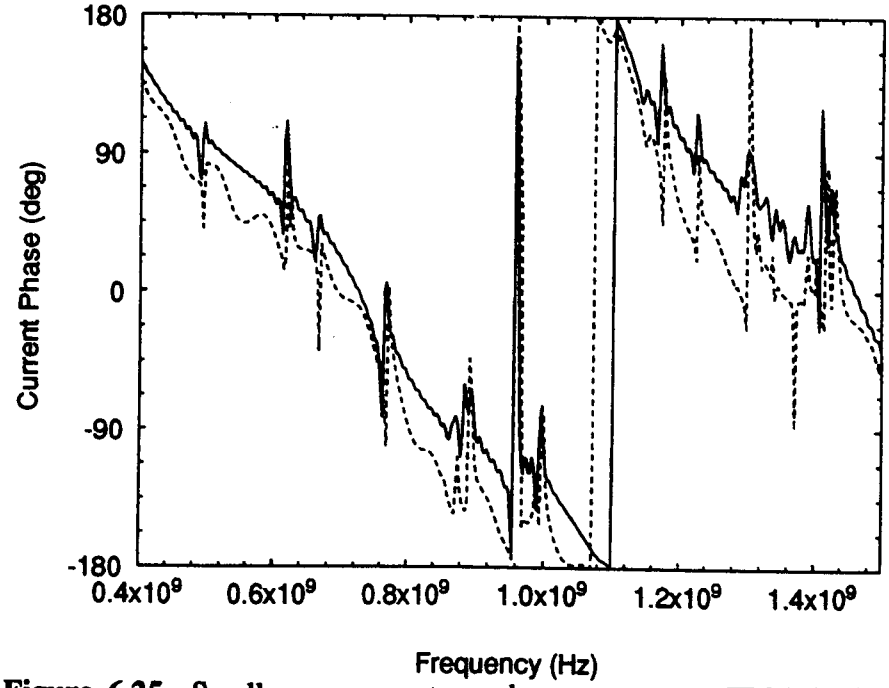

Figure 6.25 Small square aperture phase response. TLM (solid line) and experiment (dashed line).

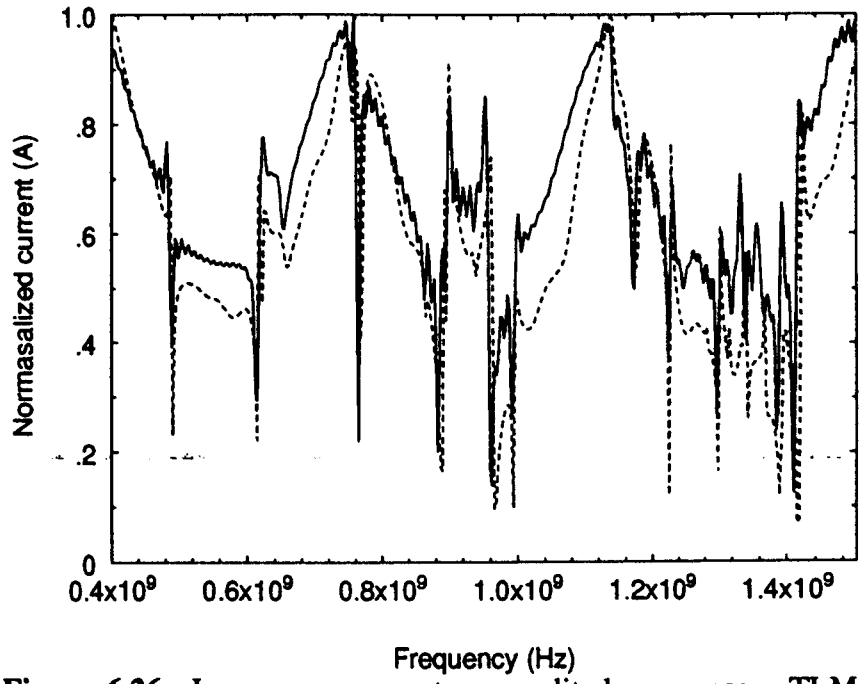

Figure 6.26 Large square aperture amplitude response. TLM (solid line) and experiment (dashed line).

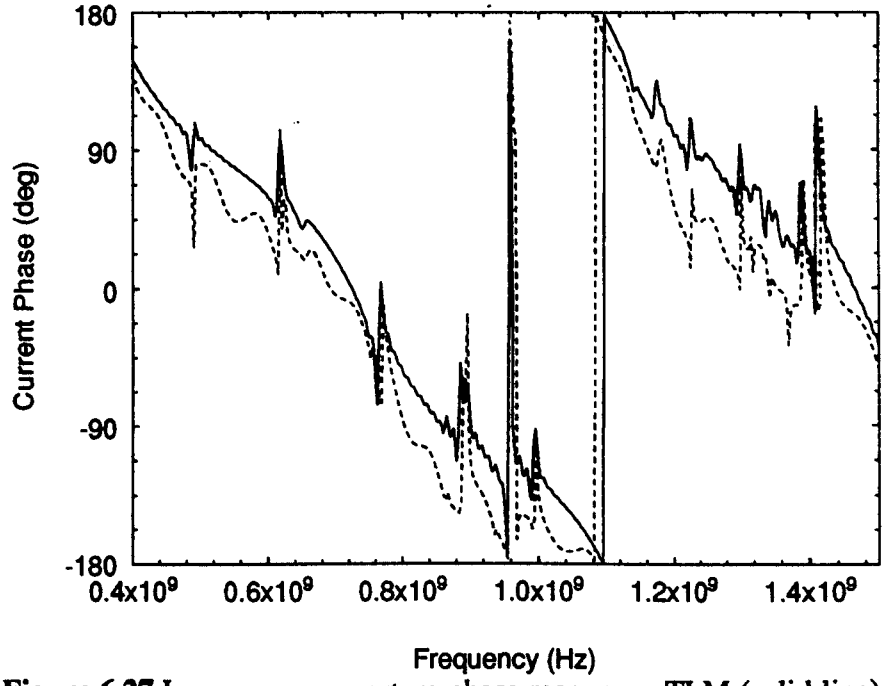

Figure 6.27 Large square aperture phase response. TLM (solid line) and experiment (dashed line).

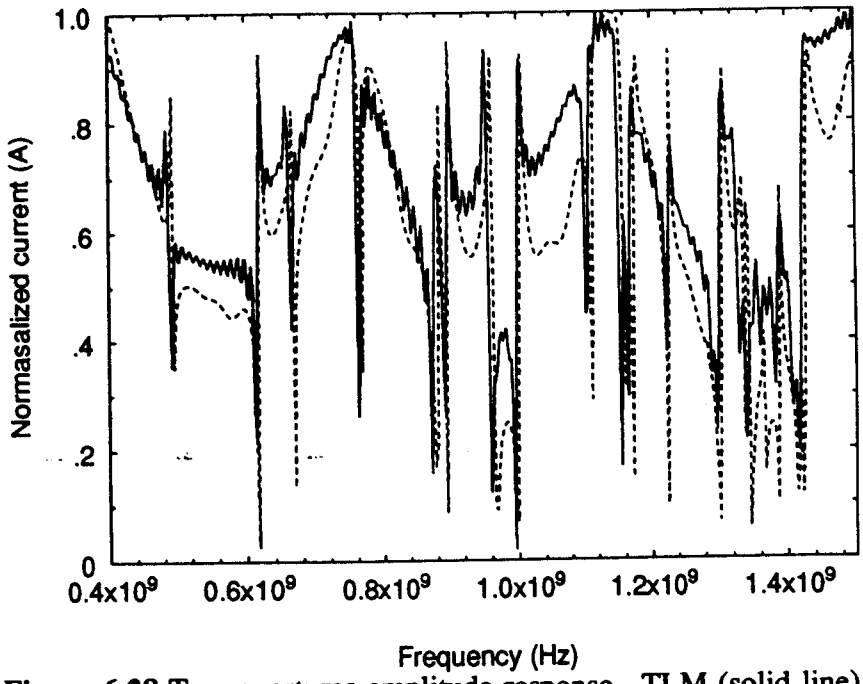

Figure 6.28 Two apertures amplitude response. TLM (solid line) and experiment (dashed line).

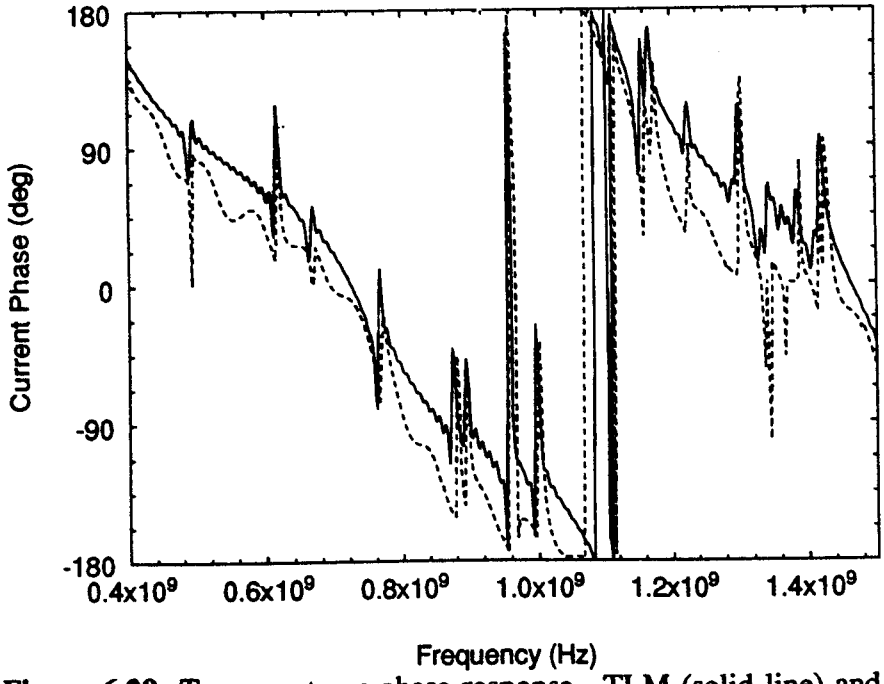

Figure 6.29 Two apertures phase response. TLM (solid line) and experiment (dashed line).

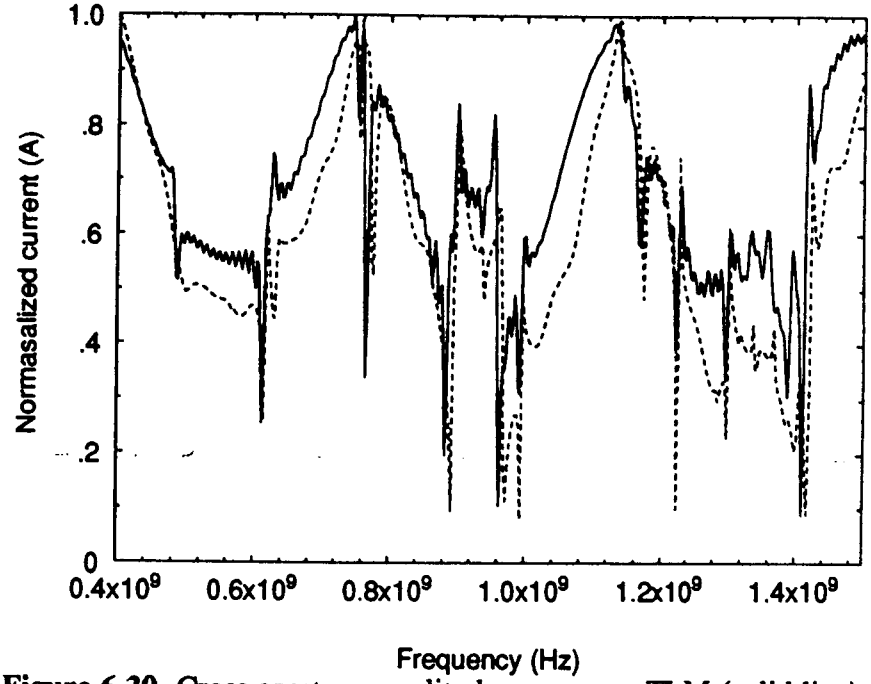

Figure 6.30 Cross aperture amplitude response. TLM (solid line) and experiment (dashed line).

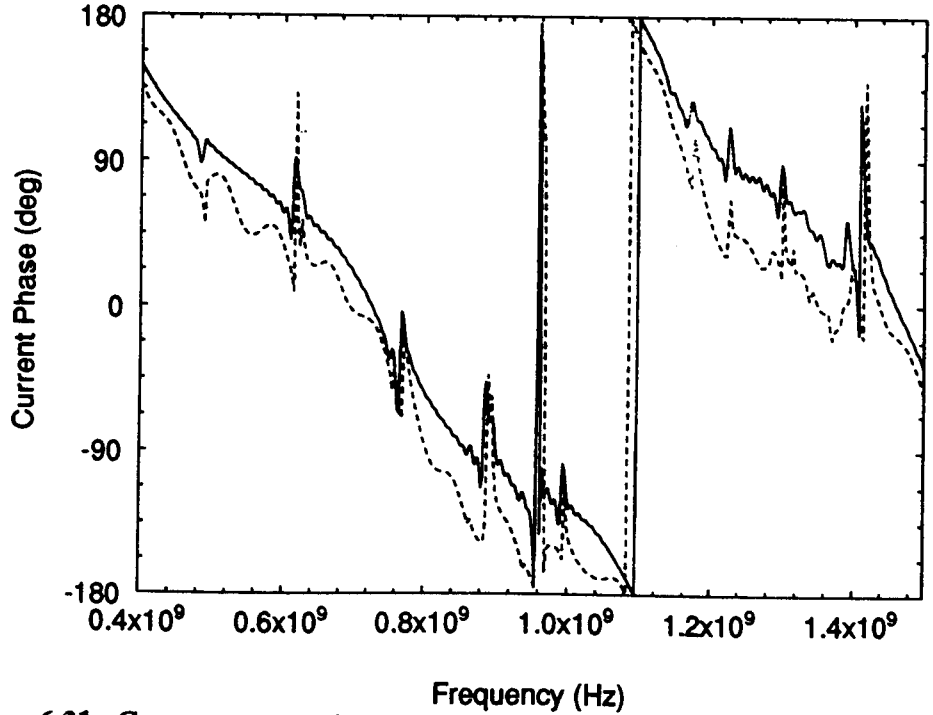

Figure 6.31 Cross aperture phase response. TLM (solid line) and experiment (dashed line).

In practical systems, such as vehicles, equipment cabinets etc., apertures of

various sizes and shapes will be found. The selection of these aperture lids was intended to reflect representative examples of those found in practice. In each case, the agreement between TLM and the experimental results is high. Further, comparison of the relative changes occurring in the response between two different apertures (comparing the TLM results together and the experimental results) is very good. The important thing to note is the relative changes in both the TLM simulations and the experimental results from one aperture type to another.

It will be seen in this set of results that the general shape of the graphs is similar and, generally, the ones with a smaller surface area of aperture have a higher density of box resonance features since the smaller aperture causes less damping. This is clearly seen when comparing the two square apertures, some of the resonances which are clearly present in the results of the small square aperture are much reduced with the large square aperture case (for example at approximately 670 MHz). The cross aperture, having the largest area, shows the smoothest curve and supports the fewest resonances. It is interesting to note the exception to this rule, which is the two aperture system. This behaves more like the enclosed system, in terms of numbers of supported box resonances and their magnitude than many of the other apertures, including those with a much smaller surface area. This is attributed to the metal separating the individual apertures dominating the overall effect by acting to support the resonances. That is, the two aperture system appears to represent a relatively insignificant loading.

For this particular cavity, there is little barrier to the size and shape of apertures which can be modelled accurately using TLM, although to model highly intricate shapes and small apertures would require a larger memory and longer run-time due to the smaller local node size required.

6.2.3. Field probed in the aperture

The field was probed in the aperture as explained in §5.3 . Figure 6.32 compares the experimental results obtained with those predicted using TLM. The agreement between the two curves in the general shape and location of features is very good.

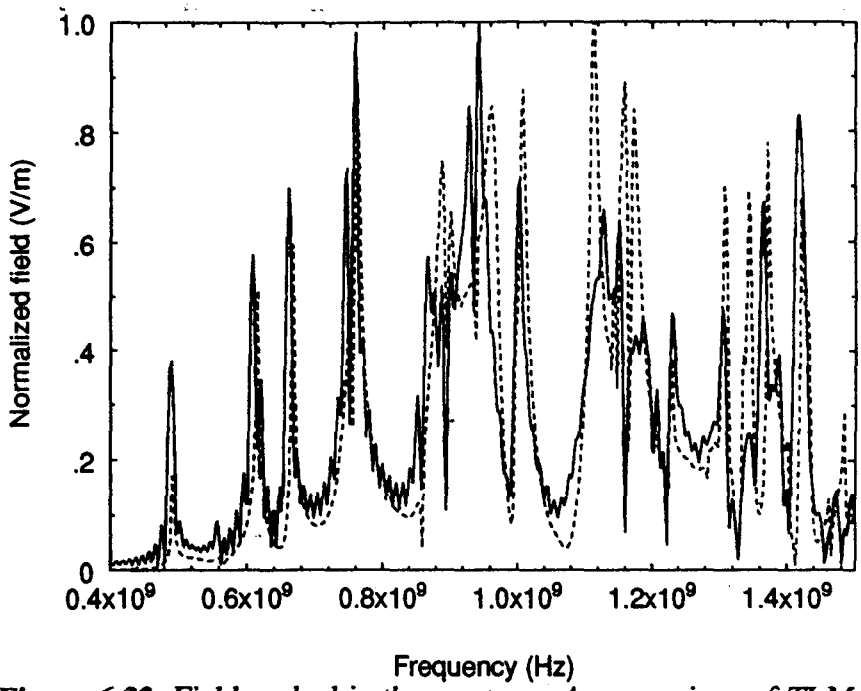

Figure 6.32 Field probed in the aperture. A comparison of TLM simulation (solid line) and experiment (dashed line). The compared electric field component is that parallel to the direction of the internal wire.

This graph shows that there are a number of frequencies at which the cavity potentially radiates well. The agreement between TLM and the experimental results indicate that TLM can be used to identify these key frequencies and those locations in the spectrum which have a very sharp response, such as at approximately 750 MHz and those which have a much broader response, such as between 800 MHz and 1 GHz. Such information may be a factor in determining

what sort of modulation could be used for an antenna, or conversely, from an electronic warfare point of view, which frequencies could be potentially problematic. Obtaining far-field data for the aperture, necessary for such analyses, would then simply require the use of TLM to map the field components at the desired frequencies in the aperture and then perform a near to far-field transform[85-87] in order to obtain the radiation pattern.

It is interesting to note the effective loss of energy from the system. Figure 6.33 shows the result of determining the difference between the output energy from the network analyzer, incident on one end of the internal wire, and that returned (both reflected from, and transmitted along, the wire). This was performed on the cavity with the small rectangular aperture, after calibrating out the cables, by measuring the reflection and transmission parameters (S_{11} and S_{21}) and determining the energy loss as:

$$E_{loss} = 1 - \sqrt{S_{11}^2 + S_{21}^2} \qquad (6.1)$$

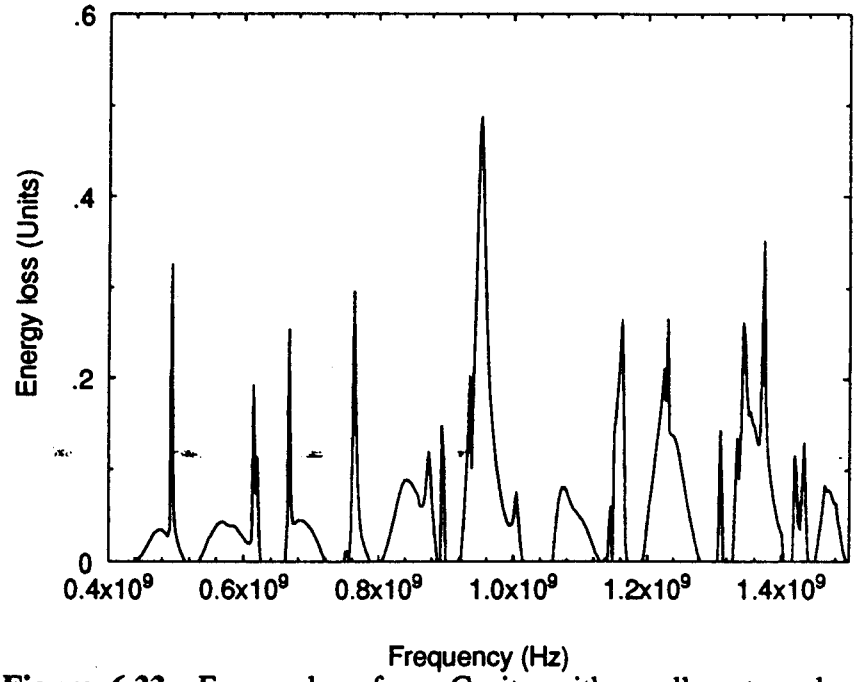

Figure 6.33 Energy loss from Cavity with small rectangular aperture, calculated from equation 6.1.

There is a close correspondence between the location of the high Q peaks of Figure 6.33 and those of Figure 6.32. This further indicates that energy is lost from the system at frequencies even below the nominal fundamental resonance of the aperture.

6.3. MODELLING CONSIDERATIONS

It is interesting to note the effect of the resonance error correction method on the run times and memory requirements for the simulations. All simulations were undertaken on a Hewlett-Packard 9000 series 710 work-station.

Without correction, the single rod screened room simulations took 7 hrs 42 mins

3 secs (7:42:3 hours) for 5000 iterations (relative to the coarse mesh). With resonance error correction they took 11:27:51 hours for the same number of iterations. The memory requirements were that the uncorrected simulations required 13 MBytes and the corrected method required 20 MBytes. 5000 iterations were found to be an adequate number for the TLM simulations in the screened room

The two receiving element simulations, again running for 5000 iterations, took 11:20:28 hours without the resonance error correction scheme and 16:55:34 hours with the correction scheme. The memory requirements were that the uncorrected simulations required 20 MBytes and the corrected method required 30 MBytes. In these cases, multigridding was used with a coarse mesh of Δl = 5 cm, requiring 91 x 47 x 45 nodes, and the two fine mesh regions totalling 80 x 115 x 25 nodes enveloping the dipole and rod individually, the single receiving rod simulation required 50 x 115 x 25 fine mesh nodes.

The cavity simulations, running for 7000 iterations took 4:21:28 hours without resonance error correction and 8:45:20 hours with the resonance error correction. The memory requirements were that the uncorrected simulations required 18 MBytes and the corrected method required 27 MBytes. 7000 iterations was an arbitrary choice which produced a result relatively free from Gibb's phenomenon[88] and ran in an acceptable time.

Clearly, the resonance error correction adds to the run time and memory requirements, with an increase in both of approximately 50%. However, these were comfortably within the memory available on the computer used, and the run times allowed the simulations to be competed overnight.

For the purposes of illustration, consider the effects of using a regular mesh or graded mesh scheme for the screened room simulations and compare these with the above figures. A Δl = 5 cm mesh took 1:32:49 hours to perform 5000 iterations, using 9 Mbytes of memory. However, this only allowed the radiating

elements to be modelled which had a much greater diameter than in the practical case (i.e. 5 cm rather than 1 cm). If this was extended to a Δl = 1 cm mesh the equivalent number of iterations for the same effective modelled time would be 25 000, giving rise to a memory requirement of 225 MBytes (assuming the platform on which this simulation was being run had sufficient space to avoid the need for memory paging) and a run time approaching 200 hours. A Δl = 0.125 cm simulation (i.e. eight nodes per side for the wires, which was previously demonstrated to have a minimal resonance error) would require 200 000 iterations, approximately 1000 hours of run time, i.e. nearly 1½ months, and 12 Gbytes of memory! Clearly these illustrative regular mesh simulations are unfeasible on the Hewlett-Packard workstation used. These figures illustrate the large saving in overhead for a low resonance error by using the resonance error correction scheme proposed in Chapter 3.

A similar analysis using graded mesh is much more difficult due to the virtually infinite permutations of node sizes. An interpretation of the possible requirements can be made by first considering that the time step, and hence the number of iterations required for a given simulated time, is determined by the smallest node size[52] (assuming cubic nodes). Thus the number of iterations would follow closely those quoted for the regular mesh case, the memory required would be determined by the actual number of nodes used and the run-time by the time-step and the number of nodes. For example, consider an hypothetical case where the Δl_{min} = 1 cm and Δl_{max} = 5 cm and the work-space required was 100 x 60 x 55 nodes. Assuming hybrid techniques were used in the implementation of the program, a memory requirement would be 20 MBytes, allowing 60 bytes per node (15 ports x 4 bytes). However, the number of iterations, required to model the same time as the multigrid simulations, would be 25 000, requiring approximately 15 hours to run.

Multigrid provides a trade-off between the potential for precise placement of objects within the work-space, provided by graded mesh and the memory and run-time advantage of a large node regular mesh.

6.4. CORRELELOGRAMS

6.4.1. The rationale for using correlelograms

An objective comparison between simulated and experimental data is difficult to undertake because of the general complexity of the signals involved. As described previously, a 'by-eye' comparison is difficult to quantify, although it is the most convenient method of comparing signals. Correlation alone is not sufficient for anything other than simple signals, i.e. those with a single peak or trough, because the resulting single value contains insufficient information to convey a clear comparison of the overall response.

Correlelograms, implicitly related to correlation, have a greater potential because there are a number of parameters which can be derived from them which adds to the generality of the comparison. Further, they reduce a potentially complex comparative graph to a much simpler curve or set of curves. This will be illustrated in the following sections.

6.4.2. Correlation and correlelograms

The correlation coefficient is widely used in signal processing to determine the extent to which two functions are related[89,90]. The correlation coefficient has a value $\leq |1|$. For example, two unrelated, random, functions will be uncorrelated and thus have a correlation coefficient of zero, whereas the auto-correlation of a function (i.e. a function correlated with itself) will have a correlation coefficient of 1.

A computationally efficient method of computing the correlation of two discrete data sets having the same number of samples, employs the Wiener-Khinchine theorem. The Wiener-Khinchine theorem states that the correlation between two signals $\{R_{xy}[p]\}$ can be computed
from the signals x(n) and y(n) as:

$$\mathcal{F}(R_{xy}(p)) = X^*(\omega) \cdot Y(\omega) \qquad (6.2)$$

i.e. the Fourier transform of the correlation is the product of the complex conjugate of the Fourier Transform of x(n) multiplied by the Fourier Transform of y(n). Consequently, the correlation coefficient can be determined by

$$R_{xy}(p) = \mathcal{F}^{-1}[X^*(\omega) \cdot Y(\omega)] \qquad (6.3)$$

Speed is the advantage of performing the correlation this way, rather than using the discrete method which is easier to program. The discrete and the Fourier Transform methods will possibly not give exactly the same results because the Fourier Transform method assumes an underlying periodicity of the signal which may not be an accurate assumption. Also, the Fourier Transform method requires that the number of data points used is a power of two.

Correlelograms are obtained by cross-correlating one function with a shifted version of the other function, shifted on a point by point basis. Thus giving rise to a graph which will, in the case of an auto-correlelogram, have a maximum of unity at zero shift and will be symmetrical about the mid-point.

It is possible that the two functions to be compared, x(n) and y(n), may be highly related, but one of them may have a linear off-set (in frequency) from the other, or it may be 'stretched' relative to the other signal, e.g. the manifestation of the wire resonance error in TLM in the time domain. These differences have been investigated with respect to DNA finger-printing, although generally applicable, and can be accounted for in the analysis[80].

6.4.3. Parameters derived from correlelograms

There are three parameters which have been derived from the correlelograms for the purpose of comparing experimental and modelled data. These are:

the maximum value of the cross-correlelogram, whether it was it obtained after a shifting or stretching process, and if so by how much.

the degree of asymmetry of the cross-correlelogram, this can be displayed graphically or as an RMS value defined by

$$S_{rms} = \frac{1}{N}\left[\sum_{p=1}^{\frac{N}{2}-1} \left(R_{xy}[p] - R_{xy}[N-p]\right)^2\right]^{\frac{1}{2}} \qquad (6.4)$$

the RMS difference between the auto-correlelogram of x $\{R_{xx}[p]\}$ and the

cross-correlelogram between x and y, $\{R_{xy}[p]\}$, which can also be displayed graphically or as an RMS value defined by

$$D_{rms} = \left[\frac{1}{N} \sum_{p=1}^{N} (R_{xx}[p] - R_{xy}[p])^2 \right]^{\frac{1}{2}} \qquad (6.5)$$

It is proposed that, when taken together, the three measures would give a more comprehensive, and quantitative, view of the comparison. If stretching or shifting is required to improve the comparison significantly, it indicates a fundamental characteristic associated with the method or the implementation of it, e.g. the resonance error described in Chapter 3. Also, the use of the correlelograms, and the graphical representation of the parameters derived from it, help to remove the 'human element', a sub-conscious bias in the analysis of the results, from the comparisons.

Examples of the application of correlelograms will be given in §6.4.4. which will consider the screened room coupling problem of a single receiving wire and the signal flow in an enclosed cavity.

6.4.4. Examples of the application of Correlelograms

Figures 6.1 and 6.2 compared the TLM simulation of the current induced in the rod in the case of the single receiving rod illuminated by a linear dipole in the screened room. A 'by-eye' comparison of these two graphs indicates that Figure 6.2 shows a better fit between the experimental and TLM results than Figure 6.1. The problem is to determine how much better. The same problem can be seen when analyzing Figures 6.18 and 6.20 for the enclosed cavity. Both these pairs of Figures compare the effects of the resonance error correction.

Figure 6.34 shows the auto-correlelogram of the experimental data and the cross-correlelograms of the modelled data in Figures 6.1 and 6.2. The frequency range adopted was 50 MHz to 177 MHz in order to allow 128 points with 1 MHz separation between them. The maximum value of the cross-correlelogram of the simulation obtained without using the resonance error correction was found to occur with a shift of one point (1 MHz) to higher frequencies, it is this pre-shifted correlelogram which has been displayed here. It will be noted that the resulting correlelograms are generally simpler in structure than the original data, making them easier to compare. The asymmetry curves and the difference curves for the two comparisons are shown in Figures 6.35 and 6.36 respectively. The peak values of the correlelograms and the asymmetry measure and the difference measure are summarised in table 6.1

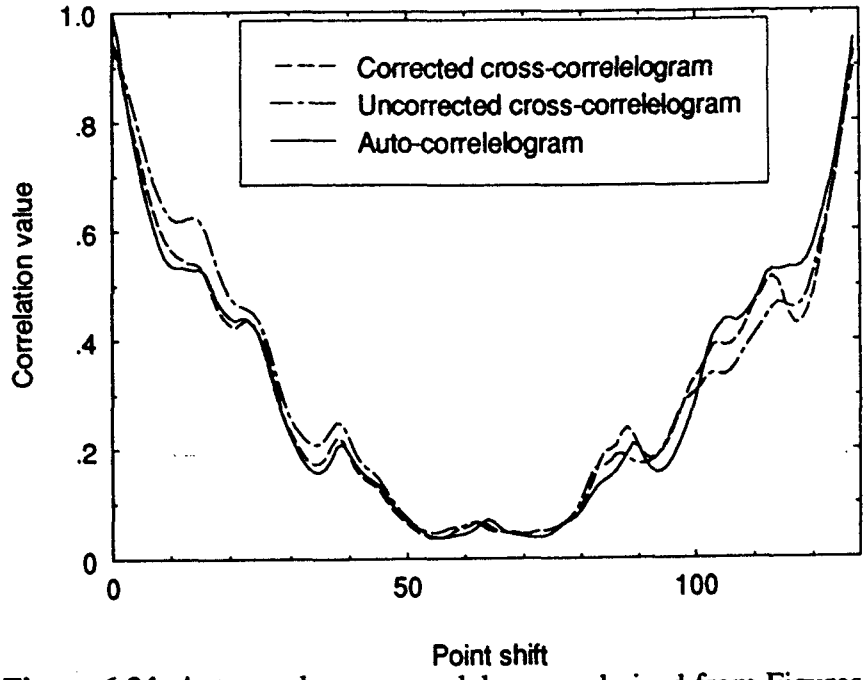

Figure 6.34 Auto- and cross-correlelograms derived from Figures 6.1 and 6.2

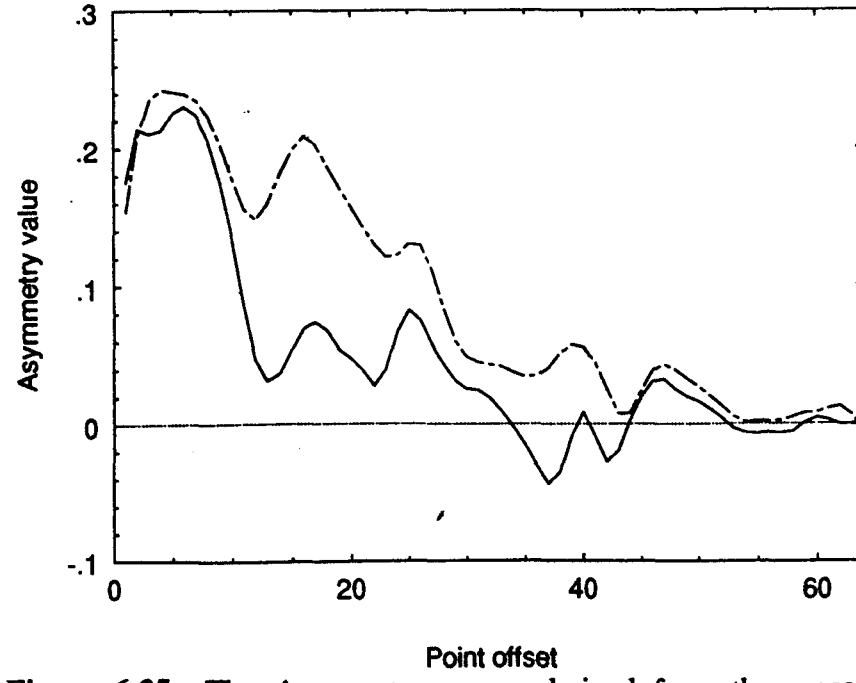

Figure 6.35 The Asymmetry curves derived from the cross-correlelograms of Figure 6.34. Solid line with resonance error correction, dashed line without.

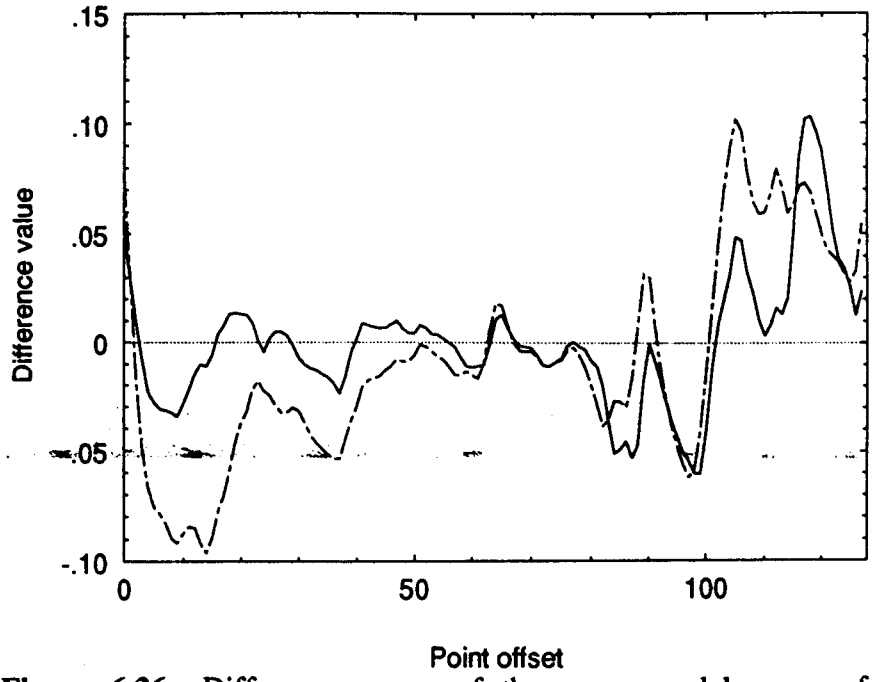

Figure 6.36 Difference curves of the cross-correlelograms of Figure 6.34 with the auto-correlelogram of Figure 6.34. Solid line with resonance error correction, dashed line without.

	Correlation Coefficient	Asymmetry (rms)	Difference (rms)
Without correction	0.925 (1 point shift)	0.12	0.047
With Correction	0.964	0.087	0.030

Table 6.1 A comparison of the three parameters (correlation coefficient, asymmetry value and difference from auto-correlelogram) obtained from the data of Figures 6.1 and 6.2.

The results confirm the 'by-eye' conclusions that the simulations obtained by using the resonance error correction method agree more closely with the experimental data than that obtained without the correction. In both cases the

correlation coefficient is high and the asymmetry and the difference measures are low, but in the case of the simulation obtained with the correction scheme these values are closer to the ideal values of unity, zero and zero respectively. Hence an objective measure of the closeness of fit of the simulations has been produced.

Figures 6.37, 6.38 and 6.39 show the correlelograms, the asymmetry curves and the difference curves for the enclosed cavity comparisons of Figures 6.18 and 6.19. Table 6.2 lists the rms values and the peak correlation coefficient.

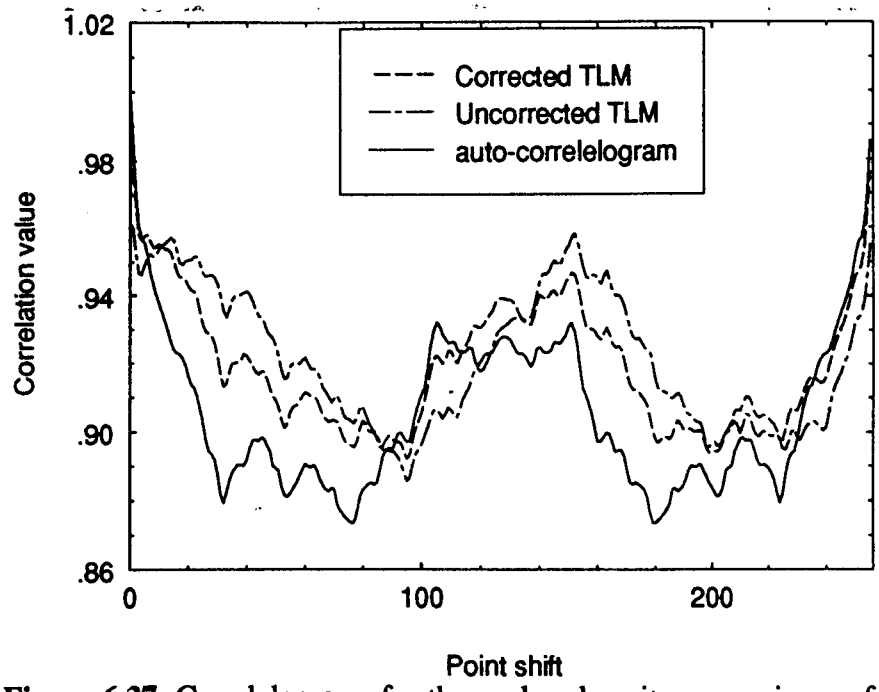

Figure 6.37 Correlelograms for the enclosed cavity comparisons of Figures 6.18 and 6.19.

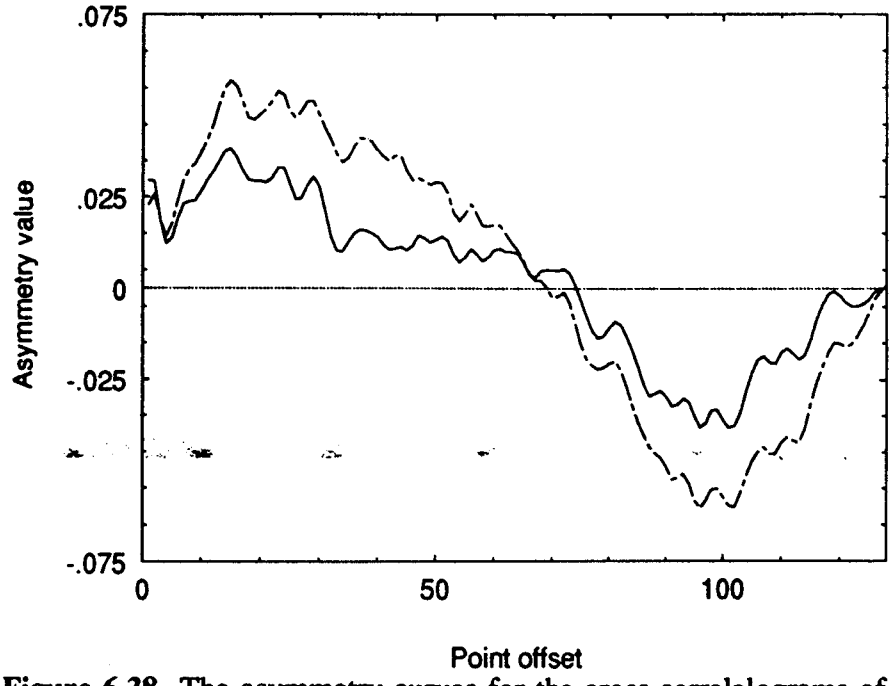

Figure 6.38 The asymmetry curves for the cross-correlelograms of Figure 6.37. Solid line with resonance error correction, dashed line without.

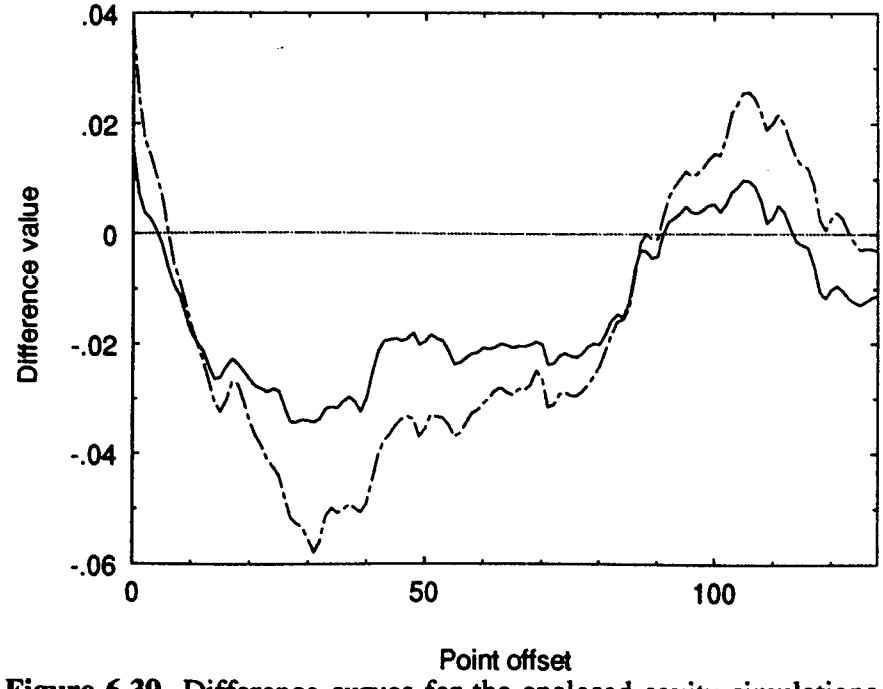

Figure 6.39 Difference curves for the enclosed cavity simulations of Figure 6.37. Solid line with resonance error correction, dashed line without.

As with Table 6.1, these values confirm the level of improvement. In the resonance error corrected results, the peak value of the cross-correlation is again closer to unity and the asymmetry and difference values are again closer to zero. However, it is interesting to note the shape of the cross-correlelograms, especially the way in which neither required a shift to gain maximum correlation, but the simulation without resonance error correction displayed a marked shift of the central portion of the cross-correlelogram away from the middle of the graph. This shift was reduced in the simulation obtained using resonance error correction. The probable explanation for this is that the high Q features of the cavity resonances dominate the overall response of the structure, hence, although the internal wire is subject to the resonance error, this is not sufficient to cause a required shift for maximum correlation. The shift in the cross-correlelogram appears to be illustrating the resonance error, this being highlighted specifically by the asymmetry value.

Further work is required to determine the significance and inter-relatedness of these values.

	Correlation Coefficient	Asymmetry (rms)	Difference (rms)
Without correction	0.962 (no shift)	0.037	0.028
With Correction	0.984	0.021	0.018

Table 6.2 A comparison of the three values (correlation coefficient, asymmetry value and difference from auto-correlation) obtained from the correlelograms of the enclosed cavity data.

6.5. SUMMARY

This Chapter has presented the experimental and modelling results for the two screened room configurations and the cavity configuration, with and without apertures. A discussion of run-times and memory requirements was presented for TLM simulations of the two test environments. Finally, a discussion of correlelograms was presented - these show promise for use in the quantitative evaluation of simulations.

CHAPTER SEVEN
DISCUSSION AND CONCLUSIONS

Chapter 6 presented results for the verification tests described in Chapter 5. This Chapter discusses those results as well as the general approach to the solution of the resonance error and measurements in screened rooms. Some general conclusions and recommendations for further work complete this chapter.

7.1. SOLUTION TO THE RESONANCE ERROR

This section considers both the solution to the resonance error proposed in this Thesis, and compares it with the solution for coarseness error proposed elsewhere[70,71].

7.1.1. Resonance error correction

A problem which affects the simulation of wires by TLM when using the integrated solution method, with wires modelled by a single node cross-section, has been identified. The problem manifests itself as a reduction in the resonances of the wire by approximately 10%, it has therefore been termed 'resonance error'. The cause of the error was determined to be due to the external corner nodes delaying signals propagating around the wire. The reason for this delay is that the path imposed on the signal by the shape of the nodes is longer than the path

which the signal would take in a practice. The method of overcoming the error was to speed up the propagation around the corners by reducing the relative material properties from the background values in the vicinity of the wires and thereby increasing the relative velocity. The correction was done in this way rather than by physically reducing the path length around the corners as the latter would rely on the development of new node type, or types (one of the requirements of the solution to this error was that no new node types, other than the standard symmetrical condensed node, would be used). Preliminary results for a simple test structure were very encouraging. A more rigorous validation was undertaken by comparison with experimental results.

The experimental verification tests required a high level of confidence to be placed on the results obtained from them. As a result, a significant effort was put into the determination of the accuracy and repeatability of the test environments. The investigations undertaken into the test environments will be discussed in §7.2.

It would be possible to provide a 'fix' for this error in a simple linear response system by re-scaling the frequency axis to account for the error. Unfortunately, the wire resonances are usually combined with those of other structures, such as the cavity or screened room, which makes a simple frequency-scaling correction impractical because of the wire resonances being subject to the error but the enclosure resonances are not. Thus, because realistic situations exhibit such a compound behaviour, the error needs to be corrected at its source.

7.1.2. A comparison of resonance and coarseness error correction.

The term 'resonance error' was used initially in this Thesis as it summarises the manifestation of the problem. A similar problem has been reported in 2D structures with external corners, i.e. the resonant frequencies of such structures are modelled as being lower than the theoretical ones[91]. This error was worse as the model bacomes coarser, i.e. the resolution of the model is decreased, and was thus termed coarseness error. This coarseness error was recently discussed and a compensation scheme was proposed[70]. Also, the modelling of strip-line structures in 3D was investigated[71] and it was found that the strip-line resonances were lower than the expected values. Both the 2D and 3D systems discussed are subject to errors which have the same manifestation as the resonance error.

Both the 2D coarseness error and the stripline resonance error problems were attributed by other researchers to poor direct communication of nodes adjacent to the corner or edge with the appropriate corner or edge.

The specific explanation given of the cause of the coarseness error in these cases was that the node diagonally adjacent to a corner had no direct electromagnetic interaction with that corner. Two solutions were proposed by other workers for the 2D coarseness error, these were direct compensation and non-direct compensation methods. The first, the direct compensation method, relies on adding a short circuit stub to the 2D node which effectively provides a direct connection between the node and the corner. Figure 7.1 describes the method and indicates the value of the link-line admittances. The stub admittance was determined empirically.

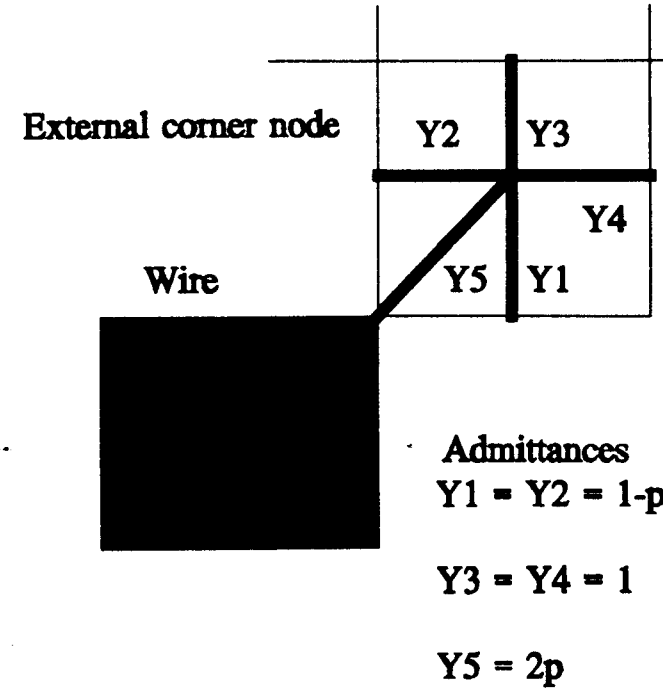

Figure 7.1 Node used in reference 70 to compensate for 2D coarseness error, showing the admittances of the link-lines and stub.

The non-direct compensation relied simply adding a $\Delta l/2$ stub and leaving the link-line admittances unchanged. Again, the value of the stub admittance was determined empirically.

The 3D stripline error correction involved the modification of the symmetrical condensed node so that the metal boundaries would lie within the nodes, rather than as shorted link-lines. Two types of nodes were introduced, these were a 'half node' which was a symmetrical condensed node bisected by the boundary and the an 'edge node' which modelled the edge of the boundary within the node. The results obtained from both the 2D and 3D correction showed a significant improvement over the uncorrected methods. Both also attributed the cause of the error to the poor communication of the nodes adjacent to the corners or edges, although neither presented any evidence to support this. The work presented in this Thesis indicates that the cause of error is the actual communications path differing from the desired path, although this is partly caused by the poor communication of the corner nodes with the corner it is subtly different. It is

highly likely that the analysis of the cause and solution to the resonance error is also appropriate to the other problems discussed in this section such as the modelling of striplines, although this needs further investigation.

7.2. EXPERIMENTAL CONFIGURATIONS

Two configurations were investigated experimentally, these were a linear dipole illuminating a rod (or rods) of the same dimensions as the dipole in a screened room, and a rod passing along the length of an enclosed cavity. These two configurations were used as the basis for the validation tests

Factors investigated for the screened room configurations included the cables and the positioning of the dipole and rod. It was found that with ferrite beads placed at intervals around the cables, the experiments were highly repeatable. Further, the accuracy of the measurements were found to be high, based on the comparisons with the TLM results obtained.

Factors specific to the cavity were mainly involved with determining the optimum connection of the internal rod to the outside world. This was performed simply by using BNC connectors which satisfied the list of requirements presented in §4.4.1. Again, the results were highly repeatable and, as will be discussed in §7.4., agreed closely with the predictions of the TLM model.

7.3. SCREENED ROOM VERIFICATION TESTS

The test results presented were of the coupling from a feed dipole placed within a screened room to both a single receiving rod and two closely spaced rods. The current in one arm of the dipole was also measured. It was previously found that the currents in both arms of the dipole were the same - provided the cables were loaded with ferrite clamps.

The dipole signal contained a large number of features over the frequency range chosen. These features were a combination of the high Q room resonances and the broader, low Q, dipole resonance. In the case where the resonance error correction was not used, the frequency shift in the TLM results was such that, in certain cases, nominally adjacent features were almost overlapping when compared with experimental results. With correction, the TLM results became much closer to the measurements. In both cases, the distinct shapes of the individual features were predicted well, showing the way TLM predicts the latent behaviour of such a source of radiation and its interaction with a complex environment.

The results for the rod(s) appeared more sensitive to the resonance error correction method than the dipole current. This was because the rod results were combinations of their natural resonances, the source effects of the dipole, and also effects due to the proximity of the bench. The current on the single rod showed how well the resonance error correction method worked, especially with regard to the broadness of the main peak.

Two receiving rods replaced the single receiving rod in a further set of experiments. This allowed the comparison experimental and TLM results for a system with closely coupled (mutual) impedance. TLM predicted both the behaviour of two closely spaced conductors in the screened room and also the effect of changing the separation of two conductors. In both cases, simulations

agreed well with experimental observation.

Both the corrected and the uncorrected TLM simulations showed that the general behaviour of such systems could be determined well. The results obtained using the correction scheme were in better agreement with the experimental results.

In general, the predictions made using TLM, incorporating the correction to the resonance error, are sufficient for most EMC purposes in that the location of the features in the frequency domain agreed well between the simulations and the experimental observations.

7.4. CAVITY RESULTS

Studies were undertaken which compared the effect of a cavity and associated apertures on the signal passing along a wire internal to the cavity. Initial comparisons of the TLM and experimental amplitude and phase response, obtained by exciting one end of the internal wire and taking output at the other end, show how well TLM predicts the behaviour of the cavity studied. The overall response of the signal is a combination of the high Q box resonances and the low Q rod resonances. Without resonance error correction, the rod resonances are subject to a shift in response to lower frequencies. This has the effect of causing the overall response to appear dramatically different at certain frequencies (for example 800 MHz in Figure 6.18). With the wire resonance error correction scheme incorporated into the model, TLM has been shown to predict resonant frequencies and the effect of apertures to a high degree of accuracy.

The number of high Q features can be seen to be higher in the cases where the aperture area, and hence the amount of damping, is lower. Clearly, this is a straightforward effect of energy loss for certain frequency components, although

the level of the effect of particular components may not be easy to determine analytically. The overall agreement between TLM and the experimental results is good vindicating the use of TLM for this type of study.

The field probed in the aperture gave good agreement between the TLM prediction and the measurements for the location of features.

Although rarely used in the EMC community, phase was used as a means of comparing results due to its sensitivity to change. The phase comparison results also showed a high level of agreement and provided further evidence of the applicability of TLM to the propagation and coupling of electromagnetic radiation in complex environments, typical of many EMC problems.

7.5. RESOURCE REQUIREMENTS

Values were presented in §6.3 which compared the effects of the correction scheme on both the memory requirements and the run-time of the simulations. It is clear that more memory and a longer run-time is required to undertake simulations with such a correction scheme due to the addition of stubs to the nodes in most of the work-space. However, the decision to be made is whether the extra resource required is justified by the improvements in the results obtained. That question is rather subjective and the answer would be dependent on the person answering as well as on the limitations of the host equipment. It was considered that, for the simulations undertaken here, the trade-off between the run time and accuracy of the simulation was acceptable. Also, the length of time the simulations took to run allowed them to be run overnight on a standard Industry platform, adding further credibility to the use of TLM to model realistic coupling problems in an acceptible time.

7.6. THE APPLICATION OF CORRELELOGRAMS TO VALIDATION

Correlelograms were introduced in §6.4 as a means of quantifying the closeness of a simulation to the experimental results. The examples given showed their potential use.

It is envisaged that correlelograms will be particularly useful when comparing the results of several different modelling methods, especially when the results are quite complex - such as the screened room or cavity results - and a single number such as that obtained from a straightforward correlation of the data therefore conveys very little information. Three values were identified as being of particular use. These were the peak values of the correlelograms, the RMS value of the difference of the cross-correlelogram from the auto-correllelogram of the experimental data, and the RMS value of the asymmetry of the cross-correlelogram. Although these values are related, they are considered sufficiently different so that, taken together, quantitative comparisons of several simulations with experimental results can be undertaken relatively objectively.

Further work is required in order to determine the significance of the actual numerical values of each of the three parameters.

7.7. GENERAL CONCLUSIONS

This thesis has addressed the coupling of electromagnetic waves into wires on two fronts: experimentally and by modelling using TLM. These two approaches were unified in the use of TLM for electromagnetic coupling between wires in complex environments which can be considered to be representative of typical EMC problems. Further validation was provided of a modification of the TLM method which was designed to overcome a problem with the modelling of wires.

The points which can be stated as the main conclusions of the work described in this Thesis are that:

experiments in the screened room and the cavity can be made repeatable and accurate provided that certain 'good experimental practices' are employed.

the good comparisons between the experimental results and the TLM simulations indicate that TLM is a powerful numerical modelling tool to be used for EMC studies.

the modelling of wires using the resonance error correction scheme allows them to be modelled with a high degree of accuracy, thus overcoming one of the fundamental problems associated with the modelling of wires in TLM.

A perenial limitation on numerical modelling methods is that the complexity of problems required to be solved will always be greater than the abilities of the method or its implementation. TLM is no exception to this, the main limitation being that of the computer resource available. The simulations described in this Thesis are generally within the maximum size which can be run on a standard platform. By way of example, consider a work-station whose available volatile

memory is 32 MBytes (this is a typical figure and will undoubtedly appear small in the relatively near future). Assume also that the real and imaginary parts of material properties will be required to be changed and stub loaded symmetrical condensed nodes will be used. Hence, each node would have 24 ports and, with four bytes per real variable, would require 96 bytes of storage. Thus a workspace of approximately 350 000 nodes would result. This is approximately equivalent to 7^3 wavelengths, a system requiring no stub loading of symmetrical condensed nodes would be able to model a work-space of approximately 9^3 wavelengths. These figures are only illustrative, as the amount of available memory depends on the actual machine used.

The other limitation is run-time. Generally, end-users do not want to have simulations running for days, except very ocassionally. It is more common for them to require an almost instantaneous answer or at worst to run simulations overnight, giving a maximum permisible run-time of the order of 16 hours. In this respect, the problems undertaken in this Thesis have been approaching the acceptable limit.

With these limits in mind, the simulations which can be undertaken at present are relatively simple as the methods and the computers on which they run have not developed sufficiently to allow a full pcb and cabinet electromagnetic analysis. However, it is important that the simpler systems are understood first as they form the basis of more detailed studies and allow the user an insight into the fundamental mechanisms involved in interference propagation.

The complexity of models which can realistically be tackled will increase as the speed and available memory of standard Industrial computing platforms improves. Further increases in complexity will occur as the efficiency of the TLM method increases. This will come about through optimisation of the algorithms, possibly for particular applications and also further development of techniques such as multigridding, accurate matched (free-space) boundary modelling and the hybridization of several different methods to utilize the beneficial features of each

without any of their shortcomings.

It was found that the use of TLM simulations and experiments in tandem was much more beneficial than doing either in isolation. The benefits of mutual validation were found to be important in the identification of problems: for example, TLM helped to identify the problems originally caused by the cables in the screened room and the experimental results helped to identify the resonance error problem and the generality of its solution.

7.8. SUGGESTIONS FOR FURTHER WORK

The work reported in this Thesis has verified the TLM method against experimental results for a number of EMC configurations. Taken together, these comparisons give a high level of confidence in the generality of this approach. Several further investigations would be beneficial for a fuller understanding of the coupling of electromagnetic waves into wires both experimentally and using models. By the very nature of research, as one question is answered, further questions arise. However, the following are some of the more fundamental areas where further work is required:

to extend the frequency ranges of the experiments. Current EMC regulations extend to 1 GHz and are likely to extend beyond this in the forseeable future. Also specific interest may be given to certain spot frequencies, such as 2.45 GHz, the frequency used for microwave heating, if equipment may be operated in that sort of environment.

to investigate further wires being modelled with diameters less than the Δl of the node in which they are placed, but without any of the disadvantages of wire nodes and separated solution methods described previously. This

may be achieved by using the resonance error correction method with material properties lowered further than those used to correct for the error. This would have the effect of making the wire diameter appear smaller than it is in the model. For example, it may be possible to get adequate simulations of the screened room configurations using only Δl = 5 cm nodes, but model the transmitter and receiver with 1 cm diameters.

to study the coupling into the enclosure through the apertures from an external source. This is the natural next step from the work which has been presented in this Thesis, and is particularly important for the consideration of susceptibility.

to implement the resonance error correcetion scheme in a hybrid TLM code, currently it is used in the regular mesh or multigrid schemes. This would involve automatic compensation for the path length differences based on the nodal aspect ratios

to apply the principle of resonance error correction, namely the path length correction, to other structures, such as strip-line and further verify the generality of the solution. This has direct application for pcb modelling.

to model multi-conductors. The work presented here has concentrated on a single wire or two closely spaced wires. The extension of this to wire looms is of practical importance for EMC and it is a complex task, and possibly a major research projrct, to develop the required modelling techniques.

to further investigate, using both experimental and modelling investigations, the behaviour of wire terminations and in particular, the effects of stray capacitance and inductance (for example caused by pig-tails) and the behaviour of terminations whose impedance changes with

frequency.

to investigate the hybridization of TLM with other modelling methods, or even with experimental results. Some of the benefits of TLM were discussed in Chapter 2. However, a limitation is that the maximum size of work-space which can be used is generally less than 10^3 wavelengths. Thus, the combination of TLM with other methods, which could extend the maximum size of the model would be a great advantage.

CHAPTER EIGHT
REFERENCES AND PUBLICATIONS

This Chapter lists the references cited in the main body of the Thesis and notes the publications arising from the work undertaken in preparation of this Thesis.

8.1. References

1 IEC50 (161): (BS4727: pt 1: Group09) Glossary of electrotechnical, power telecommunication, electronics, lighting and colour terms. Electromagnetic Compatibility.

2 Williams T.; EMC for product designers - meeting the European EMC directive; Newnes, an imprint of Butterworth-Heinemann Ltd; 1992.

3 Council Directive of 3rd May 1989 on the approximation of the laws of the Member States relating to Electromagnetic Compatibility (89/336/EEC); Official Journal of the European Communities; No L 139, 23 May 1989.

4 Bond AEJ; Implementation of the electromagnetic compatibility (EMC) directive (89/336/EEC) in the UK; Eighth International Conference on Electromagnetic Compatibility; **IEE Publ. 362**; 1992; pp. 1-11.

5 WS Atkins Management Consultants; The UK market for EMC testing and consultancy services; Department of Trade and Industry; April 1988.

6 Gravelle LB, Wilson PF; EMI/EMC in printed circuit boards - a literature review; IEEE Transactions on Electromagnetic Compatibility; **34,** no. 2; 1992; pp. 109-116.

7 Johns PB, Beurle RL; Numerical solution of 2-dimensional scattering problems using a transmission-line matrix; Proc IEE; **118,** no. 9; 1971; pp. 1203-1208.

8 Hoefer WJR; The transmission-line matrix method - theory and application; IEEE Transactions on Microwave Theory and Techniques; **MTT-33,** no. 10; 1985; pp. 882-892.

9 Herring JL, Naylor P, Christopoulos C; Transmission-line modelling in electromagnetic compatibility studies; International Journal of Numerical Modelling; **4**; 1991; pp. 143-152.

10 Naylor P; Coupling between electromagnetic waves and wires using transmission-line modelling; PhD Thesis; 1986; University of Nottingham.

11 Herring JL; Developments in the Transmission-Line Modelling method for electromagnetic compatibility studies; PhD Thesis; 1993; University of Nottingham.

12 Duffy AP, Benson TM, Christopoulos C; Numerical modelling of cavity backed apertures using transmission-line modelling (TLM); Eighth International Conference on Antennas and Propagation, 30 March - 2 April 1993; IEE Conf. Pub. 370; pp 107 - 110.

13 Daher JK, Donaldson EE, Woody JA; Evaluation of radiated emission and susceptibility measurement techniques; IEEE International Symposium on EMC, Sept 8-10; 1982; pp. 244-251.

14 Wilson P, Gassmann F; Theoretical and practical investigation of the field distribution inside a loaded/unloaded GTEM cell; 10th International Zurich Symposium and Technical Exhibition on Electromagnetic Compatibility, 9-11 March 1993; pp. 595-598.

15 Heirman DN; The open area test site - still the key to radiated emission testing; 10th International Symposium and Technical Exhibition on Electromagnetic Compatibility, 9-11 March 1993; pp. 79-82.

16 Cruz JE, Larson EB; Alternative techniques for some typical MIL-STD-461/462 types of measurements; National Institute of Standards and Technology (NEL), Boulder, Co.; Electromagnetic Fields Division; NIST/TN-1320; Mar 1989.

17 Marx KD, Eastin RI; A configuration-oriented SPICE model for multiconductor transmission lines with homogeneous dielectrics; IEEE Transactions on Microwave Theory and Techniques; **38**, no 8; 1990; pp. 1123-1129.

18 Sadiku MNO, Peterson AF; A comparison of numerical methods for computing electromagnetic fields; Proceedings - 1990 Southeastcon; 1990; pp. 42-47.

19 Itoh T. (ed.); Numerical techniques for microwave and millimeter-wave passive structures; John Wiley and Sons; 1989.

20 Booton RC, jr.; Computational methods for electromagnetics and microwaves; John Wiley and Sons Inc; 1992.

21 Sadiku MNO, Obiozor CN; Annotated bibliography of numerical modelling in electromagnetic compatibility; International Journal of Numerical Modelling; **4**; 1991; pp. 259-269.

22 Hayes TF, Barrett JJ; Modeling of multiconductor systems for packaging and interconnecting high-speed digital ic's; IEEE Transactions on Computer-Aided Design; **11,** no.4; 1992; pp. 424-431.

23 Hrennikov A; Solution of problems in elasticity by the framework method; Journal of Applied Mechanics; **A8**; 1941; pp. 169-75.

24 Steele CW; Numerical computation of electric and magnetic fields; Van Nostrand Reinhold; 1987.

25 Binns KJ, Lawrenson PJ, Trowbridge CW; The analytical and numerical solution of electric and magnetic fields; John Wiley and Sons; 1992.

26 Yamabuchi T, Fujii S, Murai T, Hirose S, Futagami T, Kagawa Y; Finite element analysis of electromagnetic field via three-dimensional hexagonal edge elements; Electronics and Communication in Japan part 2 (Electronics); **75**, no. 9; 1992; pp. 1-13.

27 George PL; Automatic mesh generation application to finite element methods; John Wiley and Sons, Paris; 1991

28 Cushman JH; Difference schemes or element schemes?; International Journal of Numerical Methods in Engineering; **14**; 1979; pp. 1643-1651.

29 Harrington RF; Field computation by moment methods; Macmillan; 1968.

30 Yee KS; Numerical solution of initial boundary value problems involving Maxwell's equations in isotropic media; IEEE Transactions on Antennas and Propagation; **AP-14**; 1966; pp. 302-307.

31 Cangellaris AC; Time domain finite methods for electromagnetic wave propagation and scattering; IEEE Transactions on Magnetics; **27**, no. 5; 1991; pp. 3780-3785.

32 Fusco M; FDTD algorithm in curvilinear coordinates; IEEE Transactions on Antennas and Propagation; **38**, no. 1; 1990; pp. 76-89.

33 Johns PB; On the relationship between TLM and finite-difference methods for Maxwell's equations; IEEE Transactions on Microwave Theory and Techniques; **MTT-35**, no. 1; 1987; pp. 60-61.

34 Gwarek WK, Johns PB; Comments on "on the relationship between TLM and finite-difference methods for Maxwell's equations" and reply; IEEE Transactions on Microwave Theory and Techniques; **MTT-35,** no. 9; 1987; pp. 872-873.

35 Chen Z, Ney MM, Hoefer WJR; A new finite-difference time-domain formulation and its equivalence with the TLM symmetrical condensed node; IEEE Transactions on Microwave Theory and Techniques; **MTT-39**; 1991; pp. 2160-2169.

36 Huygens C; Traite de la Lumiere; Leiden; 1690.

37 Hoefer WJR; Linear and Nonlinear field modelling in the time domain with the transmission line matrix (TLM) method; Alta Frequenza; **LVIII,** no. 5-6; 1989; pp. 541-549.

38 Whinnery JR, Ramo S; A new approach to the solution of high frequency field problems; Proceedings of the Institution of Radio Engineers; **32**; 1944; pp. 284-288.

39 Kron G; Equivalent circuit of the field equations of Maxwell - Pt. I; Proceedings of the Institution of Radio Engineers; **32**; 1944; pp. 289 - 299.

40 Johns PB; Application of the transmission-line matrix method to homogeneous waveguides of arbitrary cross-section; Proceedings of the Institution of Electrical Engineers; **119**, no. 8; 1972; pp. 1086-1092.

41 Akhtarzad S, Johns PB; Transmission-line matrix solution of waveguides with wall losses; Electronics Letters; **9**, no. 15; 1973; pp. 335-336.

42 Akhtarzad S, Johns PB; Numerical solution of lossy waveguides: TLM computer program; Electronics Letters; **9**, no. 21; 1973; pp. 309-311.

43 Johns PB, Slater GF; Transient analysis of waveguides with curved boundaries; Electronics letters; **9**, no. 21; 1973; pp. 486-487.

44 Johns PB; The solution of inhomogeneous waveguide problems using a transmission-line matrix; IEEE Transactions on Microwave Theory and Techniques; **MTT-22**, no. 3; 1974; pp. 209-215.

45 Akhtarzad S, Johns PB; Solution of 6-component electromagnetic fields in three space dimensions and time by the TLM method; Electronics Letters; **10**, no. 25/26; 1974; pp. 535-537.

46 Saguet P, Pic E; Utilisation d'un nouveau type de noeud dans la method TLM en 3 dimensions; Electronics Letters; **18**, no. 11; 1982; pp. 478-480.

47 Johns PB; A symmetrical condensed node for the TLM method; IEEE Transactions on Microwave Theory and Techniques; **MTT-35,** no 4; 1987; pp. 370-377.

48 Nielsen J; Spurious modes of the TLM-condensed node formulation; IEEE Microwave and Guided Wave Letters; **1,** no. 8; 1991; pp. 201-203.

49 Nielsen J, Hoefer WJR; A complete dispersion analysis of the condensed node TLM; IEEE Transactions on Magnetics; **27,** no. 5; 1991; pp. 3982-3985.

50 Nielsen JS, Hoefer WJR; Modification of the condensed 3-D TLM Node to improve modeling of conductor edges; IEEE Microwave and Guided Wave Letters; **2,** no. 3; 1992; pp. 105-107.

51 Al-Mukhtar DA, Sitch JE; Transmission-line matrix method and irregularly graded space; Proc. IEE; **128**; 1981; pp. 299-305.

52 Scaramuzza R, Lowery AJ; Hybrid symmetrical condensed node for the TLM method; Electronics Letters; **26,** no. 23; 1990; pp. 1947-1948.

53 Herring JL, Christopoulos C; Multigrid transmission-line modelling method for solving electromagnetic field problems; Electronic Letters; **27,** no. 20; 1991; pp. 1794-1795.

54 Meliani H, De Cogan D, Johns PB; The use of orthogonal curvilinear meshes in TLM models; International Journal of Numerical Modelling; **1**; 1988; pp. 221-238.

55 Ward DD; A three-dimensional model of the lightning return stroke; PhD Thesis; University of Nottingham; 1991.

56 Tong C-yE, Fujino Y; Transmission line matrix analysis for three-dimensional electromagnetic problems using personal computer; The 3rd Asia-Pacific Microwave Conference Proceedings, Tokyo; 1990; pp. 423-425.

57 Naylor P; Ait-Sadi R; A simple method for determining 3D TLM nodal scattering in non-scalar problems; Electronics Letters; **28**, no. 5; 1992; pp. 2353-2354.

58 Simons NRS, Bridges E; Method for modelling free space boundaries in TLM situations; Electronics Letters; **26,** no. 7; 1990; pp. 453-455.

59 Eswrappa, Costache G, Hoefer WJR; Transmission line matrix modelling of dispersive wide-band absorbing boundaries with time-domain diakoptics for S-parameter extraction; IEEE Transactions on Microwave Theory and Techniques; **38**, no. 4; 1990; pp. 379-386.

60 German FJ; Infinitesimally adjustable boundaries in symmetrical condensed node TLM simulations; 9th Annual Review of Progress in Applied Computational Electromagnetics at the Naval Postgraduate School; Monterey, Ca; March 22-26, 1993; pp. 482-490.

61 Forest M, Hoefer WJR; TLM synthesis of microwave structures using time reversal; IEEE Microwave Theory and Techniques Symposium Digest, Albuquerque, NM; May 1992; pp 791-792.

62 Sorrentino R, So PPM, Hoefer WJR; Numerical microwave synthesis by inversion of the TLM process; 21st European Microwave Conference digest, Stuttgard, Germany; Sept. 1991; pp. 1273-1277.

63 Naylor P, Christopoulos C, Johns PB; Analysis of the coupling of electromagnetic radiation into wires using transmission-line modelling; IERE Fifth Int. Conf. on Electromagnetic Compatibility 1-3 Oct publ no 71; 1986; pp. 129-135.

64 Naylor P, Christopoulos C, Johns PB; Coupling between electromagnetic fields and wires using transmission-line modelling; IEE Proceedings; **134, pt A,** no. 8; 1987; pp. 679-686.

65 Naylor P, Christopoulos C; A new wire node for modelling thin wires in electromagnetic field problems solved by transmission line modelling; IEEE Transactions on microwave theory and techniques; **38,** no 3; 1990; pp. 328-390.

66 Wlodarczyk AJ, Johns DP; New wire interface for graded 3-D TLM; Electronics Letters; **28,** no. 8; 1992; pp. 728-729.

67 Porti JA, Morente JA, Khalladi M, Gallego A; Comparison of thin wire models for TLM method; Electronics Letters; **28,** no. 20; 1992; pp. 1910-1911.

68 Morente JA, Porti JA, Gimenez G, Gallego; Loaded wire node for TLM method; Electronics Letters; **29,** no. 2; 1993; pp. 182-184.

69 Naylor P, Christopoulos C; Coupling between electromagnetic fields and multimode transmission systems using TLM; International Journal of Numerical Modelling: Electronic Networks, Devices and Fields; **2;** 1989; pp. 227-240.

70 Mueller U, So PPM, Hoefer WJR; The compensation of coarseness error in 2D TLM modeling of microwave structures; IEEE MTT-S Digest, paper IF1 N-2; 1992; pp. 373-376.1

71 Nielsen JS, Hoefer WJR; New 3D TLM condensed node structure for improved simulation of conductor strips; IEEE Microwave Theory and Techniques Symposium digest, Albuquerque, NM; May 1992; pp. 1221-1223.

72 Kraus JD; Electromagnetics; McGraw-Hill International; Second Edition; 1984.

73 Benson FA, Benson TM; Fields, waves and transmission lines; Chapman and Hall; 1991.

74 Hewlett-Packard Company; Operating and programming manual; HP 8510 Network Analyser; 1985.

75 Halbach L, Kirschvink M; RF-absorbtive cables; Euro-EMC '90 Conference proceedings, London, 2-4 Oct 1990; pp. 18.

76 Paul CR; Effect of pigtails on crosstalk to braided-shield cables; IEEE Transactions on Electromagnetic Compatibility; **EMC-22,** no. 3; 1980; pp. 161-172.

77 Hejase HAN, Adams AT, Harrington RF, Sarkar TK; Shielding effectiveness of "pigtail" connections; IEEE Transactions on Electromagnetic Compatibility; **31,** no. 1; 1989; pp. 63-68.

78 Hejase HAN; Radiation properties of pigtail-terminated coaxial transmission line; IEEE Transactions on Electromagnetic Compatibility; **34,** no. 1; 1992; pp. 23-27.

79 Ramo S, Whinnery JR, van Douzer T; Fields and waves in communication electronics; John Wiley and Sons.

80 Menacer M, Woolfson MS, Crowe JA; Method for correction of linear distortion of signals and application to DNA fingerprint data; Electronics Letters; **28**; 1992; pp. 2126-2127.

81 Herring JL, Duffy AP, Benson TM, Christopoulos C; A transmission-line modelling study of screened room behaviour; IEE Colloquium on radiated emission test facilities; 2 June 1992; digest no. 1992/132, pp. 1/1-1/4.

82 Marvin AC, Simpson G; Screened room radiated emission measurements; a preliminary calibration procedure for the frequency range 1MHz to 30MHz; Fifth British Electromagnetic Measurements Conference; 11-14 November 1991; pp. 35/1-35/5.

83 Herring JL, Christopoulos C; Numerical simulation for better calibration and measurements; Fifth British Electromagnetic Measurements Conference; 11-14 November 1991; pp. 37/1-37/4.

84 Cook RJ (ed.); Final report, stage 3: The requirement of the origination of a draft emission calibration procedure.

85 German FJ, Gothard GK, Riggs LS, Goggans PM; The calculation of radar cross-section (RCS) using the TLM method; and fields; **2**; 1989; pp. 267-278.

86 German FJ, Gothard GK, Riggs LS; RCS of three-dimensional scatterers using the symmetrical condensed TLM method; Electronics Letters; **26,** no 10; 1990; pp. 673-674.

87 Luebbers RJ, Kunz KS, Schneider M, Hunsberger F; A finite-difference time-domain near zone to far zone transformation; IEEE Transactions on Antennas and Propagation; **39,** no 4; 1991; pp. 429-433.

88 Wills JD; Spectral estimation for the transmission-line matrix method; IEEE Transactions on Microwave Theory and Techniques; **38**, no. 4; 1990; pp. 448-451.

89 Baher H; Analog and digital signal processing; John Wiley and Sons; 1990.

90 Stremler F; Introduction to communication systems, second edition; Addison-Wesley; 1982.

91 Shih Y-C, Hoefer WJR; Dominant and second-order cutoff frequencies with a two-dimensional TLM-program; IEEE Transactions on Microwave Theory and Techniques; **28**; 1980; pp. 1443-1448.

8.2. Publications

The following papers have been published based on the work described in this Thesis.

1 Duffy AP, Benson TM, Christopoulos C; "Application of Transmission-Line Modelling (TLM) To Studying the Effectiveness of Screened Enclosures"; IEE Colloquium on 'Screening of connectors cables and enclosures'; 17th Jan 1992; digest 1992/012; pp 2/1 - 2/3

2 Duffy AP, Naylor P, Benson TM, Christopoulos C; "Computer Simulation as an aid to EMC Diagnostics"; 16th Automated RF and Microwave Measurements Society (ARMMS) Conference; Heriot-Watt University, Edinburgh; 30-31 March 92; pp. 117 - 127

3 Herring JL, Duffy AP, Benson TM, Christopoulos C; "A Transmission-Line Modelling (TLM) Study of Screened Room Behaviour" IEE Colloquium on Radiated Environment Test Facilities, 2 June 92, London; pp 1/1-1/4.

4 Duffy AP, Naylor P, Benson TM, Christopoulos C; "Coupling Measurements and Comparisons with Simulations Inside a Screened Room"; Eighth International Conference on Electromagnetic Compatibility, Heriot-Watt University, Edinburgh, 21-24 September 1992, IEE publication number 362, pp 108-114.

5 Duffy AP, Benson TM,Christopoulos C, Herring JL; "New method for accurate modelling of wires using TLM" Electron. Lett.; **29**, no. 2; 1993; pp. 224-227.

6 Duffy AP, Herring JL, Benson TM, Christopoulos C "The application of TLM to EMC design"; IEE Colloquium on "Does Electromagnetic Modelling have a role in EMC design?"; 4 Feb 1993, London, pp 5/1-5/5.

7 Duffy AP, Naylor P, Benson TM, Christopoulos C; "Numerical Simulation of Electromagnetic Coupling and Comparison with Experimental Results"; IEEE T-EMC; **35**, no. 1; 1993; pp. 46-54.

8 Duffy AP, Herring JL, Benson TM, Christopoulos C; "The Application of the Transmission-Line Modelling (TLM) Method to the Simulation of Propagation and Coupling Inside a Conducting Enclosure"; 10th EMC Zurich Symposium; 9 - 11 March 1993; pp 445 - 449

9 Duffy AP, Benson TM, Christopoulos C; "Numerical modelling of cavity backed apertures using transmission-line modelling (TLM)"; 8th International Conference on Antennas and Propagation; 30 March - 2 April 1993; IEE publ no. 370, pt. 1; pp 107 - 110.

10 Duffy AP, Herring JL, Benson TM, Christopoulos C; "Comparison of TLM simulations and experiments in EMC problems"; IEE Colloquium on "Developments in the method of Transmission-Line Modelling (TLM); 2 April 1993; pp 4/1 - 4/3.

11 Duffy AP, Herring JL, Benson TM, Christopoulos C; "The EMC Applications of Transmission-Line Modelling"; Microwave Engineering (Europe); May 1993; pp. 41 - 50.

12 Duffy AP, Herring JL, Benson TM, Christopoulos C; "A new wire representation for TLM", IEEE EMC Symposium, Dallas, Tx, 9-13 Aug 1993; pp. 434 - 435.

13 Duffy AP, Herring JL, Benson TM, Christopoulos C; "A new wire representation for TLM"; Accepted for publication by IEEE Transactions on Microwave Theory and Techniques

14 Duffy AP, Benson TM, Christopoulos C; "The effects of a cavity on a signal propagating along an internal wire: a comparison of measurements and modelling"; Accepted for publication by IEEE Transactions on EMC.